

**CENTRE FOR INFRASTRUCTURE  
PERFORMANCE AND RELIABILITY**

**RESEARCH REPORT**

---

**Ballistic Pendulum Experiments  
and Escalator Bullet Traps:  
Report of Tests  
and Development of Modified Equations**

***Dr Bruce W. Golley and Bruce B. Hughes***

**Research Report No. 284.10.2017**

**October 2017**

**ISBN 978-0-7259-0005-2**



**THE UNIVERSITY OF  
NEWCASTLE  
AUSTRALIA**

# **Ballistic Pendulum Experiments: Report of Tests and Development of Modified Equations Relating to an Escalator Bullet Trap**

Dr Bruce W. Golley<sup>1</sup>  
Associate Professor (retired)  
School of Civil Engineering  
The University of New South Wales  
Australian Defence Force Academy  
Campbell, ACT, Australia

Major Bruce B. Hughes (Rtd)  
phone: +61 412 954206 email: bruce.hughes27@bigpond.com.au

## **EXECUTIVE SUMMARY**

The Australian Department of Defence has a number of indoor firing ranges for training purposes with these ranges incorporating a variety of bullet traps including steel escalators. Defences' steel escalator traps consist of two, sloping plates which direct a projectile along the face of the impacted plate, through a rear slot/throat and thence to a projectile de-energising chamber for spent projectile collection. The steel, impact plates under examination were constituted by quenched and tempered steel with a thickness of 10 mm and a hardness of 500 HB with the trap being commissioned in 1990. The most heavily impacted area of the plate is about a metre either side of the throat with this impacted area equating to a typical shoulder/weapon firing height. It was observed in 2011 that the lower, impact plates in particular were buckling in the vicinity of the throat. This research report describes an experiment to determine the cause of the buckling effect and centred on an examination of the ratio of tangential impulse to normal impulse during the impact of a 5.56 mm round fired from M4 carbine commonly used on the range. This examination used a ballistic pendulum with tests conducted on 29-30 October 2012 and 6-7 December 2012. Details of the tests and relevant modelling are contained in this research report.

This report summarises the research achievements of Dr Bruce Golley and Bruce Hughes and in particular is dedicated to the memory of Dr Bruce Golley. The Centre for Infrastructure Performance and Reliability (CIPAR) at The University of Newcastle values these achievements and is pleased to sponsor the publication of their research findings

---

<sup>1</sup> Note that Bruce Golley retired from the ADFA in June 2004 and passed away on 8 March 2013. For information about his research please contact Bruce Hughes.  
Ph: +61 412 954206 Email: bruce.hughes27@bigpond.com.au

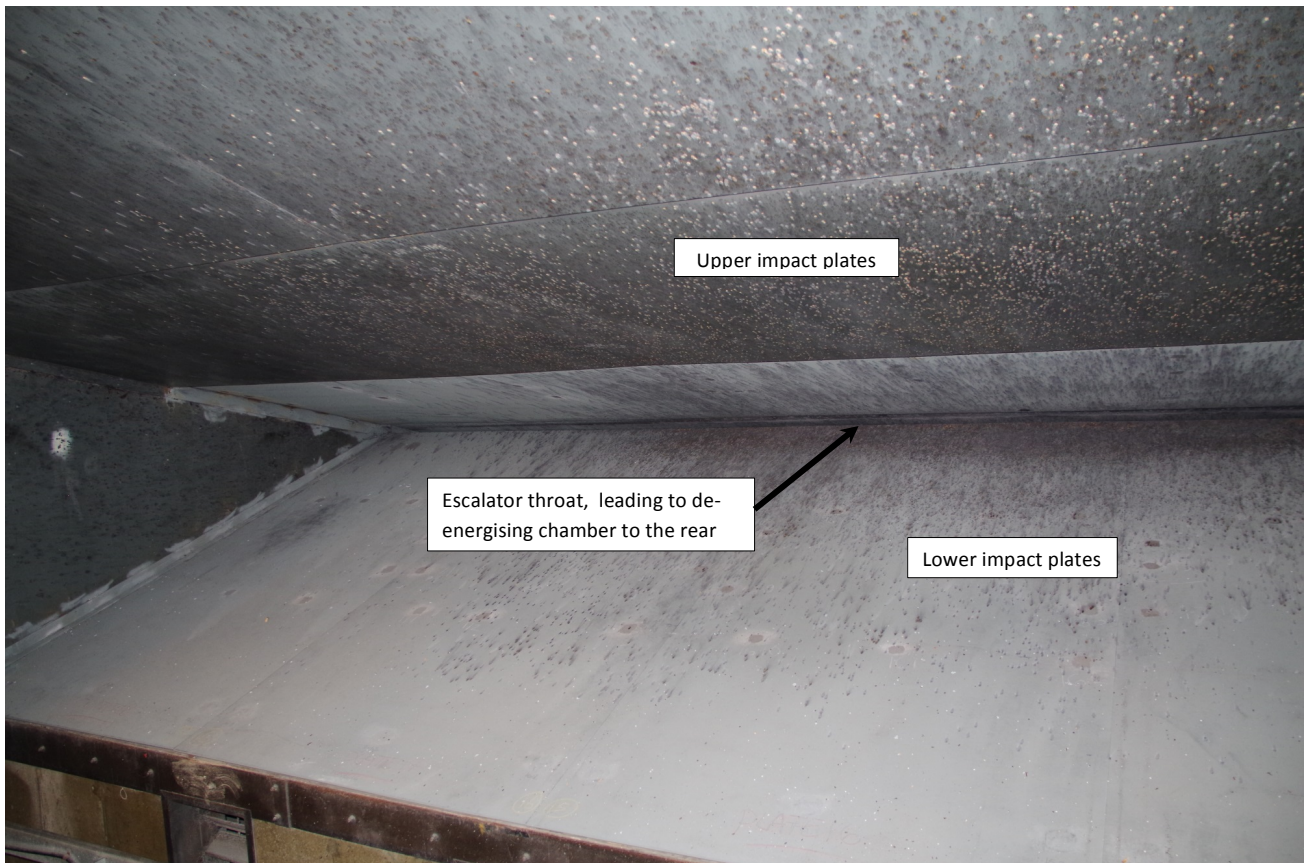


Photo of Escallator Bullet Trap.

# THE ANALYSIS OF THE DISPLACEMENT OF A THIN PLATE DUE TO SHOT PEENING AT ONE END

## SUMMARY

A thin steel plate is subjected to a large number of impacts from projectiles fired from an M4 carbine. The impacts are concentrated near one end of the plate. The impacts are at a shallow angle to the plate, but appear to have caused yielding near the impacted surface, leading to surface compression in the plane of the plate. This effect, known as shot peening, causes the plate to deform to relieve the compression stresses. To analyse the effects of peening, the compressed layer is first allowed to expand, in-plane forces are applied to the layer to restore compatibility and having restored compatibility equilibrating forces are applied to the layer. In thin plate theory, the effect is to apply line moments around the boundary of the peened layer. It is the purpose of this paper to analyse such a plate.

The plate under consideration is one of eight plates which have deformed noticeably. For the sake of this paper, the plates are 2000 mm by 5000 mm by 10 mm, with Poissons ratio  $\nu = 0.3$ . The plates are taken as simply supported on the two long sides and one short side. On the remaining short side, which is nearest the heavily peened area, the connection holding the plate to the support is compromised, or failed, and that short side is treated as a free edge. Hence the plate to be analysed and the applied loads are as shown in Figure 1.

## SUMMARY OF BASIC EQUATIONS

The following development of the solution is given mainly for the writers benefit. As the writer did not have access to finite element software, and wanted a solution reasonably promptly, an exact solution was developed. The development is lengthy, but the results for two cases of peening are given in graphical form and are consistent with the observed



deformation.

The solution involves the superposition of three loading cases, two of which involve rapidly converging sine series.

Refer to Figure 2. A thin plate is of dimensions  $a$  and  $b$  is simply supported on the ends  $x = 0$  and  $x = a$ , and is subjected to sinusoidally varying moments and shears on the sides  $y = 0$  and  $y = b$ . A stiffness relationship is required between the action and displacement coefficients

$$\begin{Bmatrix} P_{1m} \\ M_{1m} \\ P_{2m} \\ M_{2m} \end{Bmatrix} \quad \text{and} \quad \begin{Bmatrix} w_{1m} \\ \theta_{1m} \\ w_{2m} \\ \theta_{2m} \end{Bmatrix}$$

$\theta = w_{,y}$ . A comma denotes differentiation. The governing differential equation is the thin plate equation

$$w_{,xxxx} + 2w_{,xxyy} + w_{,yyyy}$$

The stress resultants per unit length shown in Figure 3 are also required. In terms of displacements, the stress resultants are

$$M_x = -D(w_{,xx} + \nu w_{,yy})$$

$$M_y = -D(w_{,yy} + \nu w_{,xx})$$

$$V_x = -D(w_{,xxx} + (2 - \nu)w_{,xyy})$$

$$V_y = -D(w_{,yyy} + (2 - \nu)w_{,xxy})$$

and

$$D = \frac{Eh^3}{12(1 - \nu^2)}$$

$E$  is the modulus of elasticity and  $h$  is the plate thickness. A Levy solution of the DE which satisfies the simply supported boundary conditions on  $x = 0$  and  $x = a$  is

$$w_m(x, y) = \left[ \cosh \frac{m\pi y}{a} \quad \sinh \frac{m\pi y}{a} \quad \frac{m\pi y}{a} \cosh \frac{m\pi y}{a} \quad \frac{m\pi y}{a} \sinh \frac{m\pi y}{a} \right] \begin{Bmatrix} A_m \\ B_m \\ C_m \\ D_m \end{Bmatrix} \sin \frac{m\pi x}{a}$$

This is written as

$$w_m(x, y) = [Y_m(y)]\{E_m\} \sin \frac{m\pi x}{a} = [F_m(x, y)]\{E_m\}$$

Derivatives are

$$\begin{aligned} w_m(x, y)_{,x} &= [F_m(x, y)_{,x}]\{E_m\} \\ w_m(x, y)_{,y} &= [F_m(x, y)_{,y}]\{E_m\} \\ w_m(x, y)_{,xx} &= [F_m(x, y)_{,xx}]\{E_m\} \\ w_m(x, y)_{,xy} &= [F_m(x, y)_{,xy}]\{E_m\} \\ w_m(x, y)_{,yy} &= [F_m(x, y)_{,yy}]\{E_m\} \\ w_m(x, y)_{,xxx} &= [F_m(x, y)_{,xxx}]\{E_m\} \\ w_m(x, y)_{,xxy} &= [F_m(x, y)_{,xxy}]\{E_m\} \\ w_m(x, y)_{,xyy} &= [F_m(x, y)_{,xyy}]\{E_m\} \\ w_m(x, y)_{,yyy} &= [F_m(x, y)_{,yyy}]\{E_m\} \end{aligned}$$

All algebra is carried out using the symbolic language MAPLE, and no details are given here. The stress resultants required in the solution are

$$M_y(x, y) = -D[[F_m(x, y)_{,yy}] + \nu[F_m(x, y)_{,xx}]]\{E_m\} = [M_{ym}(x, y)]\{E_m\}$$

$$V_y(x, y) = -D[[F_m(x, y)_{,yyy}] + (2 - \nu)[F_m(x, y)_{,xxy}]]\{E_m\} = [V_{ym}(x, y)]\{E_m\}$$

We now eliminate  $\{E_m\}$ .

$$\begin{Bmatrix} w_{1m} \\ \theta_{1m} \\ w_{2m} \\ \theta_{2m} \end{Bmatrix} \sin \frac{m\pi x}{a} = \begin{Bmatrix} [F_m(x, 0)] \\ [F_m(x, 0)_{,y}] \\ [F_m(x, b)] \\ [F_m(x, b)_{,y}] \end{Bmatrix} \begin{Bmatrix} A_m \\ B_m \\ C_m \\ D_m \end{Bmatrix}$$

or

$$\begin{Bmatrix} w_{1m} \\ \theta_{1m} \\ w_{2m} \\ \theta_{2m} \end{Bmatrix} = \frac{1}{\sin \frac{m\pi x}{a}} \begin{Bmatrix} [F_m(x, 0)] \\ [F_m(x, 0)_{,y}] \\ [F_m(x, b)] \\ [F_m(x, b)_{,y}] \end{Bmatrix} \begin{Bmatrix} A_m \\ B_m \\ C_m \\ D_m \end{Bmatrix}$$

It is a feature of the Levy solution that  $\sin \frac{m\pi x}{a}$  now cancels, and we obtain

$$\{W_m\} = [B_m]\{E_m\}$$

Therefore

$$\{E_m\} = [B_m]^{-1}\{W_m\}$$

The displacement for the  $m^{th}$  term of the series then becomes

$$\begin{aligned} w_m(x, y) &= [Y_m(y)]\{E_m\} \sin \frac{m\pi x}{a} \\ &= [Y_m(y)][B_m]^{-1}\{W_m\} \sin \frac{m\pi x}{a} \\ &= [N_m(y)]\{W_m\} \sin \frac{m\pi x}{a} \\ &= [F_m^*(x, y)]\{W_m\} \end{aligned}$$

Hence

$$M_y(x, y) = -D[[F_m^*(x, y)_{,yy}] + \nu[F_m^*(x, y)_{,xx}]]\{W_m\} = [M_{y_m}^*(x, y)]\{W_m\}$$

$$V_y(x, y) = -D[[F_m^*(x, y)_{,yyy}] + (2 - \nu)[F_m^*(x, y)_{,xxy}]]\{W_m\} = [V_{y_m}^*(x, y)]\{W_m\}$$

The relationship between edge actions and displacements is therefore

$$\begin{Bmatrix} P_{1m} \\ M_{1m} \\ P_{2m} \\ M_{2m} \end{Bmatrix} \sin \frac{m\pi x}{a} = \begin{Bmatrix} [-V_{y_m}^*(x, 0)] \\ [M_{y_m}^*(x, 0)] \\ [V_{y_m}^*(x, b)] \\ [-M_{y_m}^*(x, b)] \end{Bmatrix} \begin{Bmatrix} w_{1m} \\ \theta_{1m} \\ w_{2m} \\ \theta_{2m} \end{Bmatrix}$$

from which

$$\begin{Bmatrix} P_{1m} \\ M_{1m} \\ P_{2m} \\ M_{2m} \end{Bmatrix} = \frac{1}{\sin \frac{m\pi x}{a}} \begin{Bmatrix} [-V_{y_m}^*(x, 0)] \\ [M_{y_m}^*(x, 0)] \\ [V_{y_m}^*(x, b)] \\ [-M_{y_m}^*(x, b)] \end{Bmatrix} \begin{Bmatrix} w_{1m} \\ \theta_{1m} \\ w_{2m} \\ \theta_{2m} \end{Bmatrix}$$

As before  $\sin \frac{m\pi x}{a}$  cancels, giving the final stiffness relationship between the amplitudes

$$\begin{Bmatrix} P_{1m} \\ M_{1m} \\ P_{2m} \\ M_{2m} \end{Bmatrix} = \begin{bmatrix} K_{1,1m} & K_{1,2m} & K_{1,3m} & K_{1,4m} \\ K_{2,1m} & K_{2,2m} & K_{2,3m} & K_{2,4m} \\ K_{3,1m} & K_{3,2m} & K_{3,3m} & K_{3,4m} \\ K_{4,1m} & K_{4,2m} & K_{4,3m} & K_{4,4m} \end{bmatrix} \begin{Bmatrix} w_{1m} \\ \theta_{1m} \\ w_{2m} \\ \theta_{2m} \end{Bmatrix}$$

or

$$\{P_m\} = [K_m]\{W_m\}$$

Note

$$[K_m] = [K_m(a, b, \nu, D)]$$

## ANALYSIS OF A PLATE SHOT PEENED AT ONE END

To determine the deflection due to non-uniform shot peening, the plate shown in Figure 4 is considered. The plate has a span  $a$  between simple supports in the  $x$  direction, is free at one end and simply supported at the other. The plate is divided into two strips. Strip 1, bounded by nodal lines 1 and 2, is of width  $b_1$  in the  $y$  direction near the free end and is considered uniformly peened. Strip 2, bounded by nodal lines 2 and 3 is of width  $b_2$  and is not subjected to impacts. To determine the effect of shot peening, the plate is analysed under the moments  $M$  per unit length shown in Figure 4.

The actual loading is obtained by the superposition of three load cases.

### Case 1

Strip 1 is subjected to moments  $M$  and  $\nu M$  per unit length as shown in Figure 5(a). This causes deflections

$$w_{11} = \frac{Mx(x-a)}{2D} \quad \text{and} \quad w_{21} = 0$$

in strips 1 and 2.  $w_{11}$  may also be expressed as a sine series

$$w_{11} = \sum_{m=1,3,5}^{\infty} \frac{-4a^2 M}{m^3 \pi^3 D} \sin \frac{m\pi x}{a}$$

### Case 2

To restore compatibility on nodal line 2, displacements

$$\begin{Bmatrix} w_1 \\ \theta_1 \\ w_2 \\ \theta_2 \end{Bmatrix} = \sum_{m=1,3}^{\infty} \frac{4a^2 M}{m^3 \pi^3 D} \begin{Bmatrix} 0 \\ 0 \\ 1 \\ 0 \end{Bmatrix} \sin \frac{m\pi x}{a}$$

are applied to strip 1 along nodal lines 1 and 2. See Figure 5(b). The resulting displacements are

$$w_{12} = \sum_{m=1,3}^{\infty} \frac{4a^2 M}{m^3 \pi^3 D} F_{1,3_m}^{*1}(x, y) \quad \text{and} \quad w_{22} = 0$$

and nodal actions

$$\begin{Bmatrix} P_1 \\ M_1 \\ P_2 \\ M_2 \end{Bmatrix} = \sum_{m=1,3}^{\infty} \frac{4a^2 M}{m^3 \pi^3 D} \begin{Bmatrix} K_{1,3_m}^1 \\ K_{2,3_m}^1 \\ K_{3,3_m}^1 \\ K_{4,3_m}^1 \end{Bmatrix} \sin \frac{m\pi x}{a}$$

The superscript 1 in  $F^*$  and  $K$  refers to strip 1.

Case 3

Nodal loads are now applied to the complete plate so that when superimposed with the loads in Cases 1 and 2 the original loading is obtained. See Figure 5(c). This involves expressing the uniform moments  $M$  and  $\nu M$  on nodal lines as sine series

$$M = \sum_{m=1,3}^{\infty} \frac{M}{m\pi} \sin \frac{m\pi x}{a}$$

$$\nu M = \sum_{m=1,3}^{\infty} \frac{\nu M}{m\pi} \sin \frac{m\pi x}{a}$$

Thus we apply

$$\begin{Bmatrix} P_1 \\ M_1 \\ P_2 \\ M_2 \\ P_3 \\ M_3 \end{Bmatrix} = \sum_{m=1,3}^{\infty} \left\{ \frac{4M(1-\nu)}{m\pi} \begin{Bmatrix} 0 \\ -1 \\ 0 \\ 1 \\ 0 \\ 0 \end{Bmatrix} - \frac{4a^2 M}{m^3 \pi^3 D} \begin{Bmatrix} K_{1,3_m}^1 \\ K_{2,3_m}^1 \\ K_{3,3_m}^1 \\ K_{4,3_m}^1 \\ 0 \\ 0 \end{Bmatrix} + \begin{Bmatrix} 0 \\ 0 \\ 0 \\ 0 \\ P_{m3} \\ 0 \end{Bmatrix} \right\} \sin \frac{m\pi x}{a}$$

or

$$\begin{Bmatrix} P_1 \\ M_1 \\ P_2 \\ M_2 \\ P_3 \\ M_3 \end{Bmatrix} = \sum_{m=1,3}^{\infty} \begin{Bmatrix} P_{1m} \\ M_{1m} \\ P_{2m} \\ M_{2m} \\ P_{3m} \\ M_{3m} \end{Bmatrix} \sin \frac{m\pi x}{a}$$

We now solve

$$\begin{Bmatrix} P_{1m} \\ M_{1m} \\ P_{2m} \\ M_{2m} \\ P_{3m} \\ M_{3m} \end{Bmatrix} = \begin{bmatrix} K_{1,1m}^1 & K_{1,2m}^1 & K_{1,3m}^1 & K_{1,4m}^1 & 0 & 0 \\ K_{2,1m}^1 & K_{2,2m}^1 & K_{2,3m}^1 & K_{2,4m}^1 & 0 & 0 \\ K_{3,1m}^1 & K_{3,2m}^1 & K_{3,3m}^1 + K_{1,1m}^2 & K_{3,4m}^1 + K_{1,2m}^2 & K_{1,3m}^2 & K_{1,4m}^2 \\ K_{4,1m}^1 & K_{4,2m}^1 & K_{4,3m}^1 + K_{2,1m}^2 & K_{4,4m}^1 + K_{2,2m}^2 & K_{2,3m}^2 & K_{2,4m}^2 \\ 0 & 0 & K_{3,1m}^2 & K_{3,2m}^2 & K_{3,3m}^2 & K_{3,4m}^2 \\ 0 & 0 & K_{4,1m}^2 & K_{4,2m}^2 & K_{4,3m}^2 & K_{4,4m}^2 \end{bmatrix} \begin{Bmatrix} w_{1m} \\ \theta_{1m} \\ w_{2m} \\ \theta_{2m} \\ 0 \\ \theta_{3m} \end{Bmatrix}$$

for the unknown nodal displacement amplitudes for  $m = 1, 3, 5, \dots$ . For strips 1 and 2, the displacements are therefore

$$\{w_m^1\} = \begin{Bmatrix} w_{1m} \\ \theta_{1m} \\ w_{2m} \\ \theta_{2m} \end{Bmatrix} \quad \text{and} \quad \{w_m^2\} = \begin{Bmatrix} w_{2m} \\ \theta_{2m} \\ 0 \\ \theta_{3m} \end{Bmatrix}$$

and strip displacements are

$$w_{13} = \sum_{m=1,3}^{\infty} [F^{*1}] \{w_m^1\}$$

$$w_{23} = \sum_{m=1,3}^{\infty} [F^{*2}] \{w_m^2\}$$

Final displacements are then

$$w_{11} + w_{12} + w_{13} \quad \text{and} \quad w_{21} + w_{22} + w_{23}$$

It is found that taking three terms of the sine series is more than adequate for the determination of displacements.

### Example

A plate with the following properties was analysed.

$$a = 2, \quad b_1 = 1, \quad b_2 = 4, \quad M = 1, \quad \nu = 0.3, \quad D = 1.$$

Contours of the deformation are given in Figure 6. The deformation is consistent with the observed deformation in many of the plates.

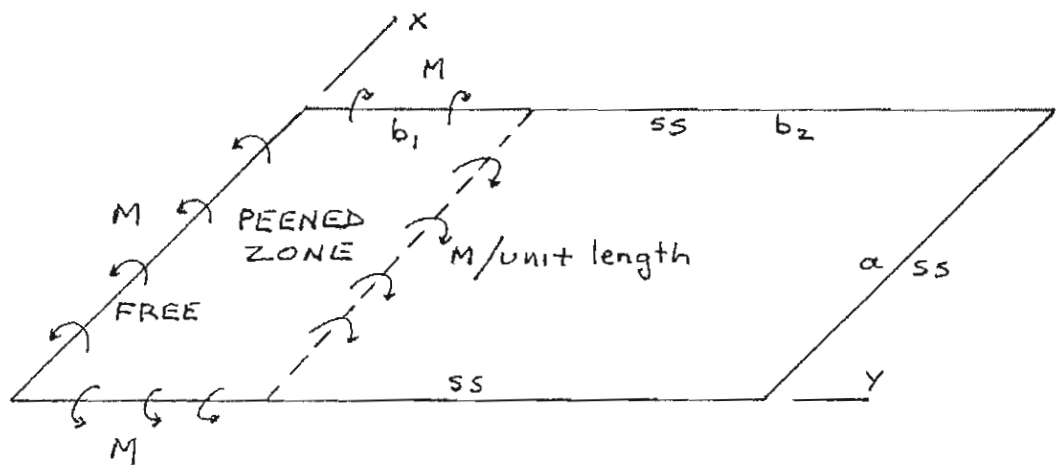


FIGURE 1

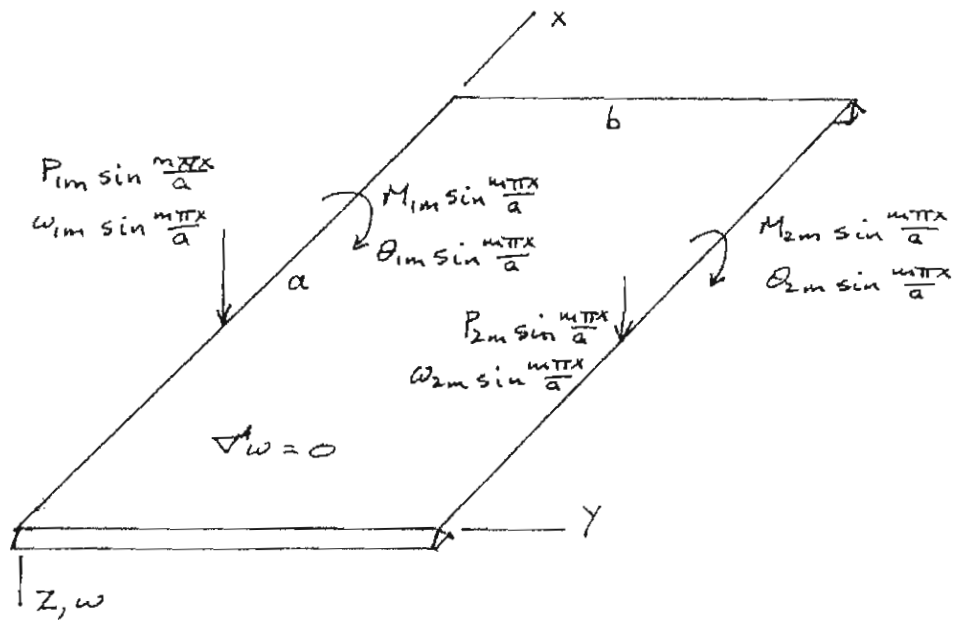


FIGURE 2

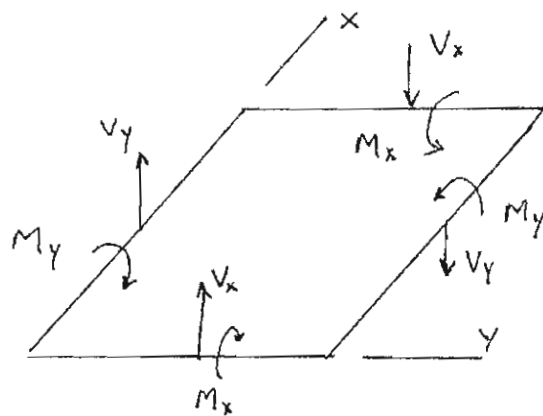


FIGURE 3

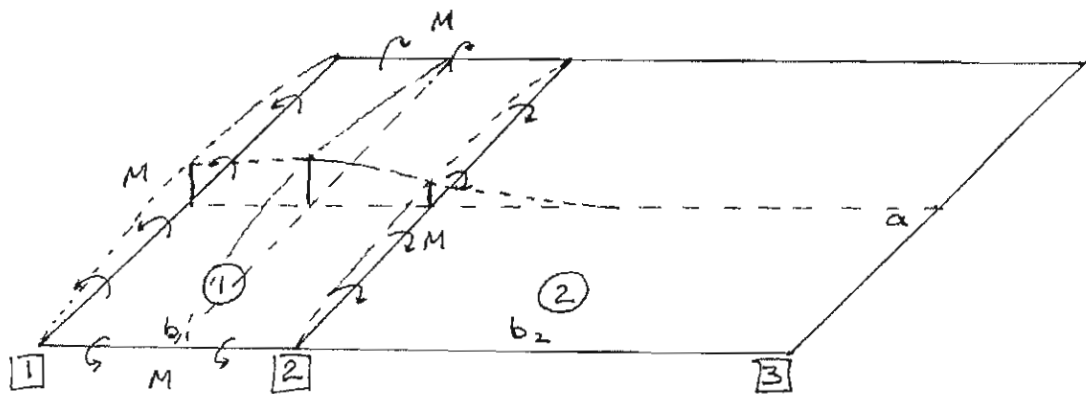


FIGURE 4

Case 1

$$w_{11} = \frac{M}{2D} x(x-a) = \sum_{m=1,3}^{\infty} -\frac{4a^2 M}{m^3 \pi^3 D} \sin \frac{m\pi x}{a}$$

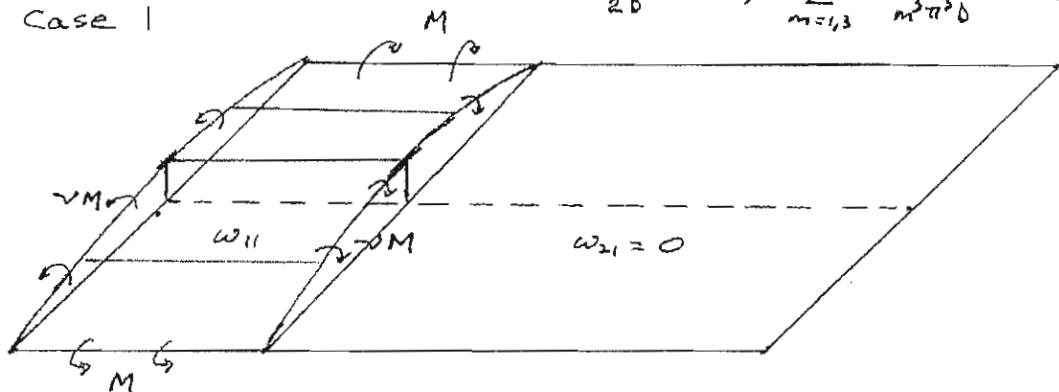


FIGURE 5(a)

$$w_{12} = \sum_{m=1,3}^{\infty} \frac{4a^2 M}{m^3 \pi^3 D} F_{1/3m}^{*1}(x,y)$$

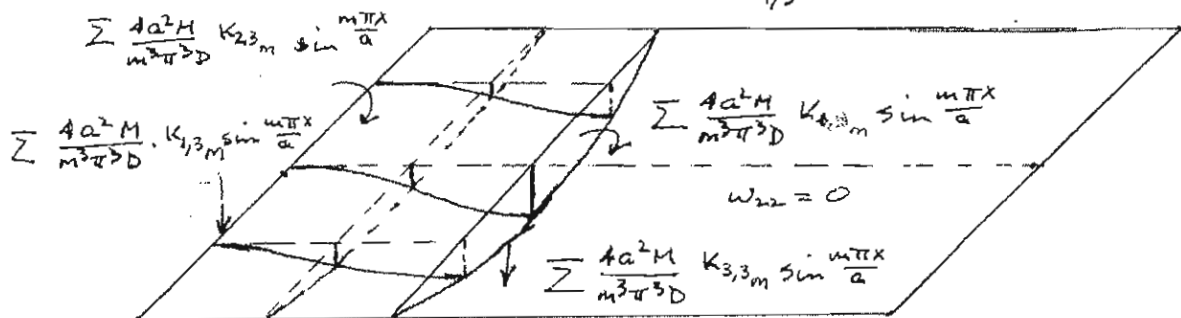


FIGURE 5(b)



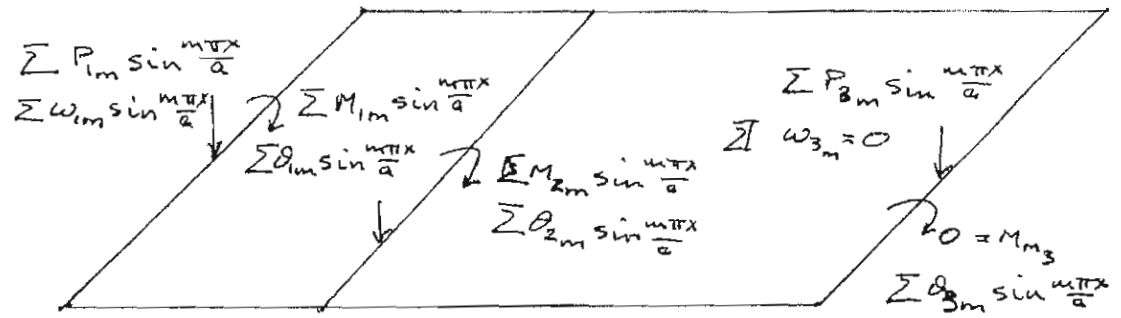


FIGURE 5(c)

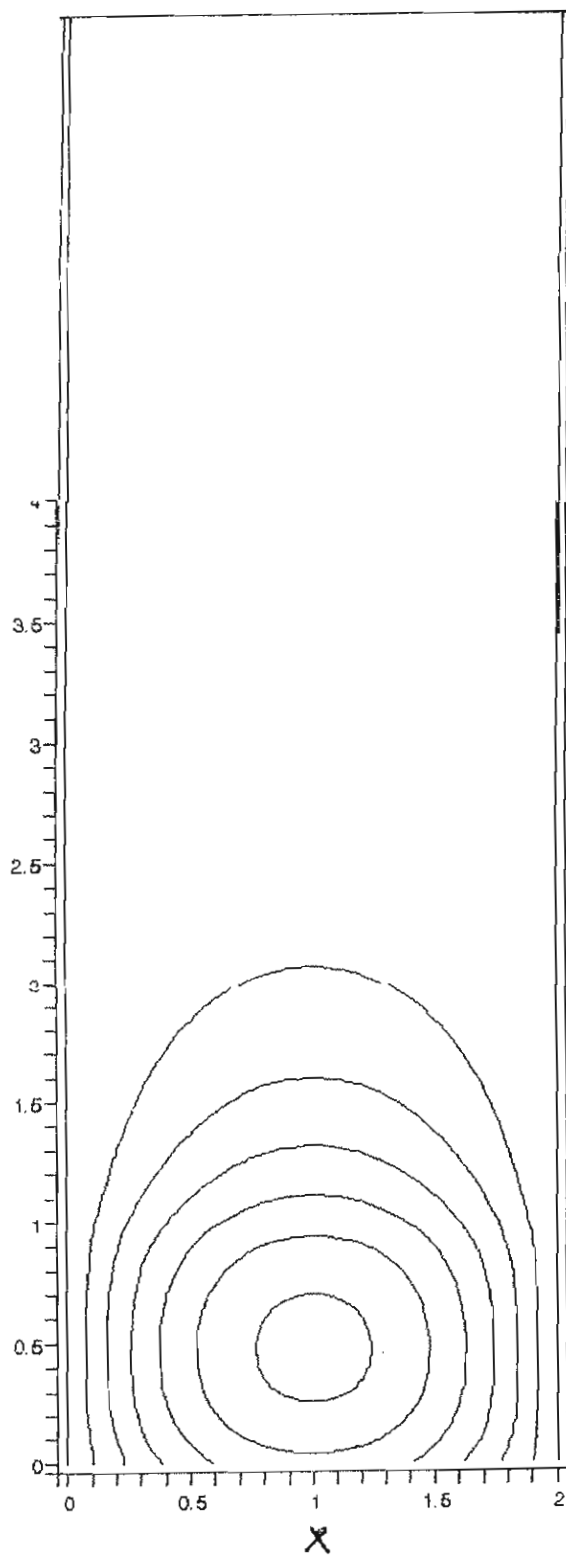


FIGURE 6

$$b_1 = 1 \text{ m}$$

## THE CASE FOR SHOT PEENING

The following are thoughts on the likely cause of distortion of steel plates in the bullet traps in two indoor [REDACTED]

The distortion of plates in the bullet traps could be due to temperature effects, plastic shear flow in the direction of impact or shot peening effects resulting from compression yielding due to the normal component of interaction during impact. [REDACTED]

[REDACTED] As the distortion of the lower plates is greatest near the throat of the bullet trap, and in the central 8 of 10 plates where the greatest intensity of impact occurs, and there are still gaps between plates, it is felt that distortion due to ambient temperature variations may be discarded.

A temporary rise in plate temperature caused by impact may be an issue and is considered later in this paper.

A theoretical investigation to show that shear deformation in the direction of impact causes plate curvature was attempted. The writer could not show that shear deformation had any effect on curvature.

### Shot peening

The effect of the normal component of interaction is considered to be the likely cause of the permanent deformation. As the determination of normal and shear stresses arising during impact is beyond the scope of this investigation, and is in any case probably not warranted, normal and tangential impulses during impact are considered to gain some idea of what is the likely cause of the permanent deformation. An impulse is the integral of the interaction force during the time of impact.

Refer to Figure 1. A projectile of mass  $m$  and velocity  $v_1$  impacts on a steel plate at an angle  $\phi$  to the horizontal and is deflected due to interactions  $F_n(t)$  and  $F_t(t)$ , and has a

velocity  $v_2$  after impact. The following equations arise:

$$mv_1 \sin \phi = \int F_n(t) dt = I_n$$

$$mv_1 \cos \phi - mv_2 = \int F_t(t) dt = I_t$$

In these equations,  $m$ ,  $v_1$  and  $\phi$  are known, but  $v_2$  and hence  $I_t$  are unknown.  $\phi = 18^\circ$  for the lower plate and  $\phi = 12^\circ$  for the upper plate.

For the sake of this discussion let  $F_n(t)$  and  $F_t(t)$  be related by a kinetic friction coefficient such that

$$F_t(t) = \mu F_n(t)$$

and hence

$$I_t = \mu I_n$$

It is stressed that  $\mu$  is not known, and would in fact itself be a function of time. The kinetic coefficient of friction between lead and mild steel is given in one table as 0.95 which is higher than a value I gave during the meeting on 05/07/2012.

The purpose of the ballistic pendulum test is to determine the relationship experimentally. Friction in the bearings made this impossible in the original equipment, which is being rebuilt using a knife edge for a pivot, which may provide satisfactory information. The maximum values  $F_t(t)$  and  $F_n(t)$  are not known, although a rough estimate of the maximum value of  $F_n(t)$  may be obtained as the duration of the impact could be estimated knowing the initial velocity  $v_1$ , and the length of the projectile. This still does not give the normal stress as contact area is not known, and so is not considered further.

However, assume that a critical normal impulse, say  $I_n^*$ , is required to cause any yielding of the plate surface. Shot preening is also cumulative, probably up to a point where plastic deformation has reached a certain depth, and impacts have reached a certain intensity measured in impacts per square metre.

The observed deformation is consistent with shot preening effects in the following ways.

1. Deformation is greatest in the lower plates nearest the throat of the bullet trap. Visual inspection shows this is the zone where the highest intensity of impacts occurs. This is also consistent with the target heights used during training. The two extreme plates are not distorted significantly. These plates corresponding to outer lanes have less use and hence lower intensity of impacts than the other lanes.
2. The upper plates show no sign of deformation due to projectile impact. Thus it would appear that the impulse when  $\phi = 12^\circ$  is below the critical level  $I_n^*$  required to cause yielding.
3. The tangential impulse is not known but yielding in shear in the direction of the impact does not appear to cause curvature of the plates.
4. Uniform shot peening on the surface of an unsupported plate causes the plate to deform to a spherical surface. It is shown below that based on observed failures and impairment of some connections the deformation of the plates is consistent with shot peening over a portion of each plate near the throat of the bullet trap.

#### Theoretical considerations

A plate with boundary supports similar to those found on the central eight plates in the XXXX range subjected to shot peening effects over a portion of the plate was analysed to estimate the deflected shape. It is stressed that magnitudes of the displacements were not determined, but only the form of the deformation. Each plate was initially supported on the edges in a manner which may be approximated as simple supports, that is with zero lateral displacement and normal moment. Some support was provided on the centreline of the plate. At the throat of the bullet trap, the connections at the midpoint of the plates had all suffered some impairment or failure, and the observed deformation of the central plates suggests limited or zero constraint is now provided by the original connections. The writer does not know if there are other connections on those edges, but assumes there are none. Hence an analysis was carried out on a single plate using thin plate theory with simply supported boundary conditions on three sides, and a free edge on the short side

near the throat of the bullet trap. Uniform shot peening was considered on a rectangular section corresponding to the full width of the plate, but extending for a limited distance only from the free edge. Details of the analysis are lengthy, with the extensive algebra and final numerical results being carried out using the symbolic language MAPLE.

To summarise, the peened section undergoing plastic deformation was prevented from expansion by the application of hypothetical in-plane forces. Equal and opposite forces were then applied, which are replaced by statically equivalent forces and normal moments around the boundary of the peened section at the middle surface of the plate. The in-plane force is then discarded as flexural deformation dominates. Details of the analysis are available, but only contours of the deflected shape are presented here. The plate analysed was taken as 5 m long by 2 m wide and peening was considered to be uniform on a 1 m length of plate in one case and a 2 m length in the second case. Poissons ratio  $\nu = 0.3$ . The form of the deflection only was investigated, as the writer had no idea of the actual depth of peening, nor the compressive stresses which may have been induced by the impacts. For the record however, values used were  $M = 1$  and  $D = 1$ .

Contours of the deflected shape are shown in Figures 2(a) and 2(b). With the dimensions and values of  $M$  and  $D$  considered, the maximum deflection was about 0.4 m, but again it is stressed that this value is meaningless, but is noted here in case a finite element analysis should be performed as a check of these calculations.

### **Temperature due to impact**

The following is included as a situation that could lead to the observed deformation, although it is not considered to be the cause. Although photographs of failed connections have been provided, the cause of failure considered in this brief section can be easily discarded by a simple check of the failed connections on plate centrelines at the throat.

If rapid fire with high intensity of impacts occurred near the throat, and caused a high rise in temperature, expansion of the plates could conceivably cause the plates to buckle upwards near the throat. It is unlikely this could cause the connections to fail, but if they

did, and failed in such a manner that on cooling, the connection maintained the deflected shape at the centre of the plate the resulting deflection would be of the form shown in Figure 3. This is consistent with the observed deformation. Hence the form of connection failure at these locations should be reviewed.

It is stressed that this is not considered the likely cause of plate deformation, as the effect would have occurred immediately the use of high velocity rounds were introduced, which does not appear to have occurred. Depending on the connections on the upper plates, this effect would also have distorted the upper plates, which has not occurred, although as these plates are at 12° rather than 18° heating would presumably be less than the lower plates.

A further reason for reviewing the connections is to check if there are connections along the full length of the plate centrelines.

### Discussion

The deflected shapes determined by considering shot peening in zones of maximum intensity of impact are similar to the observed deformation of the heavily impacted plates. This supports other observations favouring shot peening as the cause of the deformation.

### Influence of plate thickness

A simplified analysis of shot peening that must be checked in the literature suggests that the curvature  $\frac{1}{R}$  due to a certain level of peening on a plate is proportional to  $\frac{1}{h^2}$  where  $h$  is the plate thickness. Thus if this simplified analysis is a reasonable approximation, comparing the deflections of a 10 mm plate ( $d_{10}$ ) with an 8 mm plate ( $d_8$ ) and 12 mm plate ( $d_{12}$ ) we find

$$\frac{d_8}{d_{10}} = \frac{10^2}{8^2} = 1.56$$

$$\frac{d_{12}}{d_{10}} = \frac{10^2}{12^2} = 0.69$$

This observation requires discussion, as increasing the thickness from the present 10 mm to 12 mm leads to a considerable reduction of displacement following the same number of

impacts, with an expected increase in life of the structure, if shot peening is the cause of the permanent deformation.

Bruce Golley



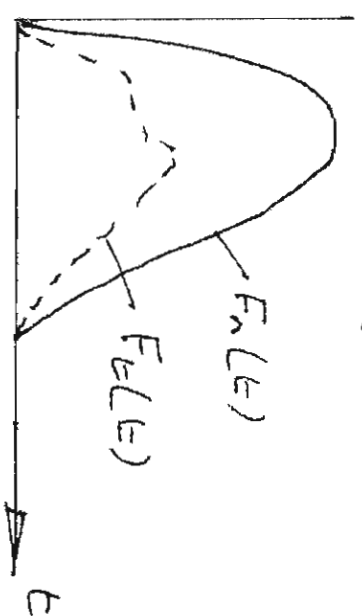
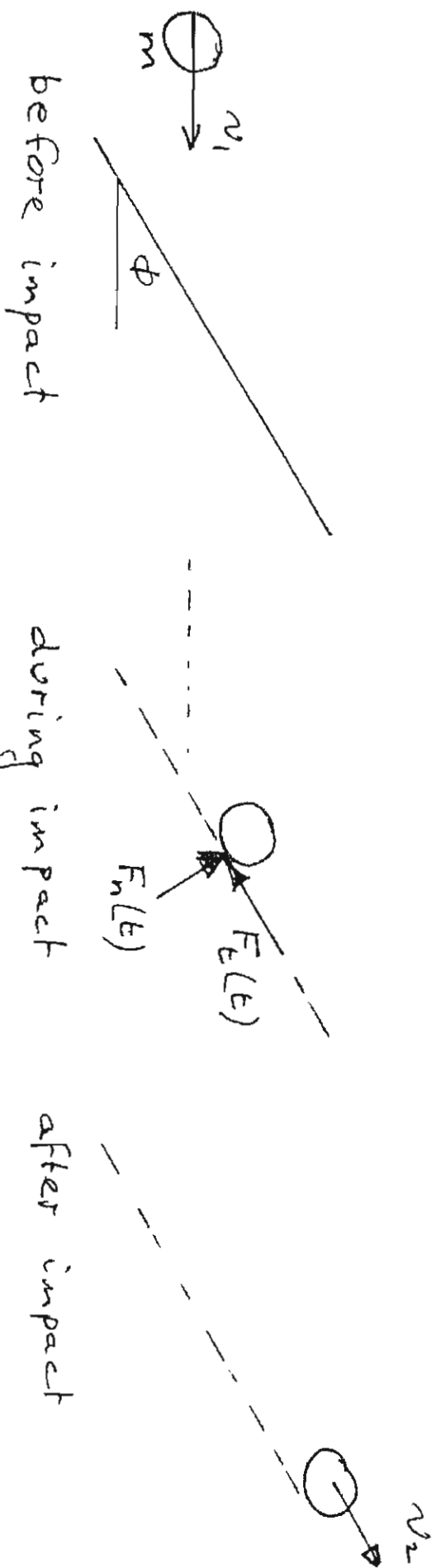


FIGURE 1

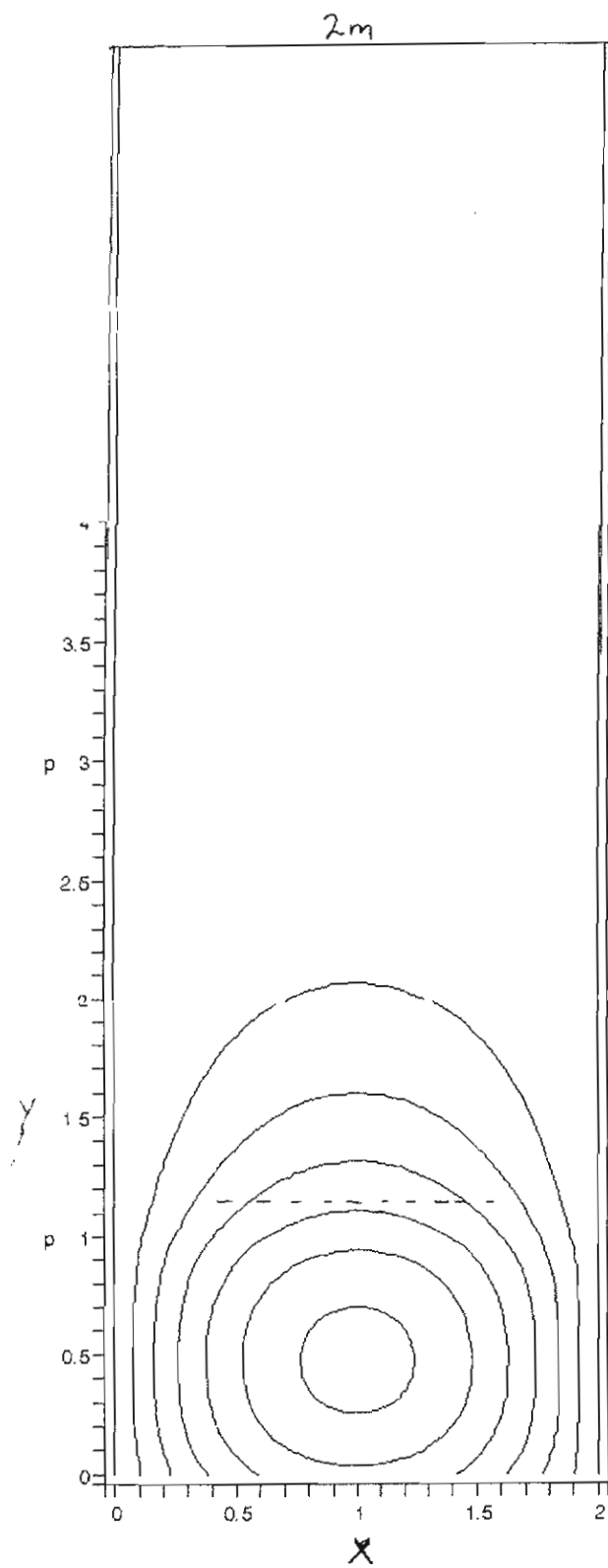


FIGURE 2(a)

$$b_1 = 1 \text{ m}$$

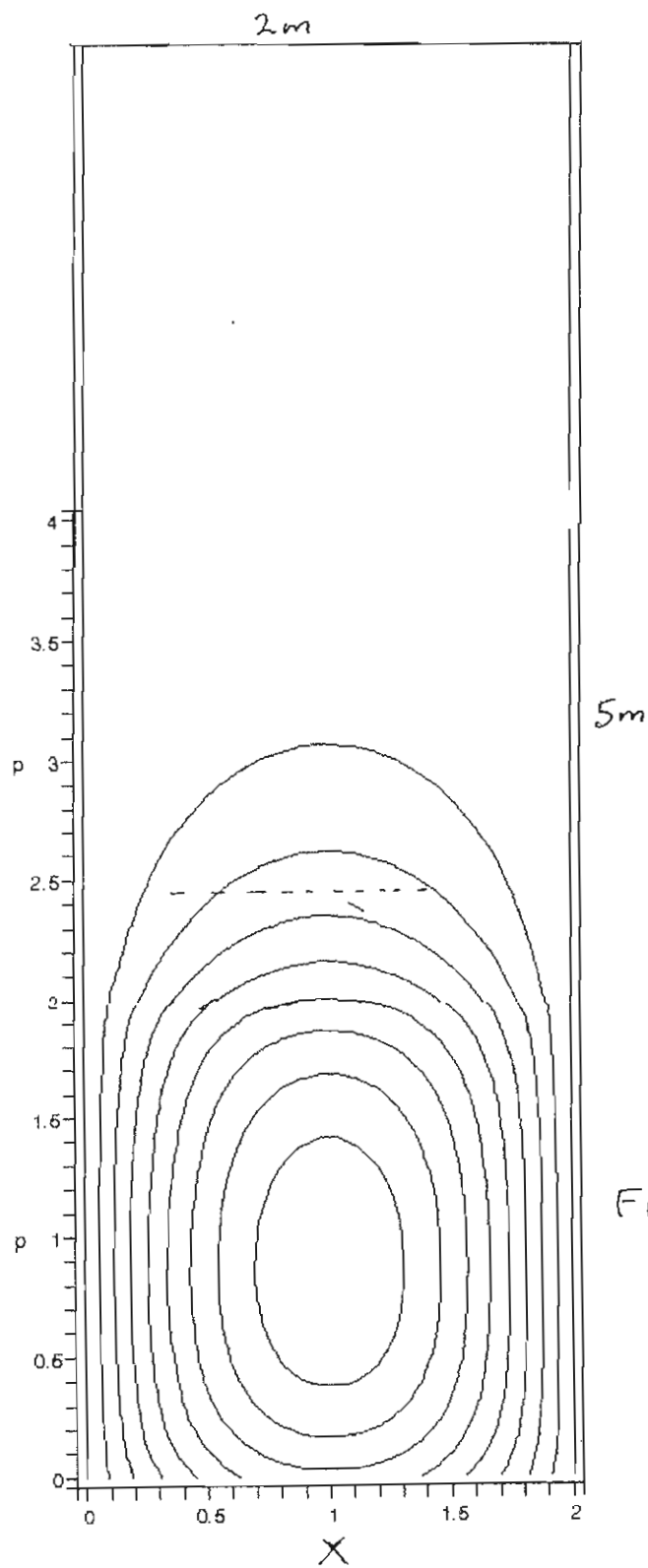


FIGURE 2(b)

$$b_1 = 2m$$

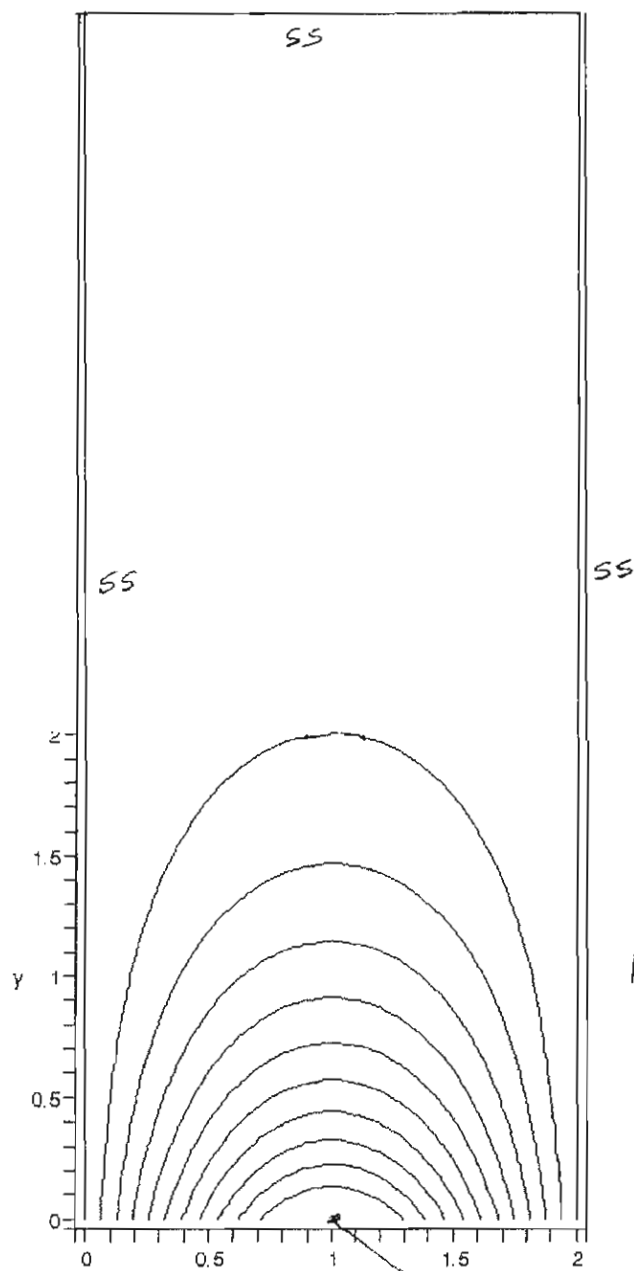


Figure 3

x

Forced displacement  
on free edge

# THE CASE FOR SHOT PEENING

Bruce Golley

The following are thoughts on the likely cause of distortion of steel plates in the bullet traps in two indoor ranges [REDACTED] The comments presented here are intended for discussion purposes only, and follow a meeting held [REDACTED] on 5 July 2012.

The distortion of plates in the bullet traps could be due to temperature effects, plastic shear flow in the direction of impact or shot peening effects resulting from compression yielding due to the normal component of interaction during impact. [REDACTED]

[REDACTED] As the distortion of the lower plates is greatest near the throat of the bullet trap, and in the central 8 of 10 plates where the greatest intensity of impact occurs, and there are still gaps between plates, it is felt that distortion due to ambient temperature variations may be discarded. Such a variation would not have caused significant distortion only in the vicinity of the throat.

A temporary rise in plate temperature caused by impact may be an issue and is considered later in this discussion paper.

A theoretical investigation to show that shear deformation in the direction of impact causes plate curvature was attempted. The writer could not show that shear deformation had any effect on curvature.

## Shot peening

The effect of the normal component of interaction is considered to be the likely cause of the permanent deformation. As the determination of normal and shear stresses arising during impact is beyond the scope of this investigation, and is in any case probably not warranted, normal and tangential impulses during impact are considered to gain some idea

of what is the likely cause of the permanent deformation. An impulse is the integral of a component of the interaction force during the time of impact.

Refer to Figure 1. A projectile of mass  $m$  and velocity of magnitude  $v_1$  impacts on a steel plate at an angle  $\phi$  to the horizontal and is deflected due to interactions  $F_n(t)$  and  $F_t(t)$ , and has a velocity of magnitude  $v_2$  after impact. Directions of  $v_1$  and  $v_2$  are shown in the figure. The following equations arise:

$$mv_1 \sin \phi = \int F_n(t) dt = I_n$$

$$mv_1 \cos \phi - mv_2 = \int F_t(t) dt = I_t$$

In these equations,  $m$ ,  $v_1$  and  $\phi$  are known, but  $v_2$  and hence  $I_t$  are unknown.  $\phi = 18^\circ$  for the lower plate and  $\phi = 12^\circ$  for the upper plate.

For the sake of this discussion let  $F_n(t)$  and  $F_t(t)$  be related by a kinetic friction coefficient such that

$$F_t(t) = \mu F_n(t)$$

and hence

$$I_t = \mu I_n$$

It is stressed that  $\mu$  is not known, and would in fact itself be a function of time. The kinetic coefficient of friction between lead and mild steel is given in one table as 0.95 which is higher than a value I gave during the meeting on 05/07/2012.

It was decided during the meeting to carry out an experiment using Bisalloy steel and M4 rounds to determine the relationship between  $I_n$  and  $I_t$ . The experiment was to be carried out using a variation of the age-old ballistic pendulum. The original ballistic pendulum apparatus was used to determine the velocity of a cannonball with the ball being fired at a wood mass which stopped the ball. In the case of the current experiment with an M4 round, the velocity  $v_1$  is simply measured using a modern instrument, but the round impacts at a shallow angle, and other information is required. The procedure is the same however, with a round being fired at an inclined plate and the angle through which the

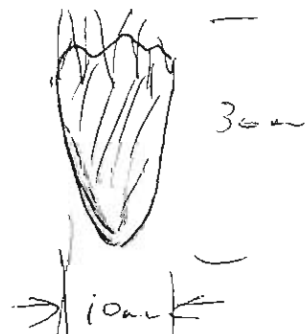
pendulum deflects enables at least in theory the information to be obtained. In the first test, friction in the bearings was excessive, and the bearings have been replaced by knife-edge supports, with tests to be conducted on 20 July 2012. The following comments are therefore premature, but are ideas for further discussion.

The maximum values  $F_t(t)$  and  $F_n(t)$  are not known, although a rough estimate of the maximum value of  $F_n(t)$  may be obtained as the duration of the impact could be estimated knowing the initial velocity  $v_1$ , and the length of the projectile. This still does not give the normal stress as contact area is not known, and so is not considered further.

However, assume that a critical normal impulse, say  $I_n^*$ , is required to cause any yielding of the plate surface. Shot preening is also cumulative, probably up to a point where plastic deformation has reached a certain depth, and impacts have reached a certain intensity measured in impacts per square metre.


The observed deformation is consistent with shot preening effects in the following ways.

1. Deformation is greatest in the lower plates nearest the throat of the bullet trap. Visual inspection shows this is the zone where the highest intensity of impacts occurs. This is also consistent with the target heights used during training. The two extreme plates are not distorted significantly. These plates, corresponding to outer lanes, have less use and hence lower intensity of impacts than the other lanes.
2. The upper plates show no sign of deformation due to projectile impact. Thus it would appear that the impulse when  $\phi = 12^\circ$  is below the critical level  $I_n^*$  required to cause yielding. The normal impulse  $I_n$  is proportional to  $\sin \phi$ , and is therefore about 1.5 times greater in the lower plates than the upper plates.
3. The tangential impulse is not known but the writer cannot show that yielding in shear in the direction of the impact causes curvature of the plates. This aspect requires further discussion.
4. Uniform shot preening on the surface of an unsupported plate causes the plate to deform to a spherical surface. It is shown below that based on observed failures and impairment



of some connections the deformation of the plates is consistent with shot peening over a portion of each plate near the throat of the bullet trap.

### Theoretical considerations

A plate with boundary supports similar to those found on the central eight plates in the  range subjected to shot peening effects over a portion of the plate was analysed to estimate the deflected shape. It is stressed that magnitudes of the displacements were not determined, but only the form of the deformation. Each plate was initially supported on the edges in a manner which may be approximated as simple supports, that is with zero lateral displacement and normal moment. Some support was provided on the centreline of the plate but the number of connections was not known, although the survey showed a number had failed. At the short edges of the plates at the throat of the bullet trap, the connections at the midpoints had all suffered some impairment or failure, and the observed deformation of the central plates suggests limited or zero constraint is now provided by the original connections. The writer does not know if there are other connections on those edges, but assumes there are none. Hence an analysis was carried out on a single plate using thin plate theory with simply supported boundary conditions on three sides, and a free edge on the short side near the throat of the bullet trap. Any connections along the plate centrelines were ignored. Uniform shot peening was considered on a rectangular section corresponding to the full width of the plate, but extending for a limited distance only from the free edge. Details of the analysis are lengthy, with the extensive algebra and final numerical results being carried out using the symbolic language MAPLE.

To summarise, the peened section undergoing assumed plastic deformation was prevented from expansion by the application of hypothetical in-plane forces. Equal and opposite forces were then applied, which were replaced by statically equivalent forces and normal moments around the boundary of the peened section at the middle surface of the plate. The in-plane force is then discarded as flexural deformation dominates. Details of the analysis are available, but only contours of the deflected shape are presented here. The



plate analysed was taken as 5 m long by 2 m wide and peening was considered to be uniform on a 1 m length of plate in one case and a 2 m length in the second case. Poissons ratio  $\nu = 0.3$ . The form of the deflection only was investigated, as the writer had no idea of the actual depth of possible peening, nor the compressive stresses which may have been induced by the impacts. For the record however, values used were  $M = 1$  and  $D = 1$ .

Contours of the deflected shape are shown in Figures 2(a) and 2(b). With the dimensions and values of  $M$  and  $D$  considered, the maximum deflection was about 0.4 m, but again it is stressed that this value is meaningless, but is noted here in case a finite element analysis should be performed as a check of these calculations.

### Temperature due to impact

The following is included as a situation that could lead to the observed deformation, although it is not considered to be the cause. Although photographs of failed connections have been provided, the cause of failure considered in this brief section can be easily discarded by a simple check of the failed connections on plate centrelines at the throat.

If rapid fire with high intensity of impacts occurred near the throat, and caused a high rise in temperature, expansion of the plates could conceivably cause the plates to buckle upwards near the throat. It is unlikely this could cause the connections to fail, but if they did, and failed in such a manner that on cooling, the connection maintained the deflected shape at the centre of the plate the resulting deflection would be of the form shown in Figure 3. This is consistent with the observed deformation. Hence the form of connection failure at these locations should be reviewed.

It is stressed that this is not considered the likely cause of plate deformation, as the effect would have occurred immediately the use of high velocity rounds were introduced, which does not appear to have occurred. Depending on the connections on the upper plates, this effect would also have distorted the upper plates, which has not occurred, although as these plates are at  $12^\circ$  rather than  $18^\circ$  heating would presumably be less than the lower plates.

A further reason for reviewing the connections is to check if there are connections along the full length of the plate centrelines.

### Discussion

The deflected shapes determined by considering shot peening in zones of maximum intensity of impact are similar to the observed deformation of the heavily impacted plates. This supports other observations favouring shot peening as the cause of the deformation.

### Influence of plate thickness

The curvature  $\frac{1}{R}$ , and hence relative displacements, of a plate uniformly peened on one face is proportional to  $\frac{1}{h^2}$  where  $h$  is the plate thickness. Thus comparing the deflections of a 10 mm plate ( $d_{10}$ ) with an 8 mm plate ( $d_8$ ) and 12 mm plate ( $d_{12}$ ) we find

$$\frac{d_8}{d_{10}} = \frac{10^2}{8^2} = 1.56$$

$$\frac{d_{12}}{d_{10}} = \frac{10^2}{12^2} = 0.69$$

This observation requires discussion, as increasing the thickness from the present 10 mm to 12 mm leads to a considerable reduction of displacement following the same number of impacts, with an expected increase in life of the structure, if shot peening is the cause of the permanent deformation.

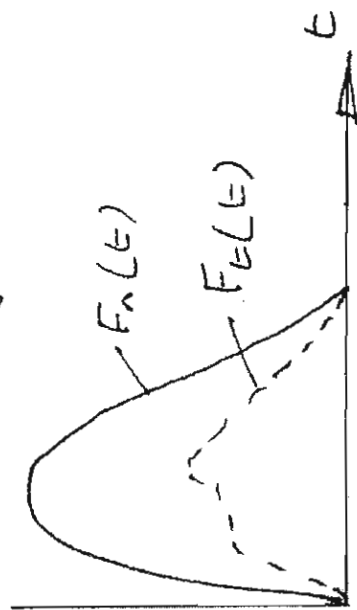
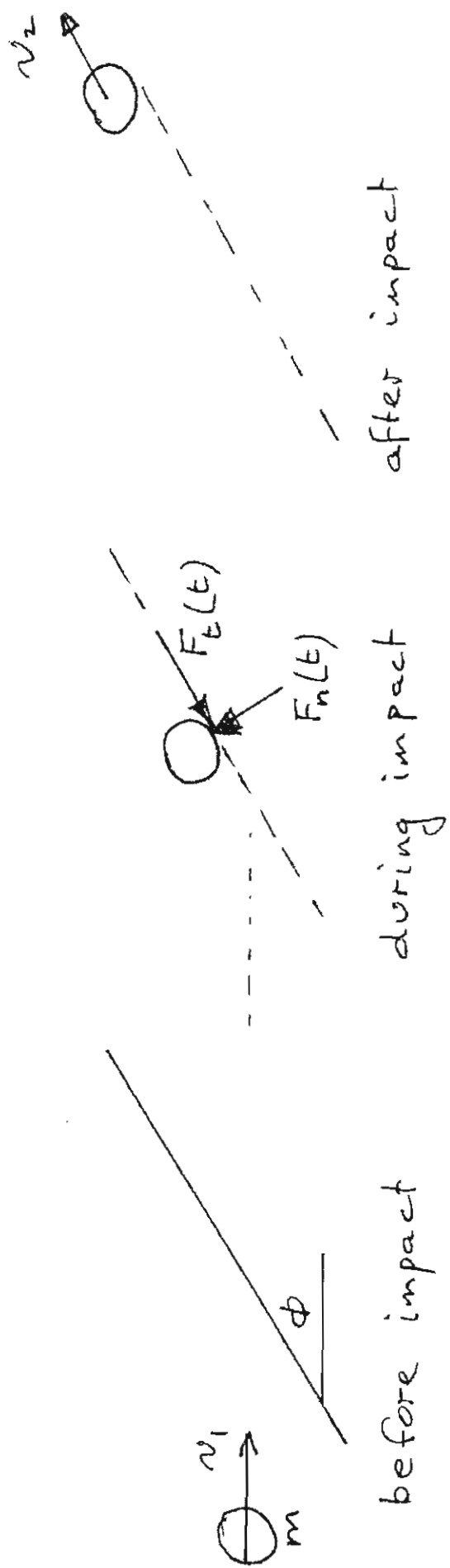


FIGURE 1

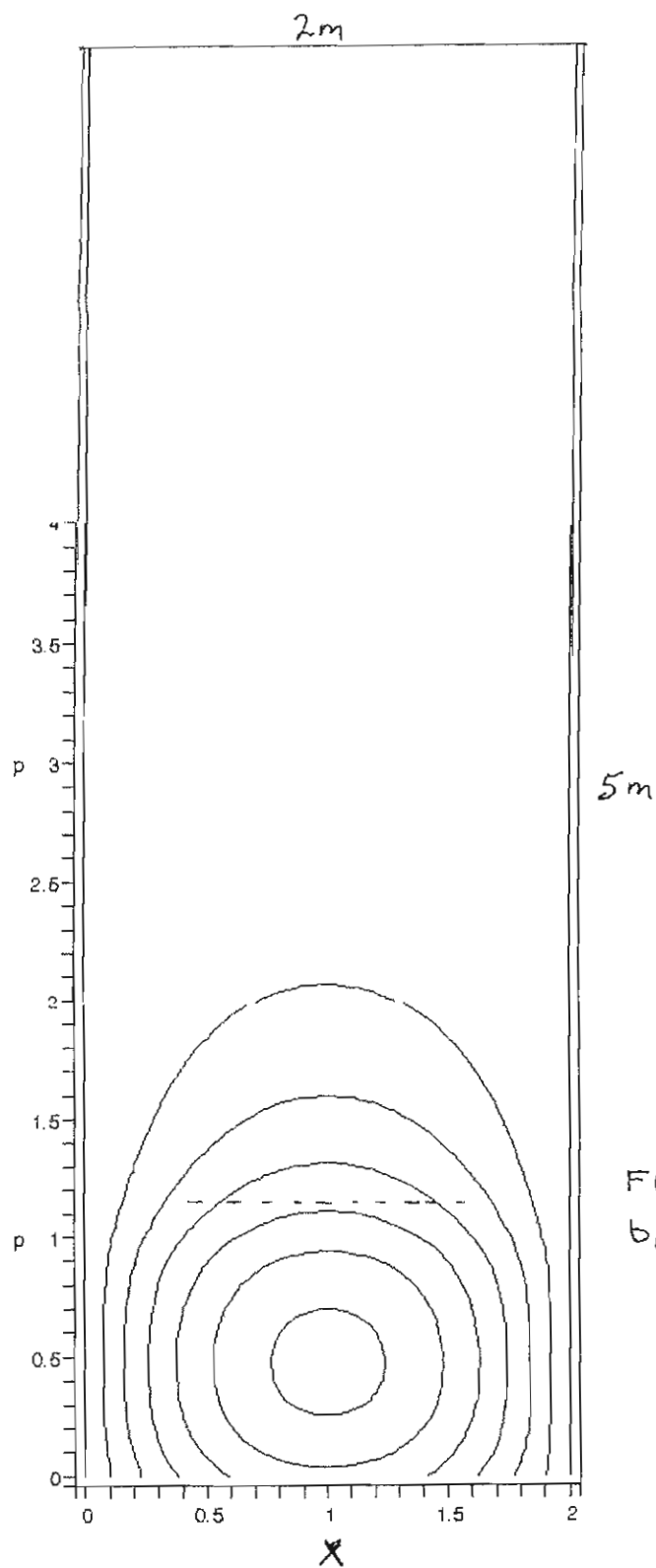


FIGURE 2(a)  
 $b_1 = 1 \text{ m}$

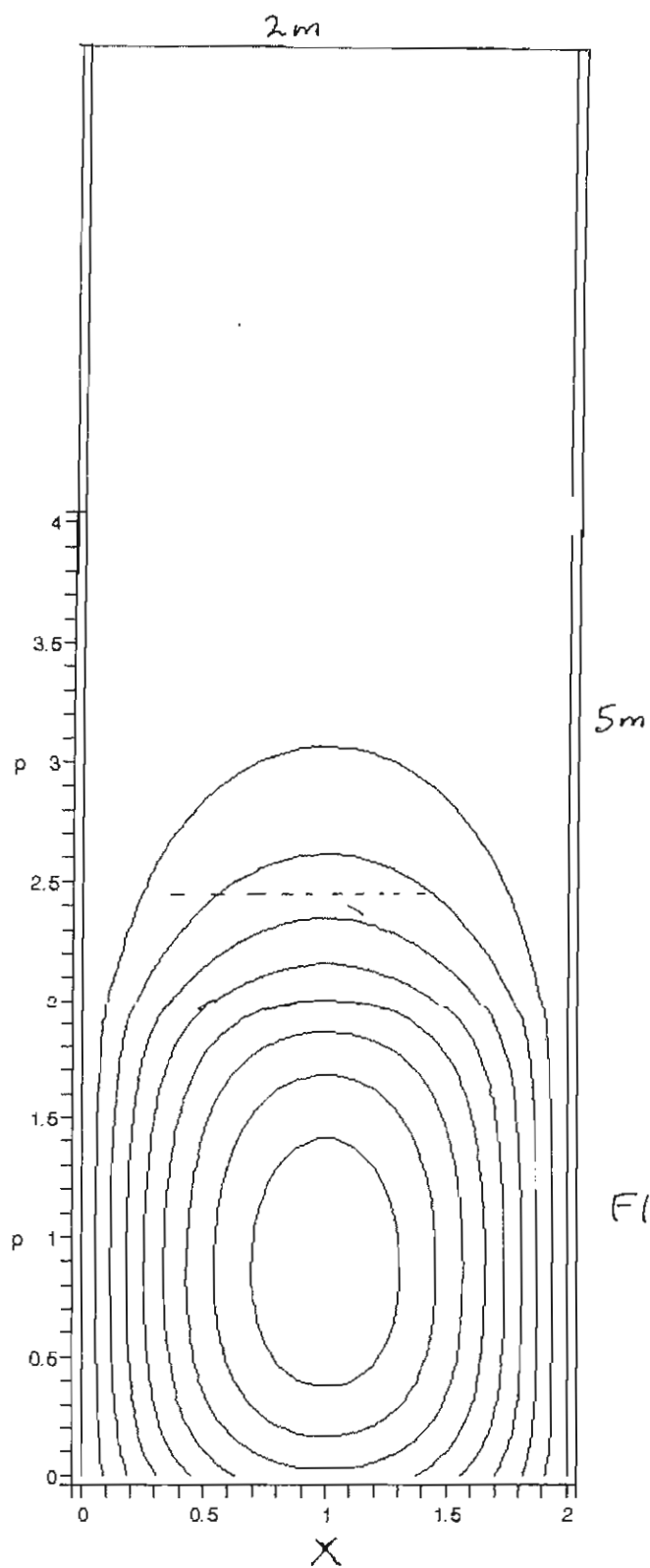


FIGURE 2(b)  
 $b_1 = 2m$

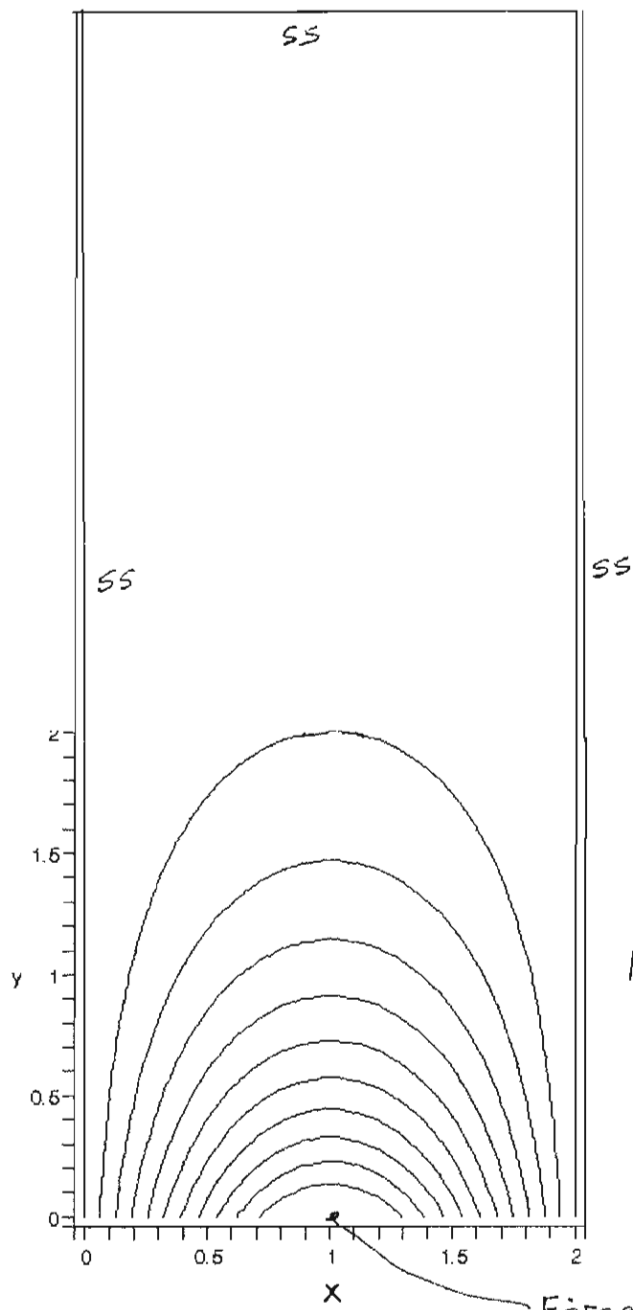


Figure 3

Forced displacement  
on free edge

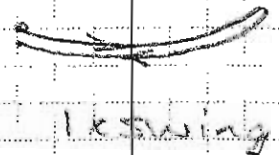
F2331

Client:			Date: 20/7/12
Project/Job: 270°/360° RANGL ESCALATOR TRAP	Job No:	Sheet No: 1	
Subject: BALLISTIC PENDULUM			By: P.B.H

## BALLISTIC PENDULUM TEST RESULTS

### PERIOD MEASUREMENT (Pendulum displaced 10°)

Dist of CG from Fulcrum	Time for 10x Swings
24 (30-6)	1' 46"
54 (60-6)	1' 12"
94 (90-6)	58"
114 (120-6)	50"



### BALLISTIC MEASUREMENT

Angle of Impact Plate (Degrees) (θ)	Dist of CG from Fulcrum (mm)	Horizontal Displacement (mm)	Dist of Proj Impact from Centre of Impact Plate (mm)	BC - Below Centre AC - Above Centre
12.5°	24	230 260 260	50 (BC) 55 (BC) 50 (BC)	
19°	24	340 340 310	Centre 15 (BC) 10 (AC)	SUSPECT
25°	24	550 520 550	15 (BC) Centre Centre	
12.5°	54	195 195 210	Centre Centre 30 (BC)	
19°	54	305 305 310	10 (BC) Centre 20 (BC)	
25°	54	430 430 420	40 (BC) Centre Centre	

Client:			Date: 20/7/12
Project/Job: 270°/360° RANGE ESCALATOR TRAP	Job No:	Sheet No: 2	
Subject: BALLISTIC PENDULUM			By: B.B.H

## AMMUNITION INFORMATION

Ammunition - Winchester 5.56mm 55gr Soft Point

Wt of 5x Projectiles - 275.2 grains

Velocity

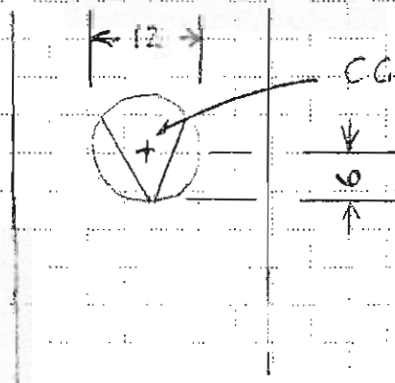
Shot No.	Velocity (fps)
1	2,784
2	2,792
3	2,829
4	2,802
5	2,782

## PENDULUM INFORMATION

1. Wt - 3.95 kg

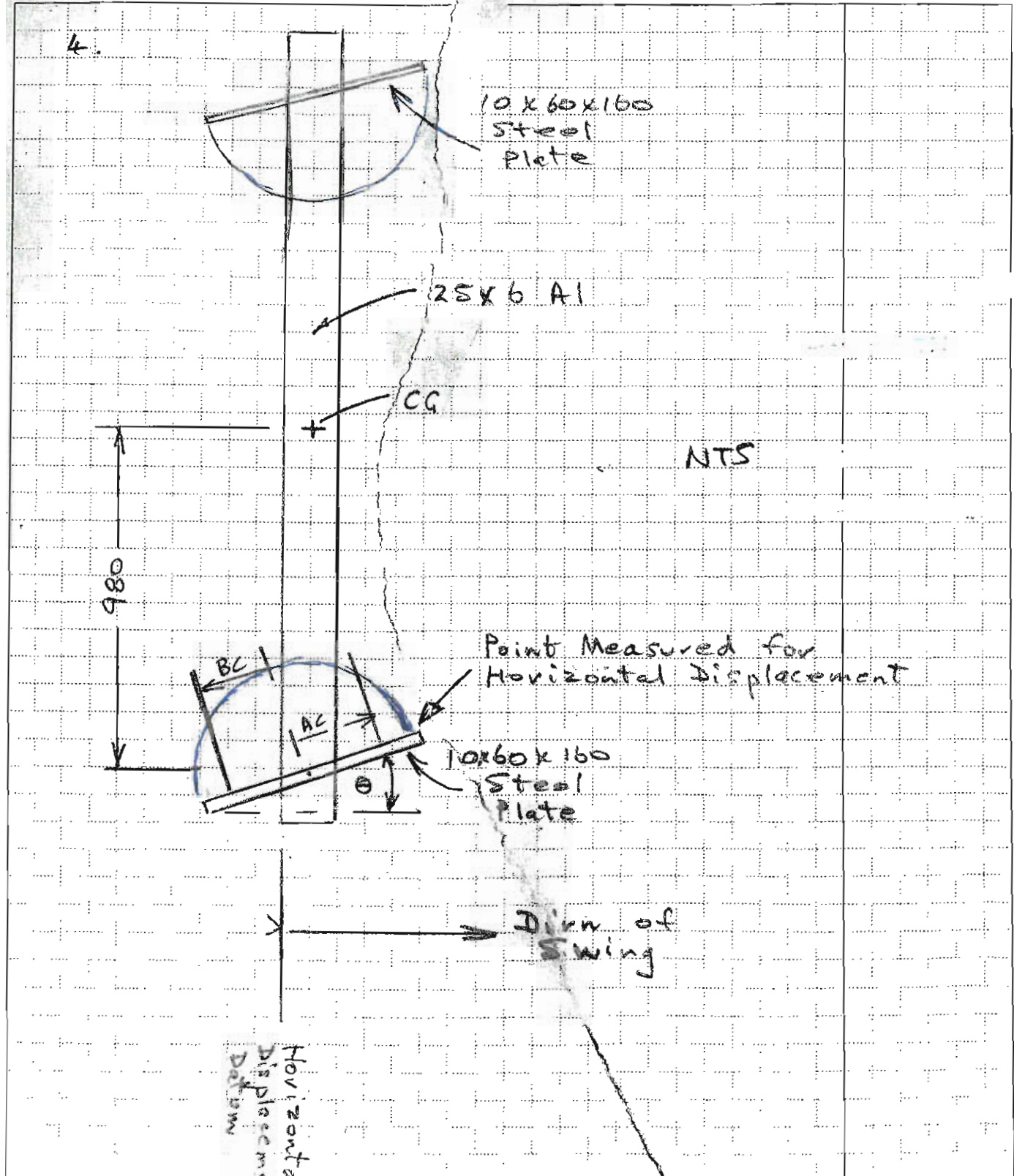
2. CG:- CG of Mass coincides with Geometric CG ( $\pm 1mm$ )

3. Dist of Fulcrum below CG - 6mm

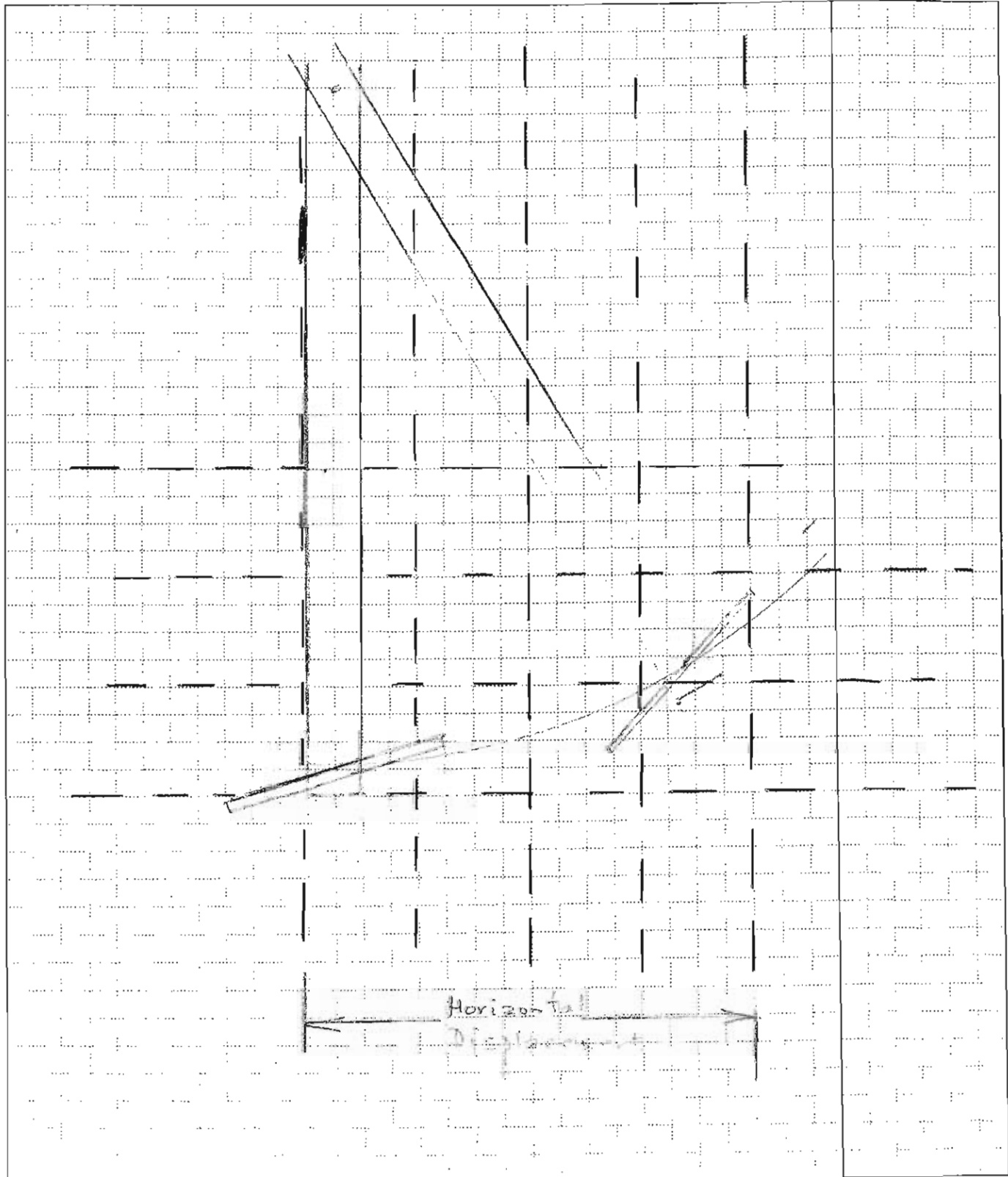




Client:		Date: 20/7/12
Project/Job: 270°/360° ESCALATOR TRAP	Job No:	Sheet No: 3
Subject: BALLISTIC PENDULUM		By: B.B.H



Client:			Date: 20/7/12
Project/Job: 22.0/12 ESCALATOR 7110	Job No:	Sheet No: 26	
Subject: BALLISTIC PENDULUM			By: B B H

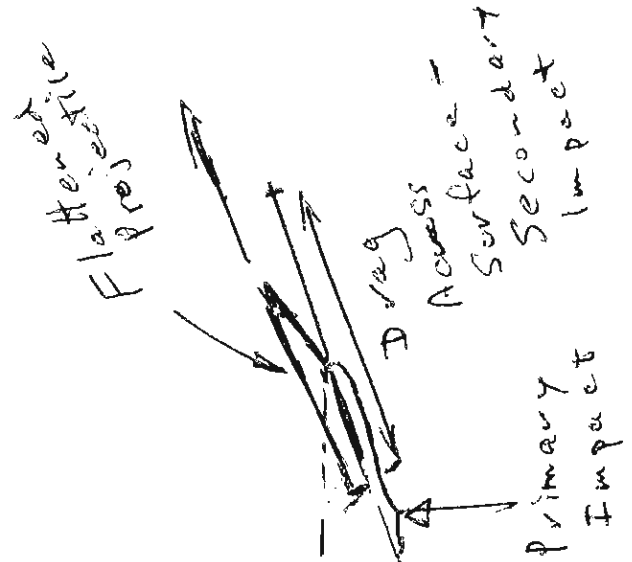
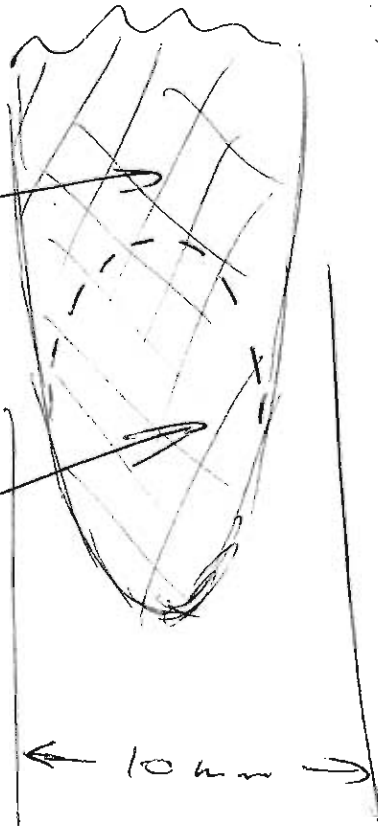


Dirn of  
Projectile  
Travel



Secondary  
Impact  
(Drag) Area

Primary  
Impact  
Area



# BALLISTIC PENDULUM EXPERIMENT

Bruce Golley

## Summary

The material presented here is a collection of equations used in the ballistic pendulum experiment, results of the first tests carried out on 17 July by Major Bruce Hughes, a discussion of those results and ideas for further discussion. The document does not need to be read in full, as many of the equations are simply for the benefit of the writer, who wanted to have the equations in a suitable form for later application if required. Hence the document may appear somewhat rambling.

Many of the equations developed herein were used to design the ballistic pendulum experiment, and are not used in analysing results. They are used to provide a check against experimental values.

## Plate and bar properties about their centres of gravity

The dimensions and  $z$  axis are shown in Figure 1.

$$\text{density of plate material} = \rho_p$$

$$\text{density of bar material} = \rho_b$$

$$\text{mass of plate} = M^* = \rho_p b h t \quad (1)$$

$$\text{moment of inertia of plate} = I_z^* = M^* \left( \frac{h^2}{12} + \frac{t^2}{12} \right) \quad (2)$$

$$\text{mass of bar} = m^* = \rho_b L A \quad (3)$$

$$\text{moment of inertia of bar} = I_z^* = \frac{m^* L^2}{12} \quad (4)$$

### Pendulum properties

The dimensions used in the following formulas are shown in Figure 2. Also note the impacted plate is an angle  $\phi$  to the horizontal or  $x$  axis.

$$\text{mass of pendulum} = M = 2M^* + 2m^* \quad (5)$$

$$\text{moment of inertia about G} = I_G = 2M^*\left(\frac{h^2}{12} + \frac{t^2}{12}\right) + 2M^*\left(\frac{L}{2}\right)^2 + 2\left(\frac{m^*L^2}{12}\right) \quad (6)$$

$$\text{radius of gyration about G} = k_G = \sqrt{\frac{I_G}{M}} \quad (7)$$

$$\text{moment of inertia about O} = I_O = I_G + 2M^*l^2 + 2m^*l^2 = I_G + Ml^2 \quad (8)$$

$$\text{radius of gyration about O} = k_O = \sqrt{\frac{I_O}{M}} \quad (8)$$

$$R = \frac{L}{2} + l + \frac{t}{2} \cos \phi \quad (10)$$

$$\text{period of vibration} = T = 2\pi\sqrt{\frac{I_O}{Mgl}} = 2\pi\sqrt{\frac{I_G + Ml^2}{Mgl}} = 2\pi\sqrt{\frac{\frac{k_G^2}{l} + l}{g}} \quad (11)$$

### Projectile impact

Refer to Figure 3. A projectile with initial velocity of magnitude  $v_1$  impacts a plate at an angle  $\phi$  shown. Interface forces  $F_n(t)$  and  $F_t(t)$  act on the projectile, which has a final velocity of magnitude  $v_2$ . With the bullet trap,  $v_2$  is always positive, and is in fact a high proportion of  $v_1$ . However for  $\phi$  close to  $90^\circ$  with low velocity projectiles and very high strength steel  $v_2$  may be zero. For completeness, the two possible interaction force-time cases are shown in the figure.

As  $I$  is used for mass moment of inertia, for convenience impulse is also used with the same letter, but in boldface, namely **I**.

$$mv_1 \sin \phi = \int F_n(t) dt = \mathbf{I}_n \quad (12)$$

$$mv_1 \cos \phi - mv_2 = \int F_t(t) dt = \mathbf{I}_t \quad (13)$$

$$\begin{aligned}
\mathbf{I}_x &= \mathbf{I}_t \cos \phi + \mathbf{I}_n \sin \phi \\
&= (mv_1 \cos \phi - mv_2) \cos \phi + mv_1 \sin \phi \sin \phi \\
&= mv_1 - mv_2 \cos \phi \quad \text{as expected}
\end{aligned} \tag{14}$$

$$\begin{aligned}
\mathbf{I}_y &= -\mathbf{I}_t \sin \phi + \mathbf{I}_n \cos \phi \\
&= -(mv_1 \cos \phi - mv_2) \sin \phi + mv_1 \sin \phi \cos \phi \\
&= mv_2 \sin \phi \quad \text{as expected}
\end{aligned} \tag{15}$$

Also

$$\mathbf{I}_t = \mathbf{I}_x \cos \phi - \mathbf{I}_y \sin \phi \tag{16}$$

$$\mathbf{I}_n = \mathbf{I}_x \sin \phi + \mathbf{I}_y \cos \phi \tag{17}$$

Determine  $\mathbf{I}_x$  using a ballistic pendulum. Consider the schematic diagram shown in Figure 4.  $O$  is the pivot point and  $G$  is the centre of gravity of the pendulum. The projectile of mass  $m$  with velocity  $v_1$  impacts the pendulum. The component of the interactive force in the  $x$  direction is  $F_x(t)$ .

$$\text{mass} = M$$

$$\text{mass moment of inertia about } O = I_O = Mk_O^2$$

$$\text{radius of gyration about } O = k_O$$

$$\text{rotation} = \theta = \theta(t)$$

$$\text{angular velocity} = \dot{\theta} = \omega(t)$$

A dot denotes differentiation with respect to time  $t$ . The projectile does not adhere to the pendulum after impact.

$$\text{torque about } O = RF_x(t) = I_O \ddot{\theta} = I_O \dot{\omega} = \frac{d\omega}{dt} \tag{18}$$

$$d\omega = \frac{R}{I_O} F_x(t) dt \tag{19}$$

Therefore

$$\omega_0 = \frac{R}{I_O} \int F_x(t) dt = \frac{R}{I_O} \mathbf{I}_x \quad (20)$$

where  $\omega_0$  is the angular velocity immediately following impact. In our case as noted earlier

$$\mathbf{I}_x = mv_1 - mv_2 \cos \phi \quad (14)$$

Now equate the kinetic energy of the pendulum immediately following impact with the maximum potential energy of the pendulum. See Figure 5.

distance from pivot O to G =  $l$

$$\frac{1}{2} I_O \omega_0^2 = Mgl(1 - \cos \theta_1) \quad (21)$$

where  $\theta_1$  is the maximum angle of  $\theta$  and  $g$  is the gravitational acceleration. Therefore

$$\frac{1}{2} I_O \left( \frac{R}{I_O} \mathbf{I}_x \right)^2 = Mgl(1 - \cos \theta_1) \quad (22)$$

from which

$$\mathbf{I}_x = \sqrt{\frac{2MglI_O(1 - \cos \theta_1)}{R^2}} \quad (23)$$

Also note the period of the pendulum,  $T$ , is

$$T = 2\pi \sqrt{\frac{I_O}{Mgl}} \quad (11)$$

giving

$$\mathbf{I}_x = \frac{MglT}{2\pi R} \sqrt{2(1 - \cos \theta_1)} \quad (24)$$

Note from the period  $T$  the moment of inertia can be determined experimentally using (11)

giving

$$I_O = \left( \frac{T}{2\pi} \right)^2 Mgl \quad (25)$$

### Experimental procedure and results

12 mm diameter holes were drilled at 30 mm centres from the centre of the pendulum. The knife edge bearings were at the bottom of the holes. Hence the distance  $l$  from the pivot to the centre of mass could be varied giving values 24 mm, 54 mm, 84 mm, 114 mm and 144 mm. The period of oscillation for various values of  $l$  was measured, giving the values in the following table.

$l$ mm	24	54	84	114
$T$ s	10.6	7.2	5.8	5.0

The mass of five projectiles was determined and averaged, the velocity of five rounds were measured and averaged and other dimensions of the completed pendulum were measured. After converting to SI units, the following values were obtained.

$M$	3.95 kg
$m$	0.003567 kg
$L$	1960 mm
$v_1$	853 m/s
$g$	9.81 m/s <sup>2</sup>

The maximum displacement  $\theta_1$  was measured by determining the maximum horizontal displacement of a point on the pendulum using lined paper and the results converted to degrees. The angle was determined for three values of  $\phi$  and two values of pendulum effective length  $l$ . Three projectiles were fired for each setting of  $\phi$  and  $l$  and the results averaged. Measured values of  $\theta_1$  and calculated values of  $\mathbf{I}_n$ ,  $\mathbf{I}_t$  and  $v_2$  using the values of  $\theta_1$  are given in the following tables.



## BALLISTIC PENDULUM EXPERIMENT

Effective pendulum length  $l = 24$  mm

$\phi$	12.5°	19°	25°
$\theta_1$	9.5°	14.6°	28.8°
$I_n$ Ns	0.66	0.99	1.28
$I_t$ Ns	0.12	0.08	0.26
$I_t/I_n$	0.18	0.08	0.20
$v_2$ m/s	799	784	699

Effective pendulum length  $l = 54$  mm

$\phi$	12.5°	19°	25°
$\theta_1$	6.3°	12.7°	20.5°
$I_n$ Ns	0.66	0.99	1.28
$I_t$ Ns	0.12	0.20	0.31
$I_t/I_n$	0.18	0.21	0.24
$v_2$ m/s	800	749	685

### Use of results

The main purpose of the experiment was to attempt to find the relationship between the normal impulse  $I_n$  and tangential impulse  $I_t$ . Although the combined effect on stresses is complicated, broadly speaking the normal impulse causes compressive stress and the tangential impulse causes shear stress.

From the above tables, it is clear that one result is in error, namely the result for  $l = 24$  mm and  $\phi = 19^\circ$ . An additional series of tests is to be performed to check this setting. From the tables, it is seen that the tangential impulse is about a fifth of the normal impulse, which was the information to be determined by the experiment.

### Some theoretical considerations

In the absence of any information, try relating the normal and tangential interactions during impact using an assumed coefficient of kinetic friction between the projectile and plate. For completeness, two cases are considered.

**Case 1** In this case,  $v_2 \geq 0$ . This is the situation in the bullet trap, where the velocity  $v_2$  is a high proportion of the initial velocity  $v_1$ . Let the normal and tangential interactions be related by

$$F_t(t) = \mu F_n(t) \quad (30)$$

where  $\mu$  is the coefficient of kinetic friction, assumed to be constant. Thus the relationship between impulses is

$$\mathbf{I}_t = \mu \mathbf{I}_n \quad (31)$$

Solving equations (12), (31), (14) and (15) for  $\mathbf{I}_n$ ,  $\mathbf{I}_x$ ,  $\mathbf{I}_y$  and  $v_2$  we obtain the relevant solutions

$$v_2 = v_1(\cos \phi - \mu \sin \phi) \quad (32)$$

$$\mathbf{I}_x = mv_1(\sin^2 \phi + \mu \cos \phi \sin \phi) \quad (33)$$

The relationship in equation (30) is only valid for  $v_2 \geq 0$ . From equation (32), this holds if

$$\cos \phi - \mu \sin \phi \geq 0 \quad (34)$$

or

$$\mu \leq \cot \phi \quad (35)$$

In the table below,  $\cot \phi$  is shown for values of  $\phi$  from  $0^\circ$  to  $90^\circ$ .

$\phi$	$10^\circ$	$20^\circ$	$30^\circ$	$40^\circ$	$50^\circ$	$60^\circ$	$70^\circ$	$80^\circ$	$90^\circ$
$\cot \phi$	5.67	2.75	1.73	1.19	0.84	0.58	0.36	0.18	0.00

Hence for example if  $\phi = 30^\circ$ ,  $\mathbf{I}_x$  obtained from equation (33) is valid if  $\mu \leq 1.73$ . If  $\mu > 1.73$ ,  $v_2 = 0$  and Case 2 applies.

**Case 2** This case is added for academic interest only, as in the bullet trap under consideration the projectiles were not stopped by the plate. In Case 2,  $v_2 = 0$  and equation (14) becomes

$$\mathbf{I}_x = mv_1 \quad (36)$$

#### Theoretical relationship between $\phi$ and $\theta_1$

Solving equation (24) for  $\theta_1$  we obtain

$$\theta_1 = \cos^{-1} \left( 1 - 2 \left( \frac{\mathbf{I}_x \pi R}{MglT} \right)^2 \right) \quad (34)$$

where  $\mathbf{I}_x$  is taken from equation (33) or (36) depending on the values of  $\phi$  and  $\mu$ . It is stressed that in the case of the bullet trap where  $\phi = 18^\circ$ , equation (33) prevails as  $v_2$  is always greater than zero. The following comments relate to that case.

Experimental values of the maximum rotation,  $\theta_1$ , for plate angles  $\phi = 12.5^\circ$ ,  $\phi = 19^\circ$  and  $\phi = 25^\circ$  are given in tables above. When  $\phi = 0^\circ$ , that is the plate is horizontal, it is obvious that  $\theta_1 = 0$ . For a given value of  $\mu$ , equation (34) gives a theoretical relationship between  $\theta_1$  and  $\phi$ . It was found that  $\mu = 0.22$  provided a very good fit to the experimental data, although one data point was clearly in error and is to be checked by an additional test. This is shown graphically in figure 6.

The fit would not be expected to apply for large values of  $\phi$ , as pitting of the plate occurs. A single round fired at the plate with  $\phi = 45^\circ$  caused a considerable pit at the point of impact.

#### Discussion

From the results of the first series of tests, direct comparison of  $\mathbf{I}_n$  and  $\mathbf{I}_t$  or determination of an approximate coefficient of kinetic friction,  $\mu$ , shows that the tangential impulse is about a fifth of the normal impulse.

### Normal stress during impact for existing lower plate

The following are some thoughts for discussion. The normal impulse  $\mathbf{I}_n$  is obtained simply using equation (12), repeated here

$$mv_1 \sin \phi = \int F_n(t) dt = \mathbf{I}_n \quad (12)$$

In the lower plate,  $\phi = 18^\circ$ , and hence in our case with  $m = 0.003567$  kg and  $v_1 = 853$  m/s

$$\mathbf{I}_n = 0.940 \text{ Ns}$$

$$\mathbf{I}_n = 0.003567 * 853 * \sin 18^\circ = 0.940 \text{ Ns}$$

The projectiles have a length of 20 mm and the impacted area when the plate in the experiment was  $19^\circ$  was approximately elliptical measuring 18 mm in the direction of motion by 10 mm laterally, or major axis 9 mm and minor axis 5 mm. This shape was observed by marking on the plate caused by the impact. The projectile slowed to about 750 m/s during the impact giving an average velocity, 800 m/s during contact. If we assume contact time of  $800/0.020$  seconds (which is about time to travel the length of the projectile or impact area), and the normal force is constant during the impact (it certainly will have a peak much greater than this) the normal force would be

$$0.940 * 800/0.02 = 37600 \text{ N} = 37.6 \text{ kN}$$

and normal stress

$$\frac{37600}{\pi * 9 * 5} = 266 \text{ MPa}$$

This normal stress is too low to cause yielding, but given the assumptions of uniform force distributed uniformly over the contact area it likely the peak normal stress would be considerably greater.

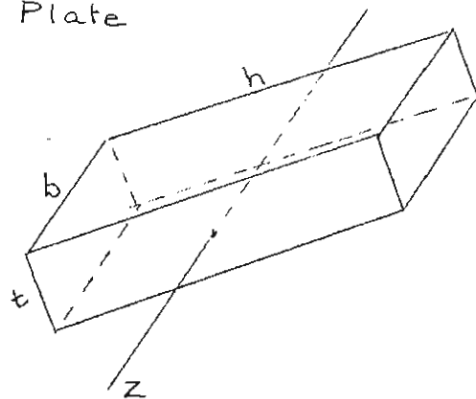
### Mechanical energy loss

Mechanical energy is kinetic energy of the projectile (before and after impact) and potential energy of the pendulum, taken as zero when the pendulum is in the equilibrium position. The initial kinetic energy of the projectile is  $\frac{1}{2}mv_1^2$  and the final kinetic energy is approximated by  $\frac{1}{2}mv_2^2$  as the shattered projectile has components in lots of directions depending on the plate angle  $\phi$ . The maximum potential energy of the pendulum is  $Mgl(1 - \cos \theta_1)$ . The mechanical energy loss during impact,  $E_{\text{loss}}$ , is given by

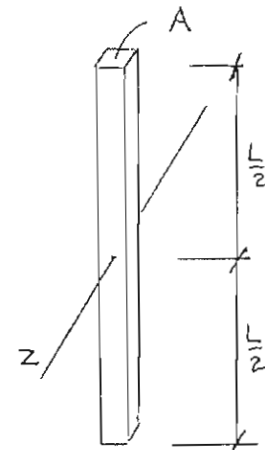
$$E_{\text{loss}} = \frac{1}{2}mv_1^2 - \frac{1}{2}mv_2^2 - Mgl(1 - \cos \theta_1) \quad (27)$$

The loss is converted to heat, fragmentation of the projectile and elastic and plastic energy in the impacted plate.

Plate



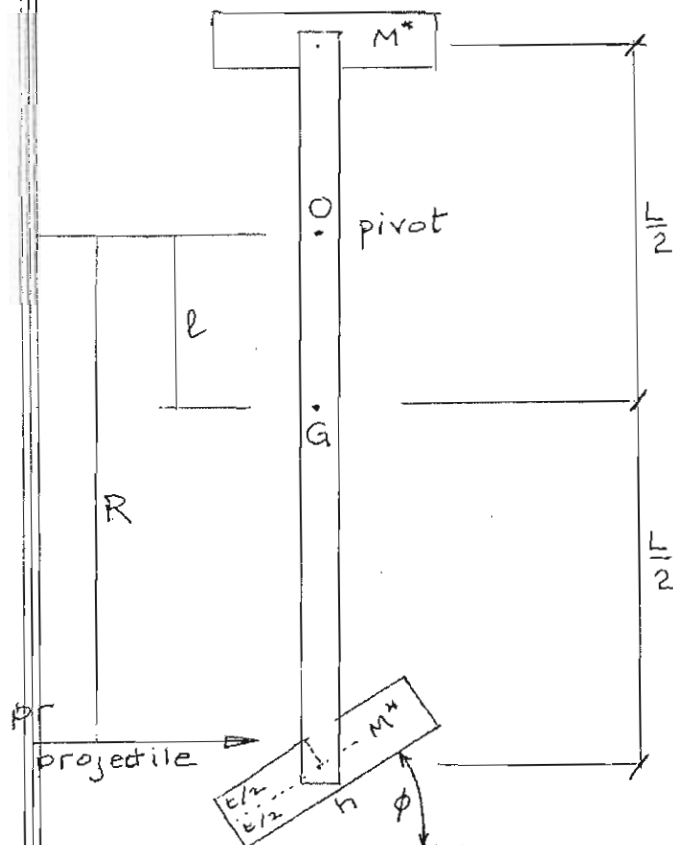
Bar



$$M^* = \rho b h t \quad I_z^* = M^* \left( \frac{b^2}{12} + \frac{h^2}{12} \right) \quad m^* = \rho A L \quad I_z^* = \frac{m^* L^2}{12}$$

Figure 1. Plate and bar properties

Pendulum

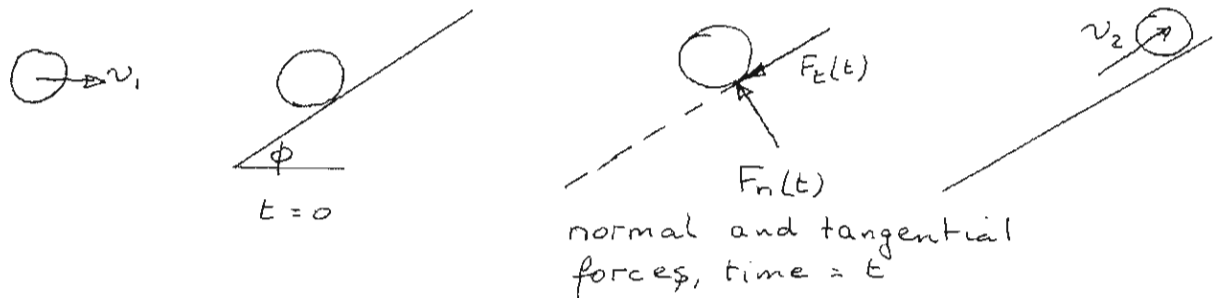


G = centre of mass

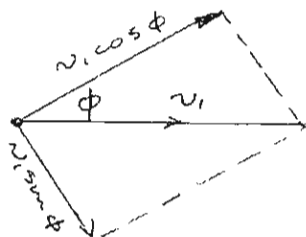
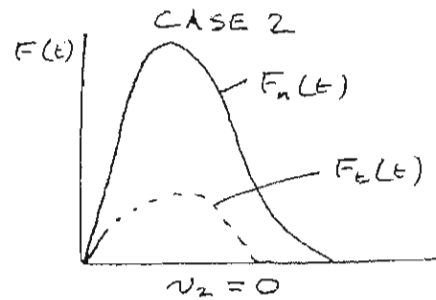
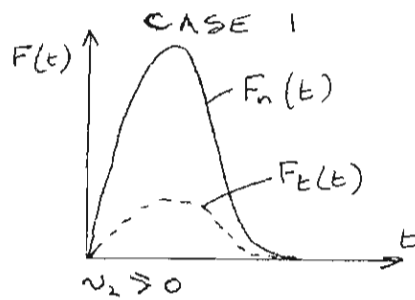
$2m^*$  = mass of bars

Figure 2. Pendulum dimensions

Projectile impact, thought experiment only.



Possible force functions



before impact

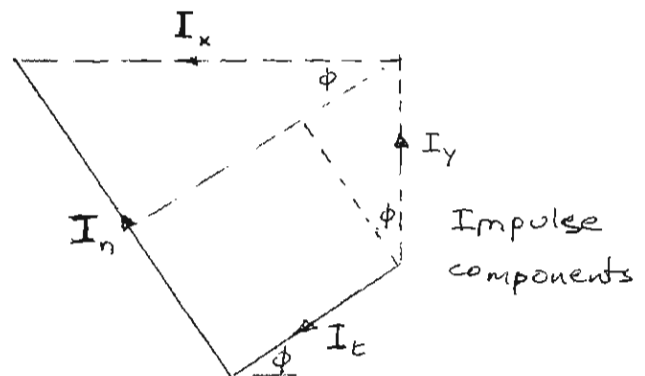
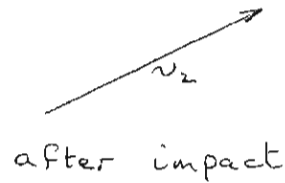


Figure 3. Velocity and impulse components

Ballistic pendulum schematic

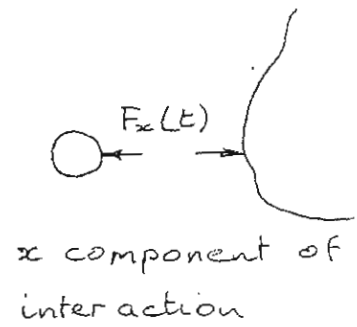
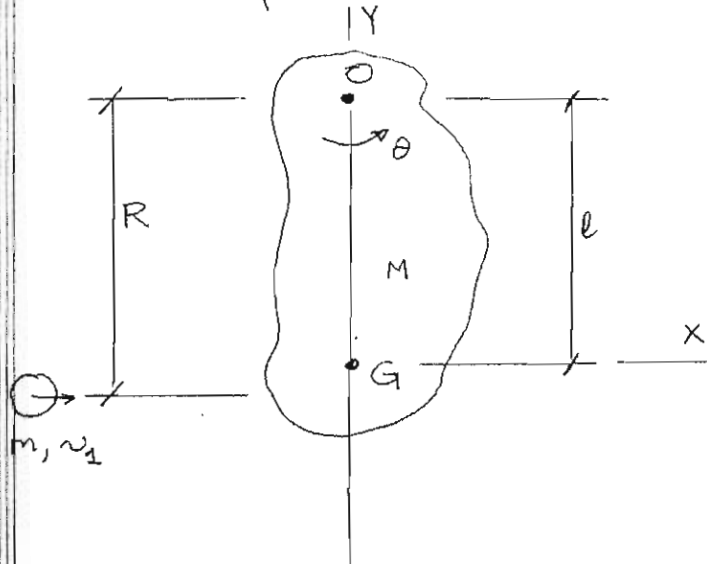
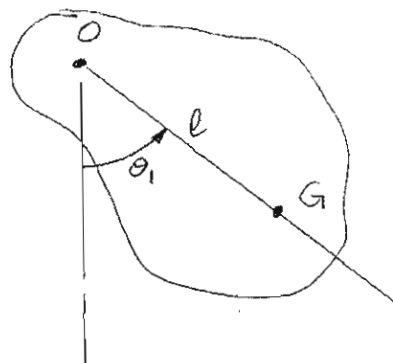


Figure 4.

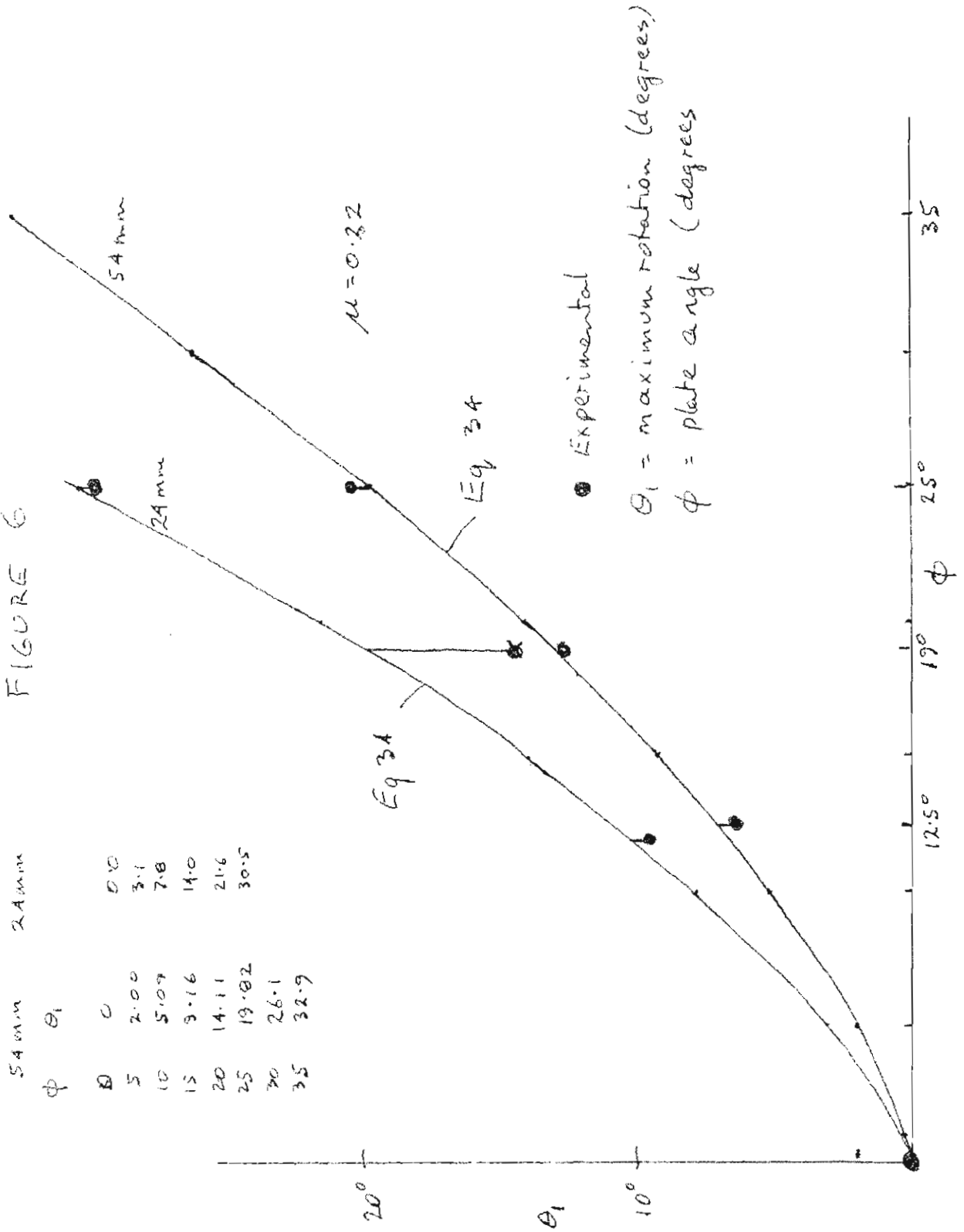


Maximum rotation.

Figure 5.



FIGURE 6



## SUMMARY OF EQUATIONS FOR BALLISTIC PENDULUM EXPERIMENT

Plate and bar properties about their centres of gravity

The dimensions and  $z$  axes are shown in Figure 1.

$$\text{density of plate material} = \rho_p$$

$$\text{density of bar material} = \rho_b$$

$$\text{mass of plate} = M^* = \rho_p b h t \quad (1)$$

$$\text{moment of inertia of plate} = I_z^* = M^* \left( \frac{h^2}{12} + \frac{t^2}{12} \right) \quad (2)$$

$$\text{mass of bar} = m^* = \rho_b L A \quad (3)$$

$$\text{moment of inertia of bar} = I_z^* = \frac{m^* L^2}{12} \quad (4)$$

### Pendulum properties

The dimensions used in the following formulas are shown in Figure 2. Also note the impacted plate is an angle  $\phi$  to the horizontal or  $x$  axis.

$$\text{mass of pendulum} = M = 2M^* + 2m^* \quad (5)$$

$$\text{moment of inertia about G} = I_G = 2M^* \left( \frac{h^2}{12} + \frac{t^2}{12} \right) + 2M^* \left( \frac{L}{2} \right)^2 + 2 \left( \frac{m^* L^2}{12} \right) \quad (6)$$

$$\text{radius of gyration about G} = k_G = \sqrt{\frac{I_G}{M}} \quad (7)$$

$$\text{moment of inertia about O} = I_O = I_G + 2M^* l^2 + 2m^* l^2 = I_G + M l^2 \quad (8)$$

$$\text{radius of gyration about O} = k_O = \sqrt{\frac{I_O}{M}} \quad (8)$$

$$R = \frac{L}{2} + l + \frac{t}{2} \cos \phi \quad (10)$$

$$\text{period of vibration} = T = 2\pi \sqrt{\frac{I_O}{M g l}} = 2\pi \sqrt{\frac{I_G + M l^2}{M g l}} = 2\pi \sqrt{\frac{\frac{k_G^2}{l} + l}{g}} \quad (11)$$

### Projectile impact

Refer to Figure 3.

As  $I$  is used for mass moment of inertia, for convenience impulse is also used with the same letter, but in boldface, namely  $\mathbf{I}$ .

$$mv_1 \sin \phi = \int F_n(t) dt = \mathbf{I}_n \quad (12)$$

$$mv_1 \cos \phi - mv_2 = \int F_t(t) dt = \mathbf{I}_t \quad (13)$$

$$\begin{aligned} \mathbf{I}_x &= \mathbf{I}_t \cos \phi + \mathbf{I}_n \sin \phi \\ &= (mv_1 \cos \phi - mv_2) \cos \phi + mv_1 \sin \phi \sin \phi \\ &= mv_1 - mv_2 \cos \phi \quad \text{as expected} \end{aligned} \quad (14)$$

$$\begin{aligned} \mathbf{I}_y &= -\mathbf{I}_t \sin \phi + \mathbf{I}_n \cos \phi \\ &= -(mv_1 \cos \phi - mv_2) \sin \phi + mv_1 \sin \phi \cos \phi \\ &= mv_2 \sin \phi \quad \text{as expected} \end{aligned} \quad (15)$$

Also

$$\mathbf{I}_t = \mathbf{I}_x \cos \phi - \mathbf{I}_y \sin \phi \quad (16)$$

$$\mathbf{I}_n = \mathbf{I}_x \sin \phi + \mathbf{I}_y \cos \phi \quad (17)$$

Determine  $\mathbf{I}_x$  using a ballistic pendulum. Consider the schematic diagram shown in Figure 4.  $O$  is the pivot point and  $G$  is the centre of gravity of the pendulum. The projectile of mass  $m$  with velocity  $v_1$  impacts the pendulum. The component of the interactive force in the  $x$  direction is  $F_x(t)$ .

$$\text{mass} = M$$

$$\text{mass moment of inertia about } O = I_O = Mk_O^2$$

$$\text{radius of gyration about } O = k_O$$

$$\text{rotation} = \theta = \theta(t)$$

$$\text{angular velocity} = \dot{\theta} = \omega(t)$$

A dot denotes differentiation with respect to time  $t$ . The projectile does not adhere to the pendulum after impact.

$$\text{torque about O} = RF_x(t) = I_O \ddot{\theta} = I_O \dot{\omega} = \frac{d\omega}{dt} \quad (18)$$

$$d\omega = \frac{R}{I_O} F_x(t) dt \quad (19)$$

Therefore

$$\omega_0 = \frac{R}{I_O} \int F_x(t) dt = \frac{R}{I_O} \mathbf{I}_x \quad (20)$$

where  $\omega_0$  is the angular velocity immediately following impact. In our case as noted earlier

$$\mathbf{I}_x = mv_1 - mv_2 \cos \phi \quad (14)$$

Now equate the kinetic energy of the pendulum immediately following impact with the maximum potential energy of the pendulum. See Figure 5.

$$\text{distance from pivot O to G} = l$$

$$\frac{1}{2} I_O \omega_0^2 = Mgl(1 - \cos \theta_1) \quad (21)$$

where  $\theta_1$  is the maximum angle of  $\theta$  and  $g$  is the gravitational acceleration. Therefore

$$\frac{1}{2} I_O \left( \frac{R}{I_O} \mathbf{I}_x \right)^2 = Mgl(1 - \cos \theta_1) \quad (22)$$

from which

$$\mathbf{I}_x = \sqrt{\frac{2MglI_O(1 - \cos \theta_1)}{R^2}} \quad (23)$$

Also note the period of the pendulum,  $T$ , is

$$T = 2\pi \sqrt{\frac{I_O}{Mgl}} \quad (11)$$

giving

$$\mathbf{I}_x = \frac{MglT}{2\pi R} \sqrt{2(1 - \cos \theta_1)} \quad (24)$$

Note from the period  $T$  the moment of inertia can be determined experimentally using (11) giving

$$I_O = \left(\frac{T}{2\pi}\right)^2 Mgl \quad (25)$$

### Experimental procedure

Plate masses  $M^*$  and bar masses  $m^*$  are determined by weighing, dimensions  $b$ ,  $h$ ,  $t$ ,  $L$  and  $l$  are measured, although  $b$  is not required. The total mass of the pendulum, including welds, bolts and bearings is also measured. The exact location of the centre of mass of the pendulum is also determined by balancing on a knife edge. If this is not almost exactly at the midpoint of the bars, the expression for determining  $I_O$  using (8) will require modification.  $I_O$  may be determined from masses and dimensions using (8) and from the period  $T$  using (25) and hence gives a useful check on a range of measurements. The mass  $m$  of the M4 projectile may be determined by pulling apart a number of rounds, or using the standard mass of 55 grains=3.56 gm. The approximate velocity of an M4 round is 915 m/s. The 9mm round is 115 grains, approximate velocity 350 m/s. Gravitational acceleration is taken as  $g = 9.81 \text{ m/s}^2$ .

$T$  is determined using a stop watch.

$v_1$  is measured using standard equipment for measuring the velocity of bullets.

$\theta_1$  is measured using the ballistic pendulum. Then determine  $\mathbf{I}_x$  using (24)

$$\mathbf{I}_x = \frac{MglT}{2\pi R} \sqrt{2(1 - \cos \theta_1)} \quad (24)$$

$v_2$  is determined using (14) giving

$$v_2 = \frac{1}{m \cos \phi} (mv_1 - \mathbf{I}_x) \quad (26)$$

$\mathbf{I}_y$ ,  $\mathbf{I}_n$  and  $\mathbf{I}_t$  are then determined using (12), (13) and (15).

### Mechanical energy loss

Mechanical energy is kinetic energy of the projectile (before and after impact) and potential energy of the pendulum, taken as zero when the pendulum is in the equilibrium position. The initial kinetic energy of the projectile is  $\frac{1}{2}mv_1^2$  and the final kinetic energy is approximated by  $\frac{1}{2}mv_2^2$  as the shattered projectile has components in lots of directions depending on the plate angle  $\phi$ . The maximum potential energy of the pendulum is  $Mgl(1 - \cos \theta_1)$ . The mechanical energy loss during impact,  $E_{\text{loss}}$ , is given by

$$E_{\text{loss}} = \frac{1}{2}mv_1^2 - \frac{1}{2}mv_2^2 - Mgl(1 - \cos \theta_1) \quad (27)$$

The loss is converted to heat, fragmentation of the projectile and elastic and plastic energy in the impacted plate.

### Estimating maximum $\theta$

This paragraph is included for experimental design purposes and information only.

Maximum  $\theta$ , namely  $\theta_1$ , occurs when  $\phi = 90^\circ$ , in which case  $v_2 = 0$ . Hence using (14) and (23), we obtain

$$\mathbf{I}_x = mv_1 - mv_2 \cos \phi = mv_1 = \sqrt{\frac{2MglI_O(1 - \cos \theta_1)}{R^2}} \quad (28)$$

And solving for  $\theta_1$  we obtain

$$\theta_{1\text{max}} = \cos^{-1} \left( 1 - \frac{(mv_1)^2 R^2}{2MglI_O} \right) \quad (29)$$

### Some thoughts on kinetic friction

In the absence of any information, try relating the normal and tangential interactions during impact using an assumed coefficient of kinetic friction between the projectile and plate. For completeness, two cases are considered.

**Case 1** In this case,  $v_2 \geq 0$ . Let the normal and tangential interactions be related by

$$F_t(t) = \mu F_n(t) \quad (30)$$

where  $\mu$  is the coefficient of kinetic friction, assumed to be constant. Thus the relationship between impulses is

$$\mathbf{I}_t = \mu \mathbf{I}_n \quad (31)$$

Solving equations (12), (30), (14) and (15) for  $\mathbf{I}_n$ ,  $\mathbf{I}_x$ ,  $\mathbf{I}_y$  and  $v_2$  we obtain the relevant solutions

$$v_2 = v_1(\cos \phi - \mu \sin \phi) \quad (32)$$

$$\mathbf{I}_x = mv_1(\sin^2 \phi + \mu \cos \phi \sin \phi) \quad (33)$$

The relationship in equation (30) is only valid for  $v_2 \geq 0$ . From equation (32), this only holds if

$$\cos \phi - \mu \sin \phi \geq 0 \quad (34)$$

or

$$\mu \leq \cot \phi \quad (35)$$

In the table below,  $\cot \phi$  is shown for values of  $\phi$  from  $0^\circ$  to  $90^\circ$ .

$\phi$	$10^\circ$	$20^\circ$	$30^\circ$	$40^\circ$	$50^\circ$	$60^\circ$	$70^\circ$	$80^\circ$	$90^\circ$
$\cot \phi$	5.67	2.75	1.73	1.19	0.84	0.58	0.36	0.18	0.00

Hence for example if  $\phi = 30^\circ$ ,  $\mathbf{I}_x$  obtained from equation (33) is valid if  $\mu \leq 1.73$ . If  $\mu > 1.73$ ,  $v_2 = 0$  and Case 2 applies.

**Case 2** This case is added for academic interest only, as in the bullet trap under consideration the projectiles were not stopped by the plate. In Case 2,  $v_2 = 0$  and equation (14) becomes

$$\mathbf{I}_x = mv_1 \quad (36)$$

Solving equation (24) for  $\theta_1$  we obtain

$$\theta_1 = \cos^{-1} \left( 1 - 2 \left( \frac{\mathbf{I}_x \pi R}{M g l T} \right)^2 \right) \quad (34)$$

where  $\mathbf{I}_x$  is taken from equation (33) or (36) depending on the values of  $\phi$  and  $\mu$ . It is stressed that in the case of the bullet trap where  $\phi = 18^\circ$ , equation (33) prevails as  $v_2$  is always greater than zero. The following comments relate to that case.

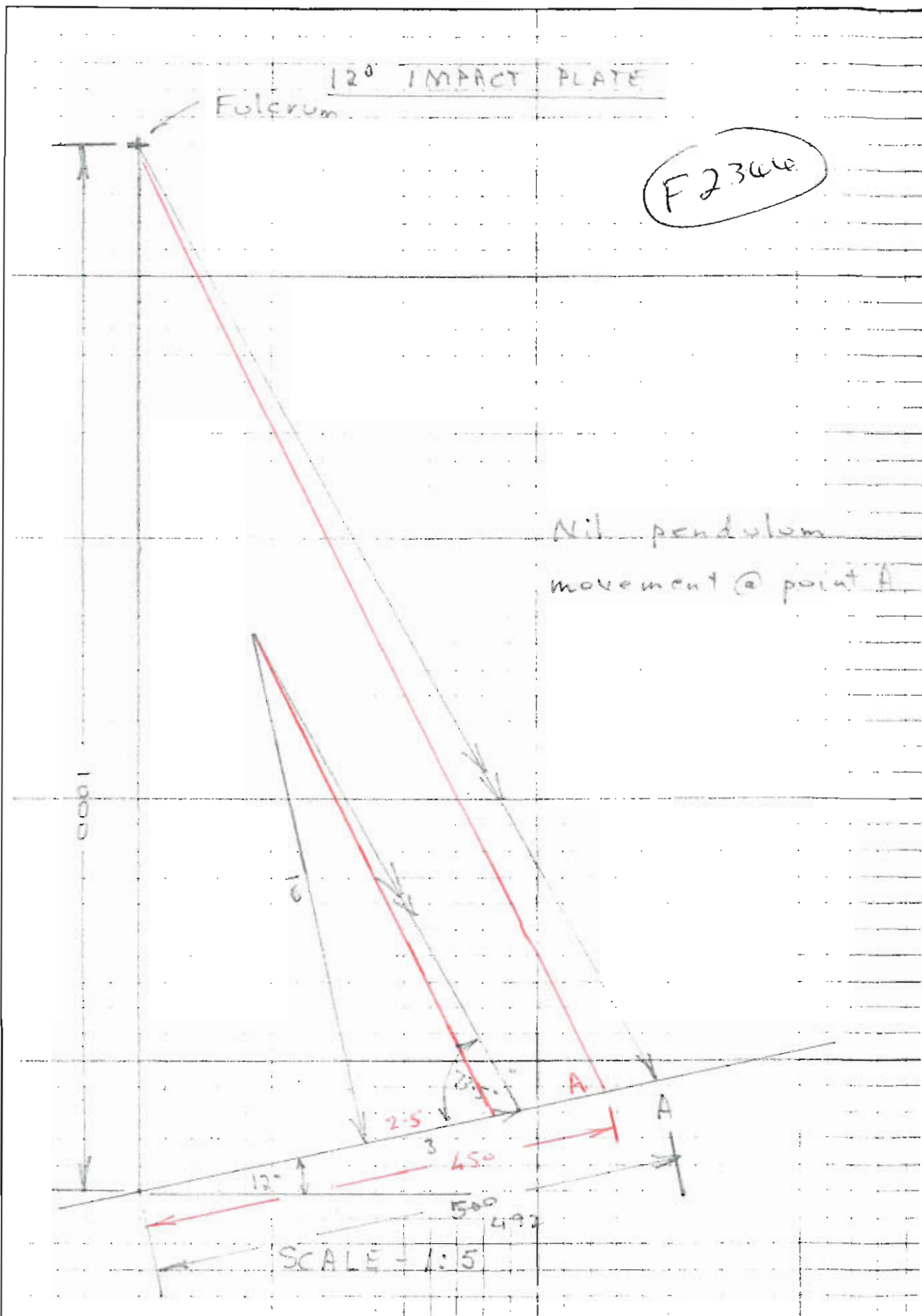
$\theta_1$  has been measured experimentally for  $\phi = 12.5^\circ$ ,  $\phi = 19^\circ$  and  $\phi = 25^\circ$ . It is also known that  $\theta_1 = 0$  when  $\phi = 0^\circ$ . Using least squares, it was found that  $\mu = 0.22$  provided a very good fit to the experimental data. This is shown graphically elsewhere.

The fit would not be expected to cover very large values of  $\phi$ , as pitting of the plate occurs. A single round fired at the plate with  $\phi = 45^\circ$  caused a considerable pit at the point of impact.

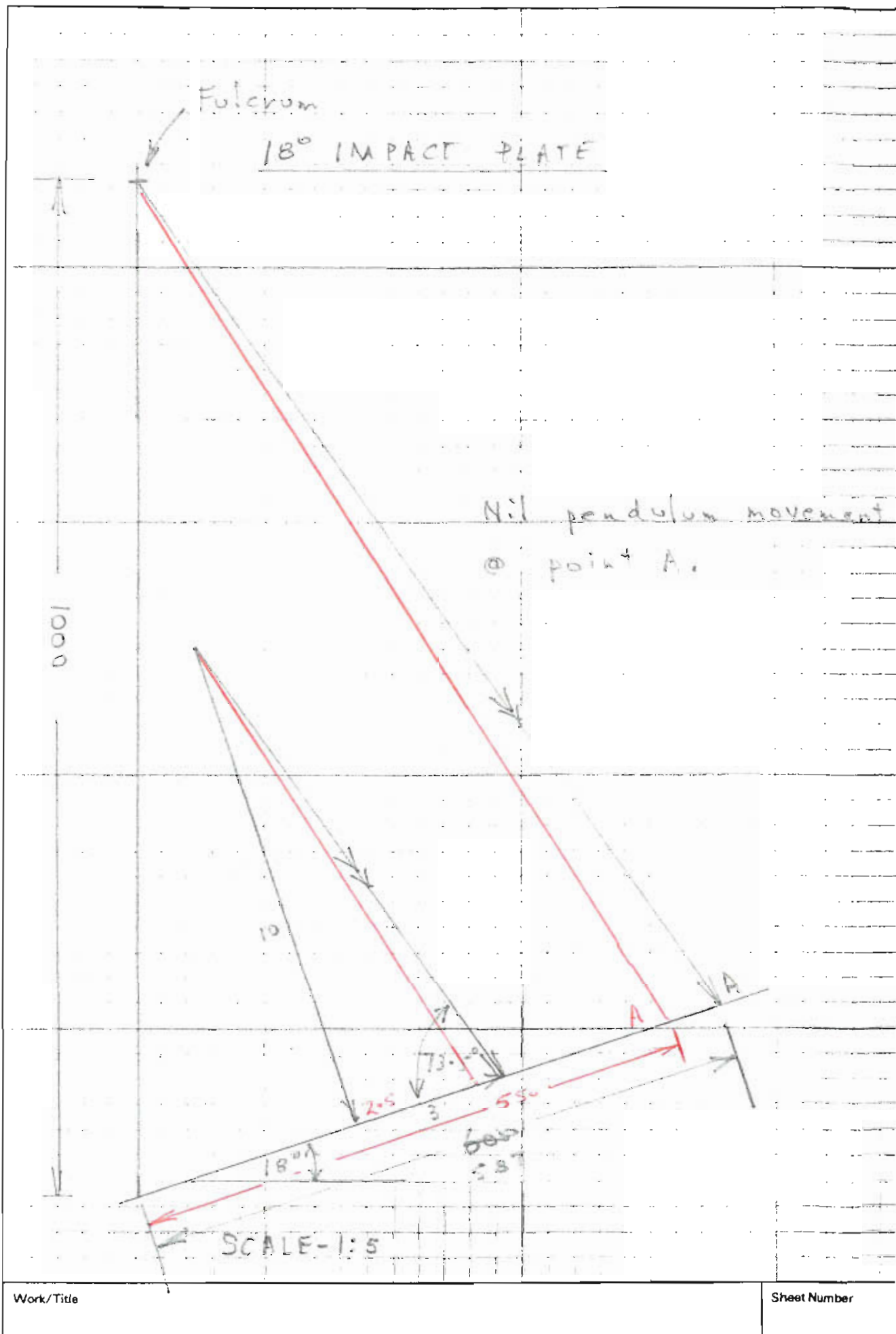
#### Thoughts following meeting 04/07/2012

The guessed relationship between the normal and tangential impulses given by Eq (29) is simply a guess, and it is the actual relationship which was hoped to be determined experimentally using the ballistic pendulum. This could not be determined with the existing experimental equipment, which was subsequently redesigned, and is now being refabricated. The evidence determined by surveying the distorted plates suggests the deformation is the result of the shot peening effect, which results from normal stresses due to impact exceeding the yield stress of the plate. The surface shear stress during impact may also exceed the yield stress, but a simple approach to determine the effect on curvature due to surface shear deformation of a thin surface layer does not lead to any curvature. The friction during impact is clearly complicated, as the projectile distorts and heats, and the plate also heats. The plate surface is also not smooth, and the surface probably roughens somewhat after long periods of use. The only figures I can find to give any idea of the coefficient of kinetic friction between lead and (mild) steel is 0.95.



W:341  
(R.1/80)

W.341  
(R.1/BO)



25° IMPACT PLATE

Nil pendulum movement  
@ point A.

1000

10

700  
181

SCALE-1:5

Sheet Number

## PENDULUM TEST RESULTS 9 AUG 12

### Impact tests

Knife Edge 30 mm above C of G.

Impact Plate Angle	Horizontal Displacement (mm) / Angular Displacement (Degrees)				
12°	110 / 8.8/ <b>5.9</b>	100 / 9.5/ <b>5.3</b>	150 / 9.2/ <b>8.0</b>	180 / 10.9/ <b>9.6</b>	150 / 9.5/ <b>8.0</b>
19°	400 / 22.9/ <b>21.8</b>	410 / 23.2/ <b>22.4</b>	330 / 19.4/ <b>17.9</b>	290 / ?/ <b>15.7</b>	370 / 21.1/ <b>20.1</b>
25°*	580 / 33.4/ <b>32.7</b>	530 / 28.9/ <b>29.5</b>	600 / 32.7/ <b>34.0</b>	600 / 32.0/ <b>33.9</b>	

Knife Edge 60 mm above C of G.

Impact Plate Angle	Horizontal Displacement (mm) / Angular Displacement (Degrees)				
12°	110 / 8.5/ <b>5.7</b>	130 / 9.9/ <b>6.8</b>	130 / 9.2/ <b>6.8</b>	130 / 9.9/ <b>6.8</b>	
19°	210 / 14.1/ <b>11.0</b>	260 / 15.8/ <b>13.6</b>	230 / 14.1/ <b>12.0</b>	220 / 14.1/ <b>11.5</b>	
25°*	480 / 27.5/ <b>25.8</b>	470 / 26.0/ <b>25.2</b>	460 / 26.4/ <b>24.6</b>	440 / 26.8/ <b>23.5</b>	

Knife Edge 90 mm above C of G.

Impact Plate Angle	Horizontal Displacement (mm) / Angular Displacement (Degrees)				
12°	100 / 7.8/ <b>5.1</b>	90 / 6.3/ <b>4.6</b>	100 / 7.8/ <b>5.1</b>	50 / 5.6/ <b>2.5</b>	
19°	240 / 14.4/ <b>12.2</b>	210 / 13.0/ <b>10.7</b>	240 / 13.7/ <b>12.2</b>	280 / 15.1/ <b>14.3</b>	
25°*	400 / 22.5/ <b>20.7</b>	390 / 21.8/ <b>20.1</b>	370 / 20.8/ <b>19.0</b>	350 / 21.5/ <b>18.0</b>	

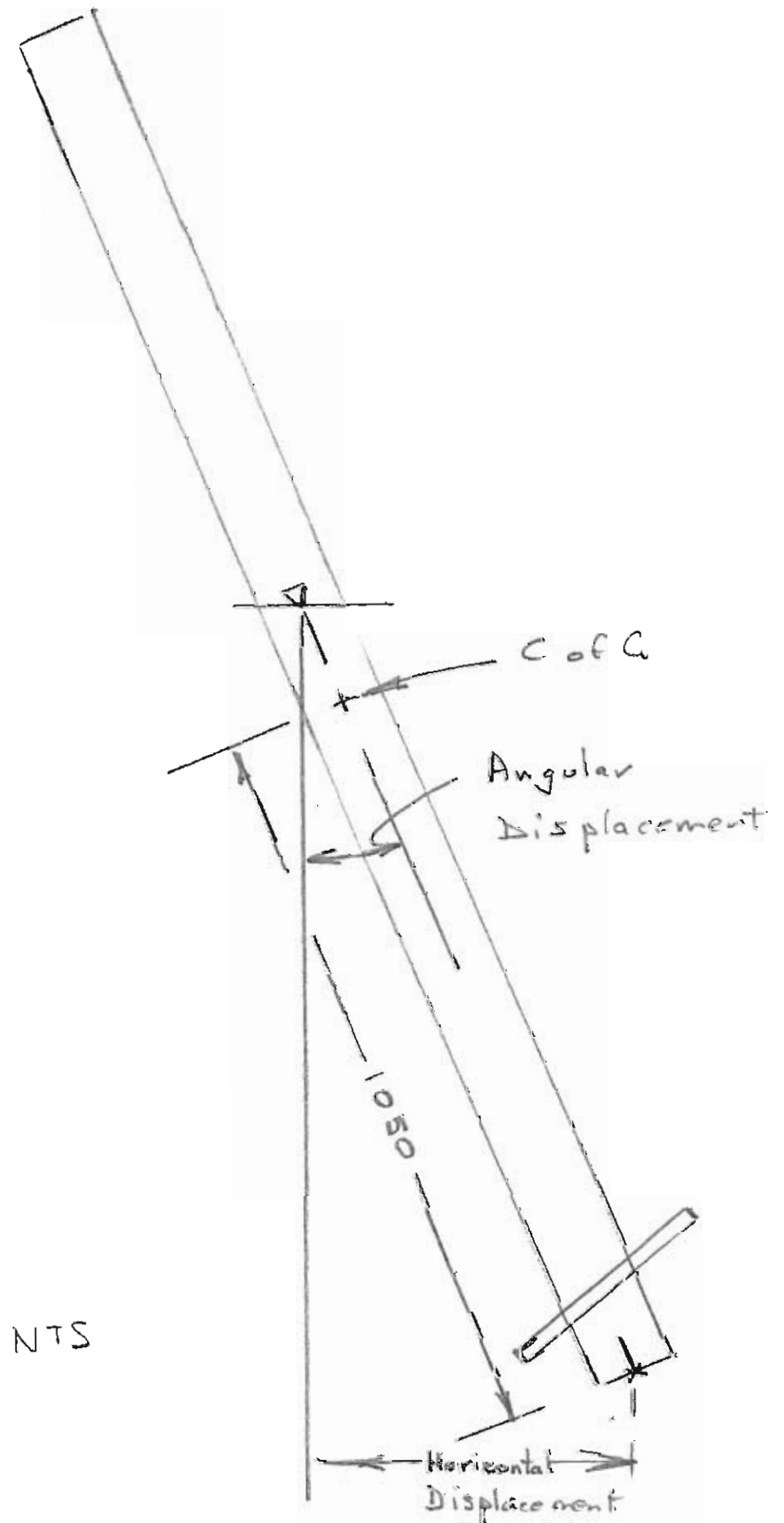
**NOTE.** (\*) With the impact plate at 25° the knife edge consistently jumped out of the slot for all knife edge positions ie 30 mm, 60 mm & 90 mm above C of G.

### Period times

The pendulum was moved to a position 20° off the vertical and released. The times noted below were for 50 x periods.

Ht of Fulcrum above C of G	Time for 50 x Periods
30	8'52"
60	6'02"
90	4'50" & 4'52"
120	4'13"

# DISPLACEMENT SKETCH



# **BALLISTIC PENDULUM EXPERIMENT**

## **MODIFIED EQUATIONS FOLLOWING TESTS 30-31/08/12**

### **SOME RESULTS INCLUDED**

Bruce Golley

#### **Summary**

Testing was conducted using the ballistic pendulum on 30/08/12 and 31/08/12. The tests were carried out with the target plate at angles  $12^\circ$ ,  $18^\circ$  and  $24.5^\circ$ . For each plate setting, the pendulum was supported at three pivots and a minimum of five rounds were fired for each plate and pivot setting. The maximum horizontal displacement of a point on the bottom of the pendulum was measured visually and using a camera. The visual readings and camera values were always similar.

The target plate was blackened with a whiteboard marker, and the transverse centreline was marked with white whiteboard marker. The rounds were fired at the centreline from about 10 metres, and the impact zone was clearly visible as the whiteboard ink was removed during impact. The impact zones were roughly elliptical, with dimensions about 20 mm by 10 mm. As the rounds were fired by a marksman, impact was not always centred on the transverse centreline. During the tests it was noted that the maximum rotation depended on the impact position. The main purpose of the experiment was to determine relative values of the normal impulse and tangential impulse during impact. It was hoped the tangential impulse would be smaller than the normal impulse, as this would support the idea that the plate deformation in the bullet traps was due to shot peening.

In developing the original equations to obtain the relative values, it was assumed that the normal and tangential impulses occurred at a single point which was at the centre of the obvious impact zone. It was also assumed that impacts away from the transverse centreline

of the plate would not influence the results. However, the larger than expected influence of location of the impact zone lead to the small changes in lever arms being introduced to account for non-central impact. A modification to this basic model leads to improved agreement between theoretical and experimental results, and is detailed in this paper.

The purpose of this discussion paper is to outline the modified scheme, provide details of the resulting equations and present some numerical results. By setting a new parameter to zero, the modified scheme reverts to the original method, and the two methods may be compared.

The modified method assumes the projectile continues to exert a tangential force on the plate after exiting the elliptical impact zone, which continues until the projectile leaves the plate. The writer cannot explain the reason why this may occur, but the resulting equations provide a superior fit to the data.

### **Experimental details**

A schematic diagram of the pendulum is shown in Figure 1. The top detail is not shown. The pendulum pivot was a knife edge, the position of which could be varied. The pivot points are referred to as 30 mm, 60 mm, 90 mm, 120 mm and 150 mm, and are shown by the letter  $O$  in the figure. The centre of gravity,  $G$ , was located initially by balancing the pendulum on a knife edge, which indicated it was at the nominal centre of the pendulum, plus or minus 1 mm. The period of the pendulum with all five pivot points were obtained by timing 50 oscillations. This enabled an alternative position of  $G$  to be determined in addition to the radius of gyration about  $G$ . The derivation is given below, but the location of  $G$  in Figure 1 is based on the periods of oscillation.

A minimum of five rounds were fired at plate angles  $12^\circ$ ,  $18^\circ$  and  $24.5^\circ$  with nominal pivots 30 mm, 60 mm and 90 mm. The maximum horizontal displacement  $h$  of point  $P$ , a point on the bottom of the pendulum was measured using a camera, and the centre of the impact zone was measured approximately using a tape measure. The centre of the impact zone can only be considered approximate, and was estimated to within 5 mm of the centreline

marked on the plate.

The increase in potential energy of the pendulum could be calculated in terms of the horizontal displacement of  $P$ , as indicated in Figure 2.

### Derivations and results

With each plate angle and pivot point, it was noted that the maximum value of the displacement  $h$  depended on the impact point. In an attempt to take this into consideration, it is assumed that the normal impulse is confined to the elliptical impact zone, but the tangential impulse has two components. The first component is confined to the elliptical impact zone, but a second component occurs along the remainder of the plate, rather like a skid, but with no accompanying normal force. There is no attempt to explain this tangential force. It can simply be set to zero to revert to the original model for comparison with the proposed model.

Refer to Figures 3 and 4. A projectile with velocity  $v_0$  impacts a plate at time  $t = 0$ . Normal and tangential components of the velocity are

$$v_{n0} = v_0 \cos \phi \quad \text{and} \quad v_{t0} = v_0 \sin \phi$$

During the time  $0 \leq t \leq t_1$ , normal and tangential forces  $F_n(t)$  and  $F_t(t)$  act on the projectile. Corresponding impulses are  $\mathbf{I}_n$  and  $\mathbf{I}_{t1}$ . At time  $t_1$ , the normal velocity is zero, and tangential velocity is  $v_{t1}$ .

From time  $t_1$  to  $t_2$  it is assumed that the normal force is zero and a tangential force  $F_t^*$  acts on the projectile. At time  $t_2$ , the tangential velocity is  $v_{t2}$ , and the projectile has reached the end of the plate.

### Location of $G$ and determination of radius of gyration

The pendulum was fabricated as a symmetrical system using aluminium bars 2100 mm long, so the centre of gravity,  $G$ , was expected to be near the midpoint of the bars. The radius of gyration with respect to  $G$ ,  $k_G$ , was required to determine moments of inertia, and the periods of oscillation were used to determine  $k_G$  and the precise location of  $G$ .



Refer to Figure 5, which simply shows the bars for convenience. Periods of oscillation were measured with five different pivots. The theoretical period with the pivot  $l_n$  above  $G$  is

$$T_n = 2\pi\sqrt{\frac{\frac{k_G^2}{l_n} + l_n}{g}}$$

For the various pivots, measured periods and corresponding values of  $l_n$  are shown in Figure 5. Lengths  $l_n$  are functions of the unknown  $x$  which is also shown in the figure. A least squares method was used to determine  $k_g$  and  $x$ . Thus

$$\sum_{n=1}^5 \left( g \left( \frac{T_n}{2\pi} \right)^2 - \left( \frac{k_G^2}{l_n} + l_n \right) \right)^2$$

where

$$l_n = 0.030n - 0.006 + x$$

was minimised with respect to the unknowns  $k_G$  and  $x$  giving  $x = 0.0016 \text{ m} = 1.6 \text{ mm}$  and  $k_G = 0.8476 \text{ m}$ . As expected,  $G$  determined using this method is close to the observed balance point. With this value of  $x$ , pivot distances are

$$l_n = 0.030n - 0.0044$$

and the  $n^{\text{th}}$  period becomes

$$T_n = \frac{2\pi}{\sqrt{9.81}} \sqrt{\frac{0.7187}{(0.030n - 0.0044)} + (0.030n - 0.0044)}$$

As the radius of gyration  $k_G$  is important in determining impulses, as a check the periods determined using this formula are compared with the observed periods in the following table, and indicate the accuracy of the formula, and hence  $k_G$ .

$n$	$T_n(\text{observed}) \text{ s}$	$T_n(\text{formula}) \text{ s}$
1	10.64	10.64
2	7.238	7.230
3	5.820	5.843
4	5.054	5.049
5	4.536	4.523

The following were also measured.

Pendulum mass  $M = 3.95$  kg

Projectile mass  $m = 0.00356$  kg

Projectile velocity  $v_0 = 875$  m/s

The projectile velocity was obtained by averaging the velocity of 10 rounds from the same batch used in the tests.

From the pendulum mass and the radius of gyration  $k_G$  the moment of inertia with respect to any pivot could be determined using the parallel axis theorem.

### Summary of equations

A number of equations used in determining impulses are presented without derivation. They are given here mainly for use by the writer. SI units (kg, m) are used. Dimensions  $A$ ,  $R$ ,  $f$ ,  $L$ ,  $h$ ,  $l$  and  $d$  are shown in the figures.  $\omega_0$  is the angular velocity of the pendulum following impact.  $I_O$  is the moment of inertia about the pivot  $O$ .

$$\mathbf{I}_n = mv_0 \sin \phi = mv_{n0} \quad (1)$$

$$\mathbf{I}_t = \mathbf{I}_{t1} + \mathbf{I}_{t2} = mv_0 \cos \phi - mv_{t2} = mv_{t0} - mv_{t2} \quad (2)$$

$$A = 0.016 \sin \phi + d \cos \phi \quad (3)$$

$$R = 1.000 + f - 0.016 \cos \phi + d \sin \phi \quad (4)$$

$$\omega_0 = \frac{1}{I_O} (\mathbf{I}_n \cos \phi A + \mathbf{I}_n \sin \phi R + \mathbf{I}_t ((1.000 + f) \cos \phi - 0.010)) \quad (5)$$

$$h = L \sqrt{\left( \frac{I_O \omega_0^2}{Mgl} \right) - \left( \frac{I_O \omega_0^2}{2Mgl} \right)^2} \quad (6)$$

$$F_t^* = -ma \quad (7)$$

where  $a$  is the acceleration in the tangential direction when  $t_1 \leq t \leq t_2$ , positive in the positive direction of  $v_t$  and the positive direction of  $F_t^*$  is shown in Figure 3.

$$v_{t2}^2 - v_{t1}^2 = 2a(d + 0.08) \quad (8a)$$

$$v_{t2} = \sqrt{v_{t1}^2 + 2a(d + 0.08)} \quad (8b)$$

### Data fitting to determine impulses

With each plate angle (12°, 18°, 24.5°) tests were conducted with three pivot settings (nominally 30 mm, 60 mm and 90 mm). For a given plate setting, the maximum horizontal displacement  $h_i$  and location of the centre of the impact zone,  $d_i$  were measured. The following calculations were carried out using the algebraic language, MAPLE. The resulting algebraic expressions are lengthy, but it should be noted that the programming would be far more complex using an arithmetic language.

Procedure.

- (1) Evaluate  $I_n$  numerically using equation (1)
- (2) Determine  $I_t$  in algebraic form using Equation (2) for impact  $i$ , namely.

$$I_t = mv_{t0} - mv_{t2} = mv_{t0} - m\sqrt{v_{t1}^2 + 2a(d_i + 0.08)} = I_t(v_{t1}, a) \quad (9)$$

- (3) Determine  $\omega_{0_i} = \omega_{0_i}(v_{t1}, a)$  using Equation (5).
- (4) Determine  $h_i(\text{theory})$  using Equation (6).
- (5) Determine  $h_i(\text{theory}) - h_i(\text{experimental}) = \epsilon_i(v_{t1}, a)$   
 $\epsilon_i(v_{t1}, a)$  is the difference (error) between the theoretical displacement and experimental displacement for the  $i^{\text{th}}$  round.
- (6) Obtain the sum of the squares of the errors for all rounds

$$E = \sum_i^I (\epsilon_i^2(v_{t1}, a))$$

$I$  is the total number of rounds fired at a plate set at one angle. The expression for  $E$  is very lengthy, and is highly nonlinear in the variables  $v_{t1}$  and  $a$ .

- (7) Minimise  $E$  with respect to the variables  $v_{t1}$  and  $a$ . This minimisation is carried out using Newton-Raphson iteration.
- (8) Calculate

$$\mathbf{I}_{t1} = m(v_{t0} - v_{t1})$$

numerically, and the impulse ratio  $\mathbf{I}_{t1}/\mathbf{I}_n$

(9) Determine  $v_{t2}$  using Equation (8b).  $v_{t2}$  and  $\mathbf{I}_{t2}$  are functions of the impact location  $d$ . To obtain the data fit with the original model, the acceleration  $a$  is simply set to zero before  $E$  is minimised.

### **Preliminary results**

Results for the  $18^\circ$  and  $24.5^\circ$  plate are presented graphically in Figures 6 and 7. The graphs show the horizontal displacement  $h$  of the bottom of the pendulum plotted as functions of the impact location  $d$ . Experimental points are shown, together with lines of best fit for the original model (dashed) and the modified model (solid). It is stressed that the best fit lines are based on the single use of all data points, the best fit lines have not been applied to each pivot setting. The modified model appears to fit the experimental data better than the original model, but there is plenty of scatter.

The impulse ratios were the object of the experiment. Values obtained were as follows.

$18^\circ$  plate. Original model  $\mathbf{I}_{t1}/\mathbf{I}_n = 0.418$ , modified model  $\mathbf{I}_{t1}/\mathbf{I}_n = 0.219$

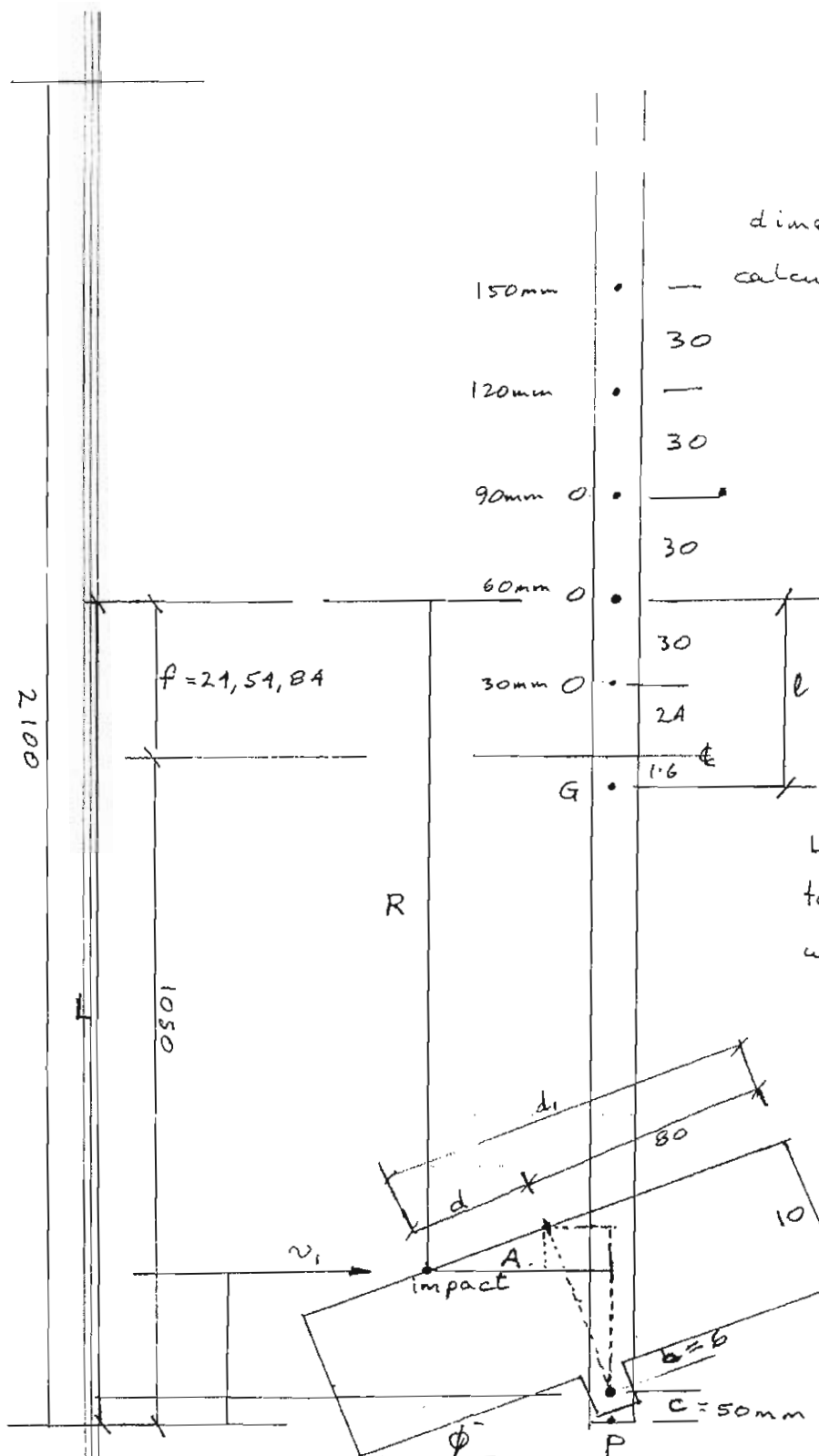
$25^\circ$  plate. Original model  $\mathbf{I}_{t1}/\mathbf{I}_n = 0.450$ , modified model  $\mathbf{I}_{t1}/\mathbf{I}_n = 0.202$

Hence the modified method leads to lower ratios, by a factor of about 2.

### **Final comments**

The outcome of these tests is inconclusive, although it is clear the normal impulse is significantly greater than the shear impulse which supports the shot peening proposal.

Additional tests are to be conducted in which more rounds are to be fired at the plate ensuring a wide range of impact zones are included.



L = distance from pivot  
to bottom of pendulum  
where h is measured

$$d_1 = d + 80 \text{ mm}$$

b to be determined.

c = 50mm 12mm bolt.

$$A = (10 + b) \sin \phi + d \cos \phi = 16 \sin \phi + d \cos \phi \text{ mm}$$

$$R = 1050 + f - c - ((10 + b) \cos \phi - d \sin \phi)$$

$$= 1000 + f - 16 \cos \phi + d \sin \phi \text{ mm}$$

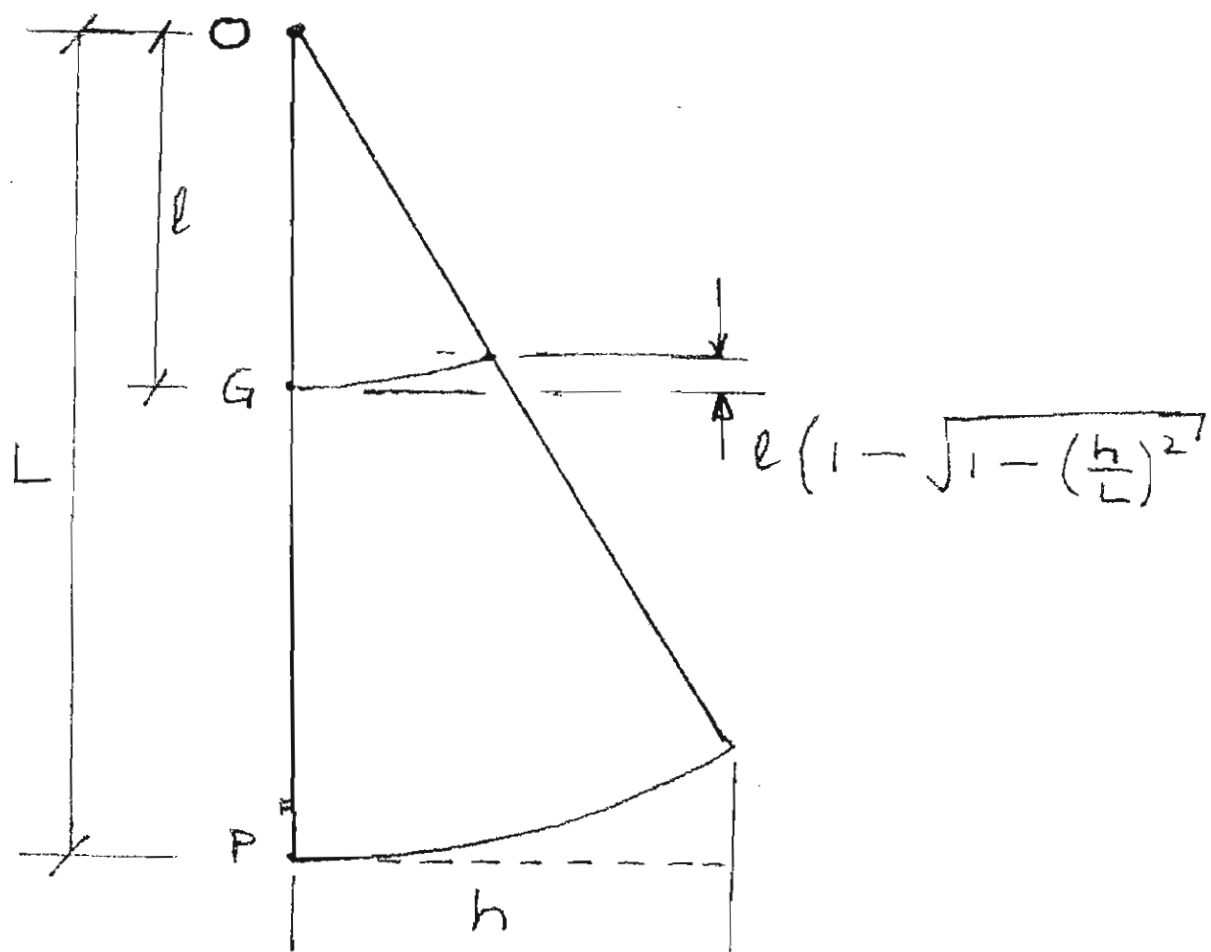


Figure 2

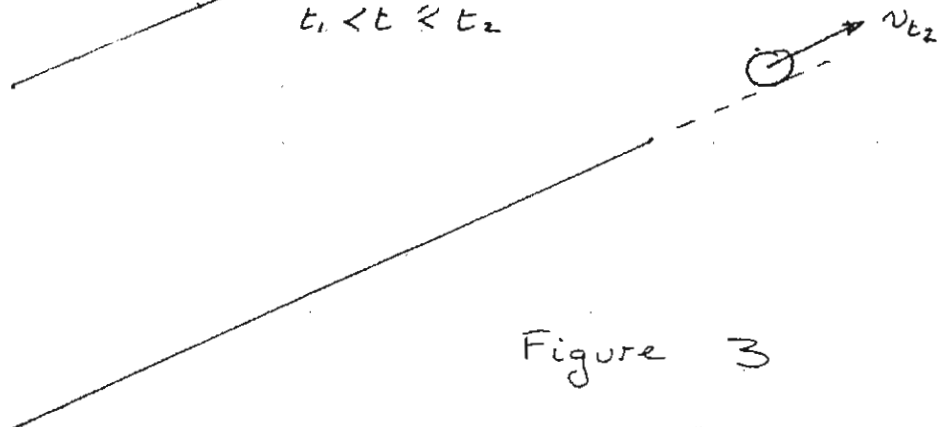
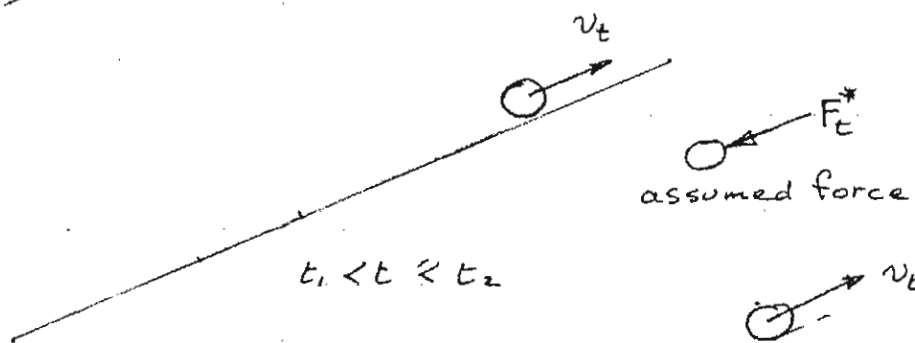
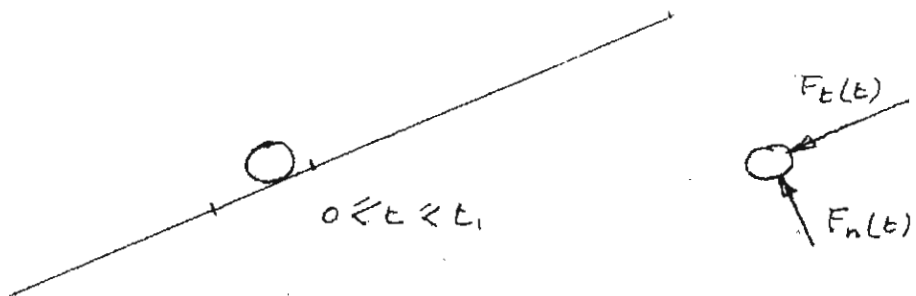
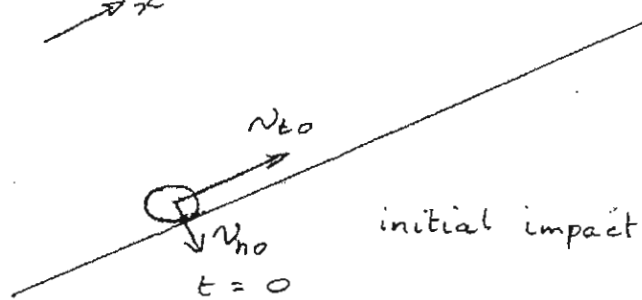
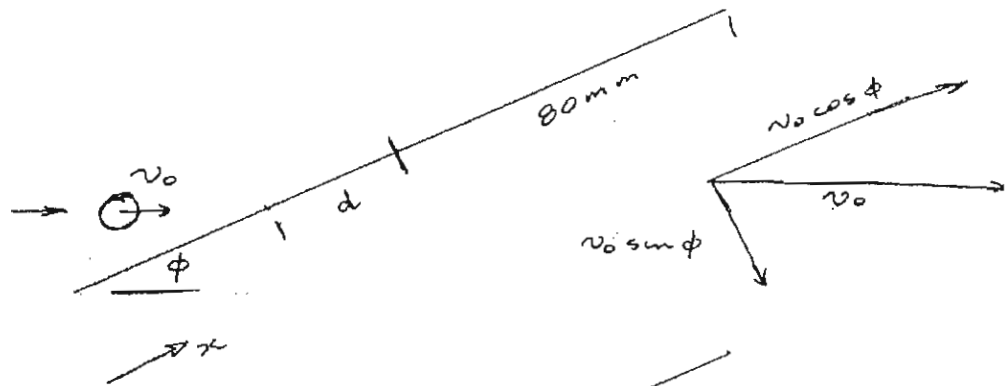


Figure 3

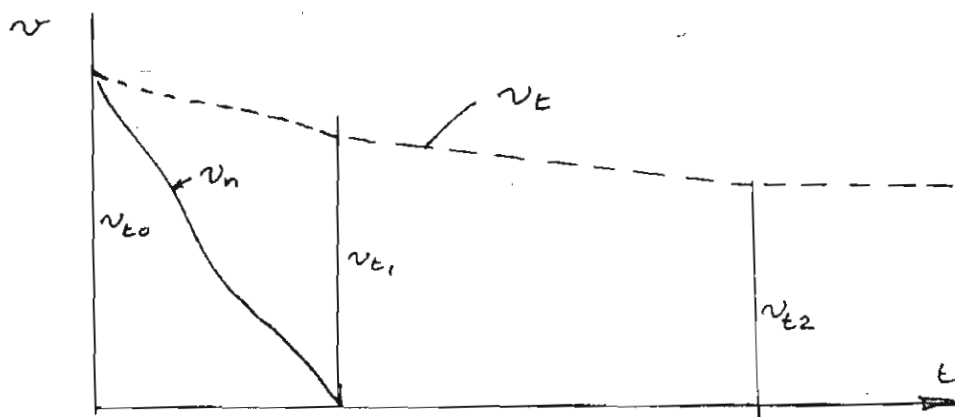
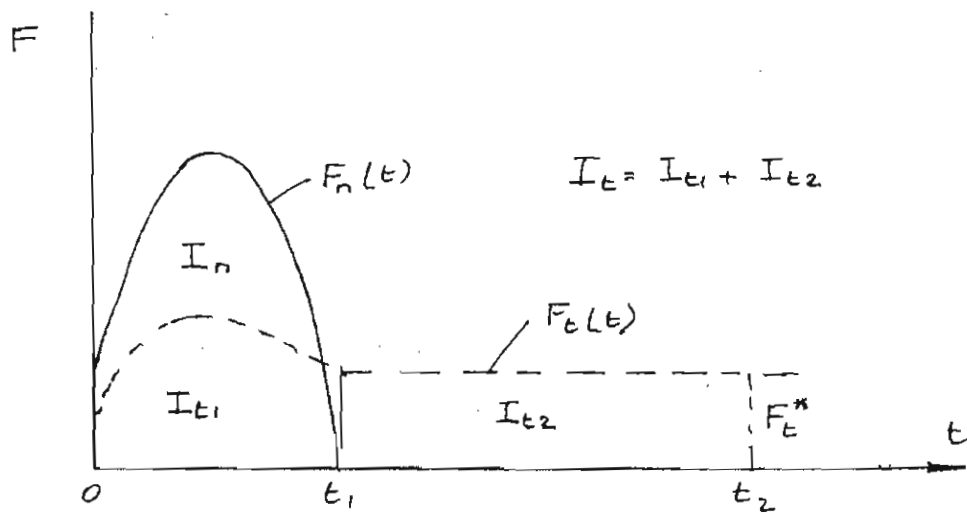


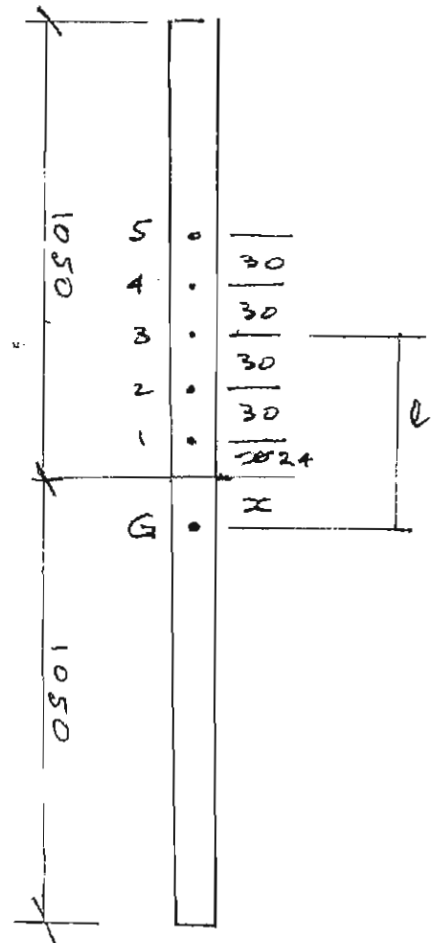
Figure 4



$$T_5 = 4.536 \quad l_5 = 0.144 + x$$

$$l_n = 0.030n - 0.006 + x$$

Figure 5



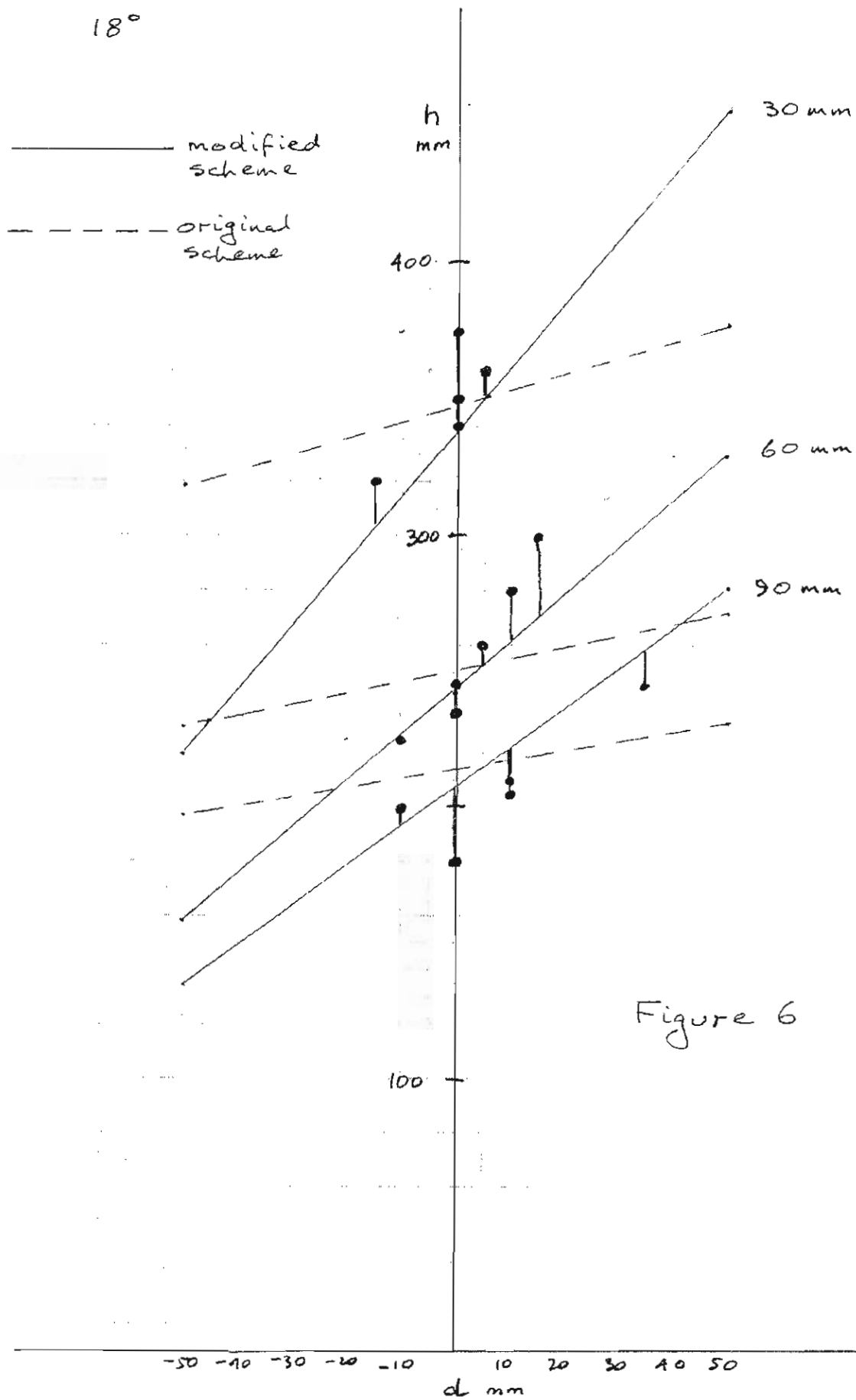
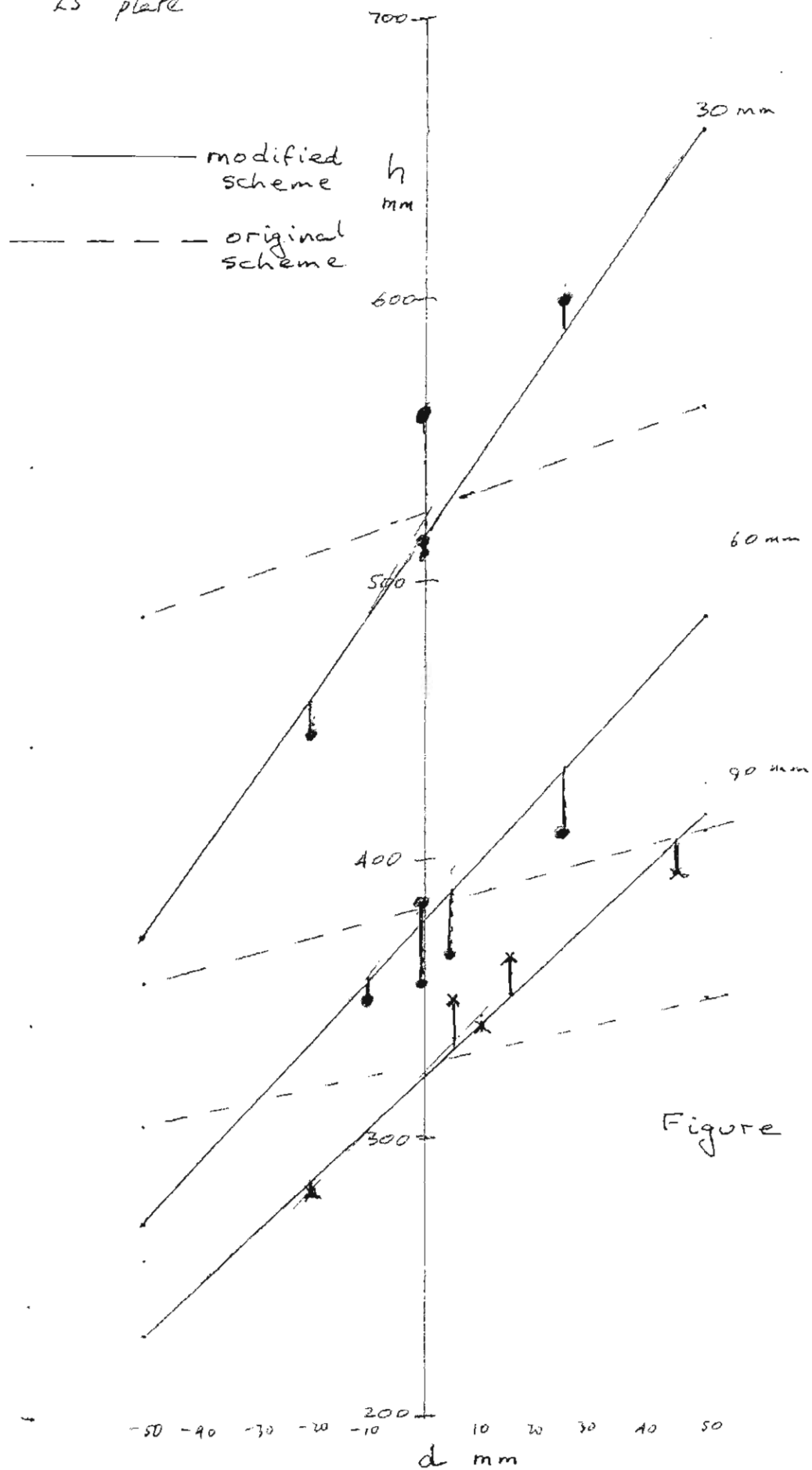


Figure 6

25° plate



12°

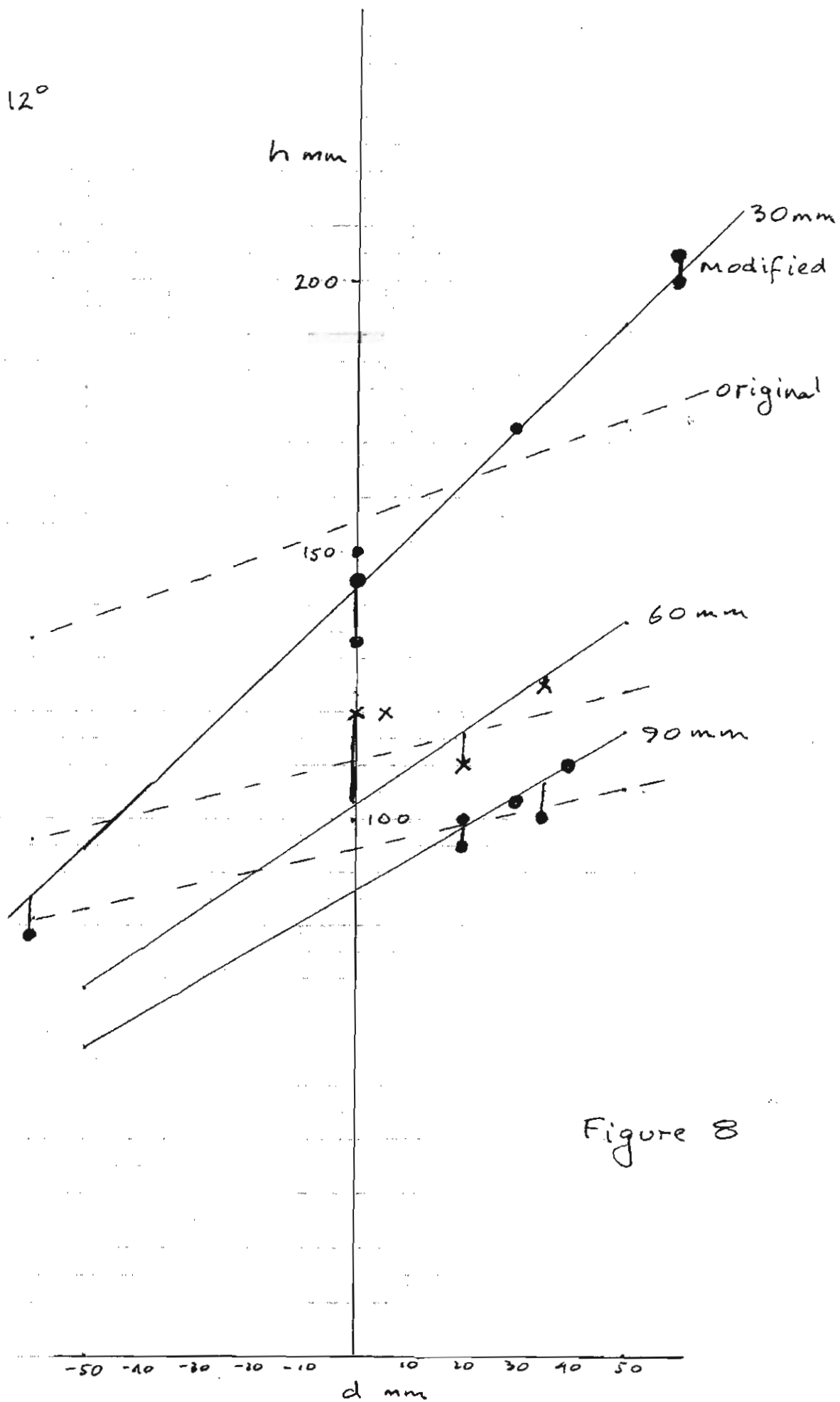


Figure 8

# **BALLISTIC PENDULUM EXPERIMENT**

## **MODIFIED EQUATIONS FOLLOWING TESTS 30-31/08/12**

### **SOME RESULTS INCLUDED**

Bruce Golley

#### **Summary**

Testing was conducted using the ballistic pendulum on 30/08/12 and 31/08/12. The tests were carried out with the target plate at angles  $12^\circ$ ,  $18^\circ$  and  $24.5^\circ$ . For each plate setting, the pendulum was supported at three pivots and a minimum of five rounds were fired for each plate and pivot setting. The maximum horizontal displacement of a point on the bottom of the pendulum was measured visually and using a camera. The visual readings and camera values were always similar.

The target plate was blackened with a whiteboard marker, and the transverse centreline was marked with white whiteboard marker. The rounds were fired at the centreline from about 10 metres, and the impact zone was clearly visible as the whiteboard ink was removed during impact. The impact zones were roughly elliptical, with dimensions about 20 mm by 10 mm. As the rounds were fired by a marksman, impact was not always centred on the transverse centreline. During the tests it was noted that the maximum rotation depended on the impact position. The main purpose of the experiment was to determine relative values of the normal impulse and tangential impulse during impact. It was hoped the tangential impulse would be smaller than the normal impulse, as this would support the idea that the plate deformation in the bullet traps was due to shot peening.

In developing the original equations to obtain the relative values, it was assumed that the normal and tangential impulses occurred at a single point which was at the centre of the obvious impact zone. It was also assumed that impacts away from the transverse centreline

of the plate would not influence the results. However, the larger than expected influence of location of the impact zone lead to the small changes in lever arms being introduced to account for non-central impact. A modification to this basic model leads to improved agreement between theoretical and experimental results, and is detailed in this paper.

The purpose of this discussion paper is to outline the modified scheme, provide details of the resulting equations and present some numerical results. By setting a new parameter to zero, the modified scheme reverts to the original method, and the two methods may be compared.

The modified method assumes the projectile continues to exert a tangential force on the plate after exiting the elliptical impact zone, which continues until the projectile leaves the plate. The writer cannot explain the reason why this may occur, but the resulting equations provide a superior fit to the data.

### **Experimental details**

A schematic diagram of the pendulum is shown in Figure 1. The top detail is not shown. The pendulum pivot was a knife edge, the position of which could be varied. The pivot points are referred to as 30 mm, 60 mm, 90 mm, 120 mm and 150 mm, and are shown by the letter  $O$  in the figure. The centre of gravity,  $G$ , was located initially by balancing the pendulum on a knife edge, which indicated it was at the nominal centre of the pendulum, plus or minus 1 mm. The period of the pendulum with all five pivot points were obtained by timing 50 oscillations. This enabled an alternative position of  $G$  to be determined in addition to the radius of gyration about  $G$ . The derivation is given below, but the location of  $G$  in Figure 1 is based on the periods of oscillation.

A minimum of five rounds were fired at plate angles  $12^\circ$ ,  $18^\circ$  and  $24.5^\circ$  with nominal pivots 30 mm, 60 mm and 90 mm. The maximum horizontal displacement  $h$  of point  $P$ , a point on the bottom of the pendulum was measured using a camera, and the centre of the impact zone was measured approximately using a tape measure. The centre of the impact zone can only be considered approximate, and was estimated to within 5 mm of the centreline

marked on the plate.

The increase in potential energy of the pendulum could be calculated in terms of the horizontal displacement of  $P$ , as indicated in Figure 2.

### Derivations and results

With each plate angle and pivot point, it was noted that the maximum value of the displacement  $h$  depended on the impact point. In an attempt to take this into consideration, it is assumed that the normal impulse is confined to the elliptical impact zone, but the tangential impulse has two components. The first component is confined to the elliptical impact zone, but a second component occurs along the remainder of the plate, rather like a skid, but with no accompanying normal force. There is no attempt to explain this tangential force. It can simply be set to zero to revert to the original model for comparison with the proposed model.

Refer to Figures 3 and 4. A projectile with velocity  $v_0$  impacts a plate at time  $t = 0$ . Normal and tangential components of the velocity are

$$v_{n0} = v_0 \cos \phi \quad \text{and} \quad v_{t0} = v_0 \sin \phi$$

During the time  $0 \leq t \leq t_1$ , normal and tangential forces  $F_n(t)$  and  $F_t(t)$  act on the projectile. Corresponding impulses are  $\mathbf{I}_n$  and  $\mathbf{I}_{t1}$ . At time  $t_1$ , the normal velocity is zero, and tangential velocity is  $v_{t1}$ .

From time  $t_1$  to  $t_2$  it is assumed that the normal force is zero and a tangential force  $F_t^*$  acts on the projectile. At time  $t_2$ , the tangential velocity is  $v_{t2}$ , and the projectile has reached the end of the plate.

### Location of $G$ and determination of radius of gyration

The pendulum was fabricated as a symmetrical system using aluminium bars 2100 mm long, so the centre of gravity,  $G$ , was expected to be near the midpoint of the bars. The radius of gyration with respect to  $G$ ,  $k_G$ , was required to determine moments of inertia, and the periods of oscillation were used to determine  $k_G$  and the precise location of  $G$ .

Refer to Figure 5, which simply shows the bars for convenience. Periods of oscillation were measured with five different pivots. The theoretical period with the pivot  $l_n$  above  $G$  is

$$T_n = 2\pi \sqrt{\frac{\frac{k_G^2}{l_n} + l_n}{g}}$$

For the various pivots, measured periods and corresponding values of  $l_n$  are shown in Figure 5. Lengths  $l_n$  are functions of the unknown  $x$  which is also shown in the figure. A least squares method was used to determine  $k_g$  and  $x$ . Thus

$$\sum_{n=1}^5 \left( g \left( \frac{T_n}{2\pi} \right)^2 - \left( \frac{k_G^2}{l_n} + l_n \right) \right)^2$$

where

$$l_n = 0.030n - 0.006 + x$$

was minimised with respect to the unknowns  $k_G$  and  $x$  giving  $x = 0.0016 \text{ m} = 1.6 \text{ mm}$  and  $k_G = 0.8476 \text{ m}$ . As expected,  $G$  determined using this method is close to the observed balance point. With this value of  $x$ , pivot distances are

$$l_n = 0.030n - 0.0044$$

and the  $n^{\text{th}}$  period becomes

$$T_n = \frac{2\pi}{\sqrt{9.81}} \sqrt{\frac{0.7187}{(0.030n - 0.0044)} + (0.030n - 0.0044)}$$

As the radius of gyration  $k_G$  is important in determining impulses, as a check the periods determined using this formula are compared with the observed periods in the following table, and indicate the accuracy of the formula, and hence  $k_G$ .

$n$	$T_n(\text{observed}) \text{ s}$	$T_n(\text{formula}) \text{ s}$
1	10.64	10.64
2	7.238	7.230
3	5.820	5.843
4	5.054	5.049
5	4.536	4.523



The following were also measured.

Pendulum mass  $M = 3.95$  kg

Projectile mass  $m = 0.00356$  kg

Projectile velocity  $v_0 = 875$  m/s

The projectile velocity was obtained by averaging the velocity of 10 rounds from the same batch used in the tests.

From the pendulum mass and the radius of gyration  $k_G$  the moment of inertia with respect to any pivot could be determined using the parallel axis theorem.

### Summary of equations

A number of equations used in determining impulses are presented without derivation. They are given here mainly for use by the writer. SI units (kg, m) are used. Dimensions  $A$ ,  $R$ ,  $f$ ,  $L$ ,  $h$ ,  $l$  and  $d$  are shown in the figures.  $\omega_0$  is the angular velocity of the pendulum following impact.  $I_O$  is the moment of inertia about the pivot  $O$ .

$$\mathbf{I}_n = mv_0 \sin \phi = mv_{n0} \quad (1)$$

$$\mathbf{I}_t = \mathbf{I}_{t1} + \mathbf{I}_{t2} = mv_0 \cos \phi - mv_{t2} = mv_{t0} - mv_{t2} \quad (2)$$

$$A = 0.016 \sin \phi + d \cos \phi \quad (3)$$

$$R = 1.000 + f - 0.016 \cos \phi + d \sin \phi \quad (4)$$

$$\omega_0 = \frac{1}{I_O} (\mathbf{I}_n \cos \phi A + \mathbf{I}_n \sin \phi R + \mathbf{I}_t ((1.000 + f) \cos \phi - 0.010)) \quad (5)$$

$$h = L \sqrt{\left( \frac{I_O \omega_0^2}{Mgl} \right) - \left( \frac{I_O \omega_0^2}{2Mgl} \right)^2} \quad (6)$$

$$F_t^* = -ma \quad (7)$$

where  $a$  is the acceleration in the tangential direction when  $t_1 \leq t \leq t_2$ , positive in the positive direction of  $v_t$  and the positive direction of  $F_t^*$  is shown in Figure 3.

$$v_{t2}^2 - v_{t1}^2 = 2a(d + 0.08) \quad (8a)$$

$$v_{t2} = \sqrt{v_{t1}^2 + 2a(d + 0.08)} \quad (8b)$$

### Data fitting to determine impulses

With each plate angle (12°, 18°, 24.5°) tests were conducted with three pivot settings (nominally 30 mm, 60 mm and 90 mm). For a given plate setting, the maximum horizontal displacement  $h_i$  and location of the centre of the impact zone,  $d_i$  were measured. The following calculations were carried out using the algebraic language, MAPLE. The resulting algebraic expressions are lengthy, but it should be noted that the programming would be far more complex using an arithmetic language.

Procedure.

- (1) Evaluate  $\mathbf{I}_n$  numerically using equation (1)
- (2) Determine  $\mathbf{I}_t$  in algebraic form using Equation (2) for impact  $i$ , namely.

$$\mathbf{I}_t = mv_{t0} - mv_{t2} = mv_{t0} - m\sqrt{v_{t1}^2 + 2a(d_i + 0.08)} = \mathbf{I}_t(v_{t1}, a) \quad (9)$$

- (3) Determine  $\omega_{0_i} = \omega_{0_i}(v_{t1}, a)$  using Equation (5).

- (4) Determine  $h_i(\text{theory})$  using Equation (6).

- (5) Determine  $h_i(\text{theory}) - h_i(\text{experimental}) = \epsilon_i(v_{t1}, a)$

$\epsilon_i(v_{t1}, a)$  is the difference (error) between the theoretical displacement and experimental displacement for the  $i^{\text{th}}$  round.

- (6) Obtain the sum of the squares of the errors for all rounds

$$E = \sum_i^I (\epsilon_i^2(v_{t1}, a))$$

$I$  is the total number of rounds fired at a plate set at one angle. The expression for  $E$  is very lengthy, and is highly nonlinear in the variables  $v_{t1}$  and  $a$ .

- (7) Minimise  $E$  with respect to the variables  $v_{t1}$  and  $a$ . This minimisation is carried out using Newton-Raphson iteration.

- (8) Calculate

$$\mathbf{I}_{t1} = m(v_{t0} - v_{t1})$$

numerically, and the impulse ratio  $\mathbf{I}_{t1}/\mathbf{I}_n$

(9) Determine  $v_{t2}$  using Equation (8b).  $v_{t2}$  and  $\mathbf{I}_{t2}$  are functions of the impact location  $d$ . To obtain the data fit with the original model, the acceleration  $a$  is simply set to zero before  $E$  is minimised.

### **Preliminary results**

Results for the  $12^\circ$ ,  $18^\circ$  and  $24.5^\circ$  plate are presented graphically in Figures 6, 7 and 8. The graphs show the horizontal displacements  $h$  of the bottom of the pendulum plotted as functions of the impact location  $d$ . Experimental points are shown, together with lines of best fit for the original model (dashed) and the modified model (solid). It is stressed that the best fit lines are based on the single use of all data points, the best fit lines have not been applied to each pivot setting. The modified model appears to fit the experimental data better than the original model, but there is plenty of scatter.

The impulse ratios were the object of the experiment. Values obtained were as follows.

$12^\circ$  plate. Original model  $\mathbf{I}_{t1}/\mathbf{I}_n = 0.263$ , modified model  $\mathbf{I}_{t1}/\mathbf{I}_n = 0.125$

$18^\circ$  plate. Original model  $\mathbf{I}_{t1}/\mathbf{I}_n = 0.418$ , modified model  $\mathbf{I}_{t1}/\mathbf{I}_n = 0.219$

$24.5^\circ$  plate. Original model  $\mathbf{I}_{t1}/\mathbf{I}_n = 0.450$ , modified model  $\mathbf{I}_{t1}/\mathbf{I}_n = 0.202$

Hence the modified method leads to lower ratios, by a factor of about 2.

### **Final comments**

The outcome of these tests is inconclusive, although it is clear the normal impulse is significantly greater than the shear impulse which supports the shot peening proposal.

The graphs show clearly the effect of the impact position on the maximum displacement, but also show that more data are required to support any theory. Additional tests are to be conducted in which more rounds are to be fired at the plate ensuring a wide range of impact zones are included.

**BALLISTIC PENDULUM EXPERIMENTS**  
**SWEET SPOT TESTS AND STANDARD TESTS**  
**REPORT OF TESTS CONDUCTED ON 29-30/10/12**

Bruce Golley

**Summary**

Two series of ballistic pendulum tests were conducted on 29/10/12 and 30/10/12. When the target plate is at shallow angles to the direction of impact, it is possible to locate a point such that the pendulum does not deflect on impact. The location of this point, referred to herein as the sweet spot, enables the ratio of tangential impulse to normal impulse to be determined. In the first series of tests, this point was determined with plate angles of  $14.6^\circ$  and  $19.2^\circ$ . In the second series of tests, tests similar to those detailed in an earlier report were carried out. The first series of tests are considered in detail in this report. As fragmentation of the projectiles in the second series of tests lead to forces on side plates which could not be dealt with theoretically the test results are only treated briefly. The pendulum is being redesigned to eliminate this problem, and further tests are to be carried out.

**Series 1 tests**

This series of tests was conducted as an alternative procedure to determine the impulse ratio  $\rho$ , where

$$\rho = \frac{\mathbf{Imp}_t}{\mathbf{Imp}_n} \quad (1)$$

and  $\mathbf{Imp}_n$  and  $\mathbf{Imp}_t$  are the normal and tangential impulses during impact respectively. The maximum displacement of the pendulum depends on the point of impact, and may be positive, negative or zero. The location of the point of impact where zero displacement

occurs provides a simple method to determine  $\rho$ , and hence the original experimental rig was modified to enable this point to be located. For convenience, the point is referred to as the sweet spot.

A photograph of the modified pendulum is shown in Figure 1, and a schematic drawing is shown in Figure 2.

### Location of G and determination of radius of gyration

The pendulum was fabricated as a symmetrical system using aluminium bars 2100 mm long, so the centre of gravity,  $G$ , was expected to be near the midpoint of the bars. The radius of gyration with respect to  $G$ ,  $k_G$ , was required to determine moments of inertia, and the periods of oscillation were used to determine  $k_G$  and the precise location of  $G$ . Refer to Figure 3, which simply shows the bars for convenience. Periods of oscillation were measured with five different pivots. The theoretical period with the pivot  $l_n$  above  $G$  is

$$T_n = \frac{2\pi}{\sqrt{g}} \sqrt{\frac{k_G^2}{l_n} + l_n} \quad (2)$$

For the various pivots, measured periods and corresponding values of  $l_n$  are shown in Figure 3. Lengths  $l_n$  are functions of the unknown  $x$  which is also shown in the figure. A least squares method was used to determine  $k_G$  and  $x$ . Thus

$$E_1 = \sum_{n=1}^5 \left( T_n - \frac{2\pi}{\sqrt{g}} \sqrt{\frac{k_G^2}{l_n} + l_n} \right)^2 \quad (3)$$

where

$$l_n = 0.030n - 0.006 + x \quad (4)$$

was minimised with respect to the unknowns  $k_G$  and  $x$  using  $g = 9.806 \text{ m/s}^2$ . Solving the nonlinear equations gave  $x = -0.006 \text{ m}$  and  $k_G = 1.015 \text{ m}$ . As expected,  $G$  determined using this method is close to the observed balance point. With this value of  $x$ , pivot distances are

$$l_n = 0.030n - 0.012 \text{ m} \quad (5)$$

and the  $n^{\text{th}}$  period becomes

$$T_n = \frac{2\pi}{\sqrt{9.806}} \sqrt{\frac{1.030}{(0.030n - 0.012)} + (0.030n - 0.012)} \quad (6)$$

As the radius of gyration  $k_G$  is important in determining impulses, as a check the periods determined using this formula are compared with the observed periods in the following table, and indicate the accuracy of the formula, and hence  $k_G$ .

$n$	$T_n(\text{observed}) \text{ s}$	$T_n(\text{formula}) \text{ s}$
1	15.179	15.171
2	9.251	9.303
3	7.333	7.311
4	6.248	6.231
5	5.551	5.531

The following were also measured or were obtained in earlier tests.

Pendulum mass  $M = 8.15 \text{ kg}$

Projectile mass  $m = 0.00356 \text{ kg}$

Projectile velocity  $v_0 = 875 \text{ m/s}$

From the pendulum mass and the radius of gyration  $k_G$  the moment of inertia with respect to any pivot could be determined using the parallel axis theorem.

### Summary of equations

A projectile with initial velocity  $v_0$  and mass  $m$  impacts a plate at an angle  $\phi$  to the horizontal. Following impact, the projectile has velocity  $v_2$ . The post impact velocity is subscripted 2 for historical reasons related to earlier tests in which an intermediate velocity  $v_1$  was considered. During the impact, normal and tangential impulses  $\mathbf{Imp}_n$  and  $\mathbf{Imp}_t$  occur.

A number of equations used in determining impulses are presented without derivation. They are given here mainly for use by the writer. SI units (kg, m) are used. Dimensions  $a, b, f, L, h, l$  and  $d$  are shown in the figures.  $\omega_0$  is the angular velocity of the pendulum

following impact.  $I_O$  is the moment of inertia about the pivot  $O$  and  $I_G$  is the moment of inertia about the centre of gravity  $G$ .

$$I_G = M k_G^2 \quad (7)$$

$$I_O = I_G + M l^2 \quad (8)$$

$$L = 1.050 + f \quad (9)$$

$$\mathbf{Imp}_n = m v_0 \sin \phi \quad (10)$$

$$\mathbf{Imp}_t = m(v_0 \cos \phi - v_2) \quad (11)$$

$$a = 0.016 \sin \phi + d \cos \phi \quad (12)$$

$$b = 1.000 + f - 0.016 \cos \phi + d \sin \phi \quad (13)$$

$$\mathbf{Imp}_O = \mathbf{Imp}_n a \cos \phi + \mathbf{Imp}_n b \sin \phi + \mathbf{Imp}_t b \cos \phi - \mathbf{Imp}_t a \sin \phi \quad (14)$$

$$\omega_0 = \mathbf{Imp}_O / I_O \quad (15)$$

$$\text{maximum KE} = KE_{\max} = \frac{1}{2} I_O \omega_0^2 \quad (16)$$

$$\text{maximum PE} = PE_{\max} = M g l \left( 1 - \sqrt{1 - \left( \frac{h}{L} \right)^2} \right) \quad (17)$$

During the tests, the lowest pivot was used to maximise displacements  $h$ , and so  $f = 0.024$  in the tests, in addition to the values  $M$ ,  $m$ ,  $v_0$ ,  $k_G$  and  $x$  already noted.

Equating  $KE_{\max}$  and  $PE_{\max}$  and with appropriate substitutions the maximum horizontal displacement  $h$  can be expressed in terms of the impact distance  $d$ , the velocity  $v_2$  and plate angle  $\phi$ . For a given value of  $\phi$ ,  $h$  is then expressed as a function of  $d$  and  $v_2$ , ie

$$h = h(d, v_2) \quad (18)$$

For a given plate angle  $\phi$  with  $N$  projectile impacts there are  $N$  pairs of data points  $(d_n, h_n)$ .

These data points are fitted to the theoretical function  $h = h(d, v_2)$  by minimising

$$E_2 = \sum_{n=1}^N (h(d_n, v_2) - h_n)^2 \quad (19)$$

with respect to  $v_2$ . Having determined  $v_2$  in this manner, the theoretical function becomes  $h = h(d)$  the value  $d = d_s$  locating the sweet spot is obtained by solving

$$h(d_s) = 0 \quad (20)$$

$\mathbf{Imp}_t$  is obtained using Equation (11). As  $\mathbf{Imp}_n$  is known from Equation (10) the required impulse ratio is determined. Alternatively, having determined  $d_s$ , the impulse ratio may be determined geometrically by noting the line of action of the resultant impulse passes through the pivot when the point of impact is the sweet spot. Thus referring to Figure 4, having located  $S$  the impulse ratio is

$$\frac{\mathbf{Imp}_t}{\mathbf{Imp}_n} = \frac{-d_s - 1.024 \sin \phi}{1.024 \cos \phi - 0.016} \quad (21)$$

### Series 1 results

Plate angles were measured using a digital spirit level. In the first test, the plate angle was  $14.6^\circ$  and fifteen rounds were fired. In the second test, the plate angle was  $21.8^\circ$  and thirteen rounds were fired. For future reference, the data pairs  $(d_n, h_n)$  are given in Appendix A. The data pairs are show graphically in Figures 5 and 6, together with the lines of best fit obtained by the minimisation procedure discussed above. The tangential component of  $v_0$ ,  $v_{t0} = v_0 \cos \phi$ , was also evaluated for comparison with  $v_2$ . Reduced results for the two tests are given in the Table 1.

T

able 1. Results for Series 1 tests

plate angle $\phi$	$14.6^\circ$	$21.8^\circ$
$d_s$ m	-0.324	-0.432
$v_2$ m/s <sup>2</sup>	832	794
$v_{t0}$ m/s <sup>2</sup>	847	812
$\frac{\mathbf{Imp}_t}{\mathbf{Imp}_n}$ Method 1	0.0678	0.0558
$\frac{\mathbf{Imp}_t}{\mathbf{Imp}_n}$ Method 1	0.0676	0.0553



## Series 2 tests

In this series of tests, the procedure followed and pendulum used were the same as detailed in an earlier report, “Ballistic pendulum experiment, modified equations following tests 30-31/08/12” by the writer. The pendulum is shown schematically in Figure 7. Properties of the pendulum were

$$M = 3.95 \text{ kg}$$

$$k_G = 0.8476 \text{ m}$$

$$x = 0.0016 \text{ m}$$

$$g = 9.803 \text{ m/s}^2$$

$$m = 0.00356 \text{ kg}$$

Nine tests were conducted, with plate angles  $12.8^\circ$ ,  $17.9^\circ$  and  $22.8^\circ$ . With each angle, pivots were set with  $f = 0.024 \text{ m}$ ,  $f = 0.054 \text{ m}$  and  $f = 0.084 \text{ m}$ . The theoretical relationship between  $h$  and  $d$  was also determined using the impulse ratio  $\rho = 0.06$ , which is approximately the average of the two values obtained in Series 1 tests. The results are presented graphically in Figures 8, 9 and 10. The theoretical relationship in each case is the solid line are drawn between two points evaluated at  $d = -80 \text{ mm}$  and  $d = 80 \text{ mm}$ , which are points at the extremes of the  $160 \text{ mm} \times 60 \text{ mm}$  target plate.

During testing, it was observed that due to fragmentation of the projectiles, forces in addition to those in the elliptical impact area appeared to arise, as the welds holding light webs used to fix the impacted plate had been polished by fragments. Thus the tests to determine the impulse ratio using the original equipment involved additional unknown forces. However, these forces do not arise with impacts near the plate end where  $d = -80 \text{ mm}$ . From the graphs, the theoretical relationship appears quite close to the experimental results where  $d = -80 \text{ mm}$  with considerable divergence as the impact moves from that edge, which is consistent with the addition force due to some lateral fragmentation.

The pendulum has been modified to eliminate any forces due to lateral fragmentation and further testing is to be conducted. Thus no further work is currently being carried out on the data obtained in Series 2 tests.

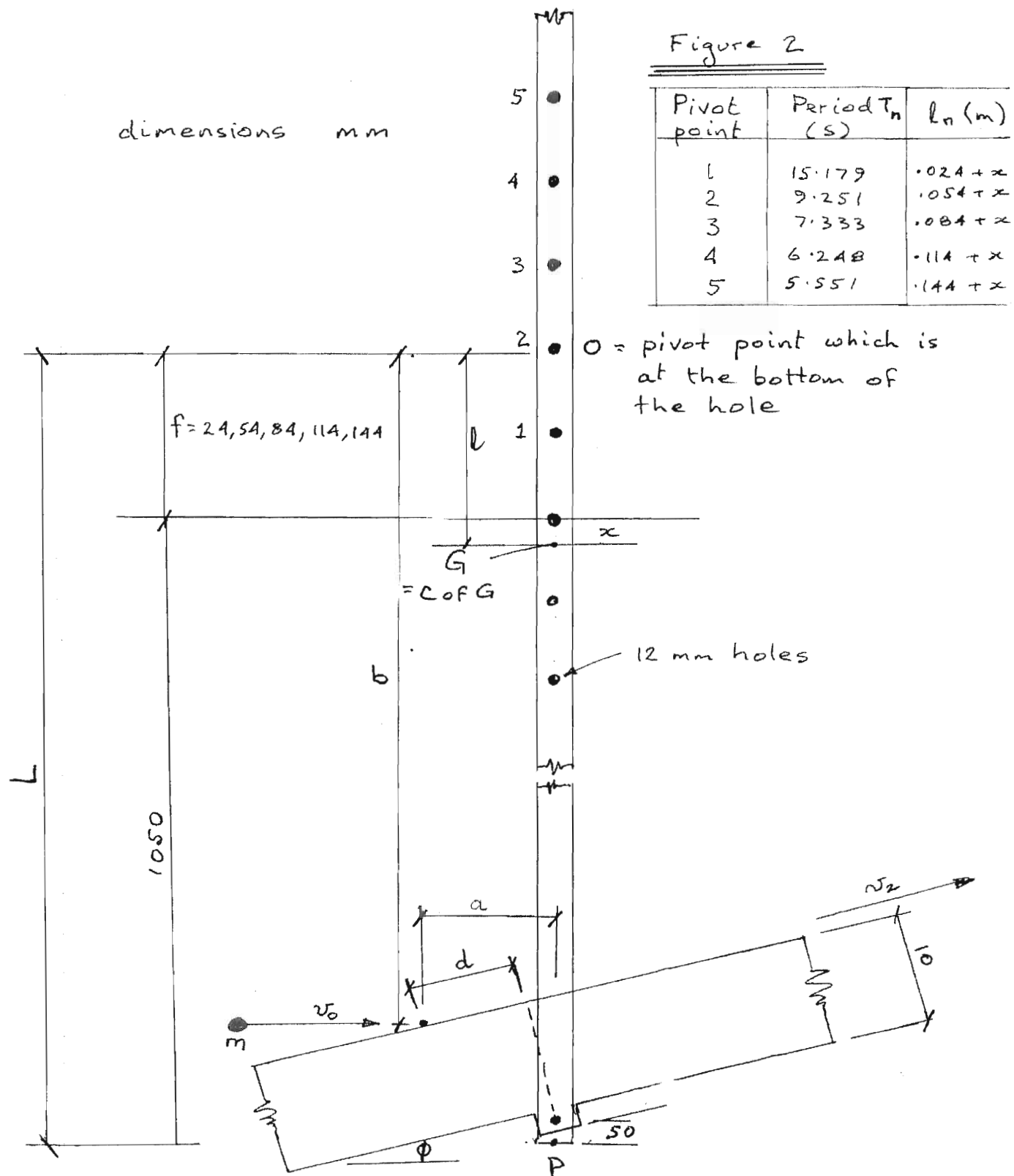
## Appendix A Series 1 test results

Table A1. Results for 14.6° plate

$n$	$d_n$ mm	$h_n$ mm
1	-605	-75
2	-590	-55
3	-580	-58
4	-525	-31
5	-500	-45
6	-465	-38
7	-410	-30
8	-385	-10
9	-360	-20
10	-335	5
11	-310	8
12	-305	0
13	-245	23
14	-235	18
15	-220	15

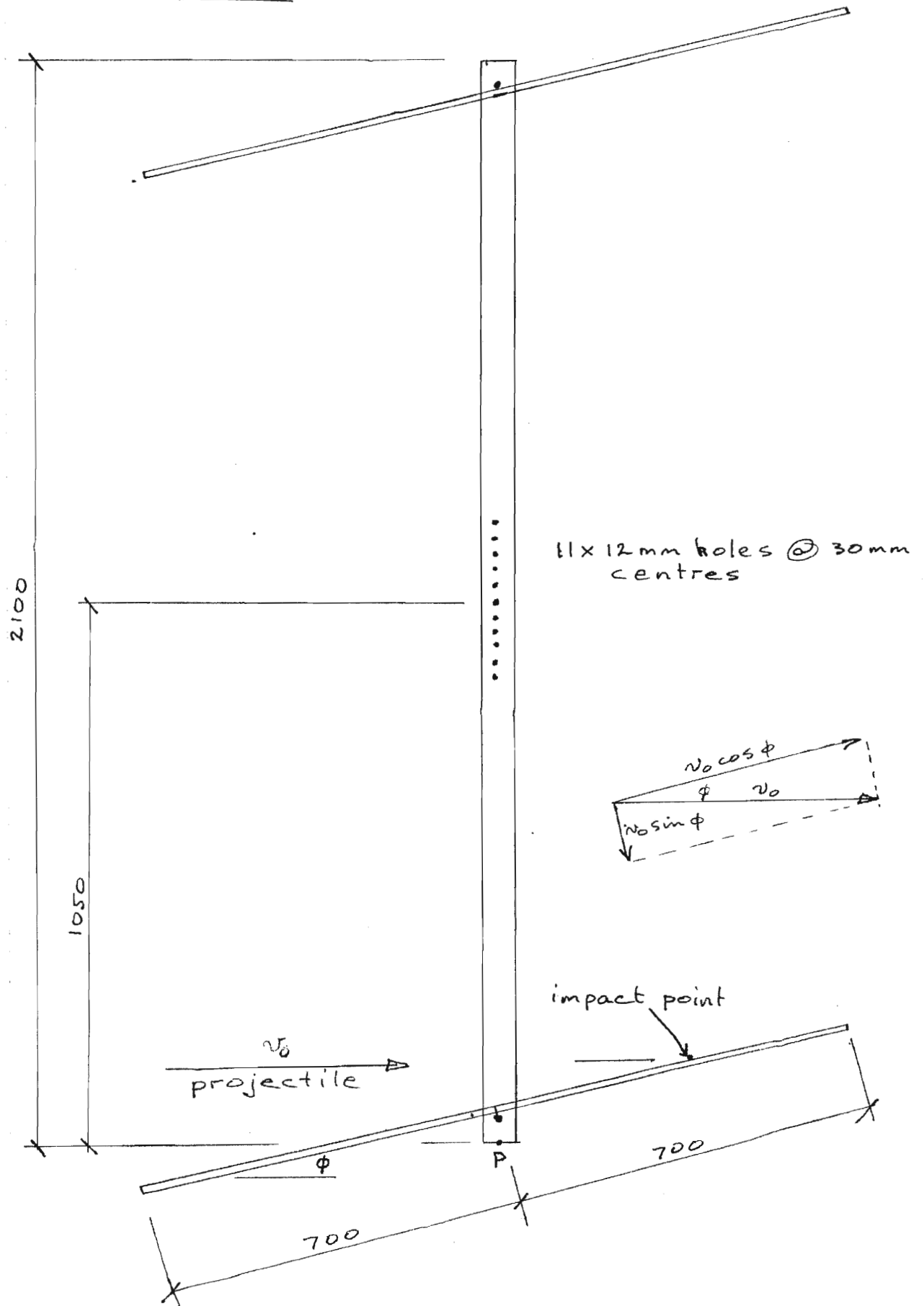
Table A2 Results for 21.8° plate

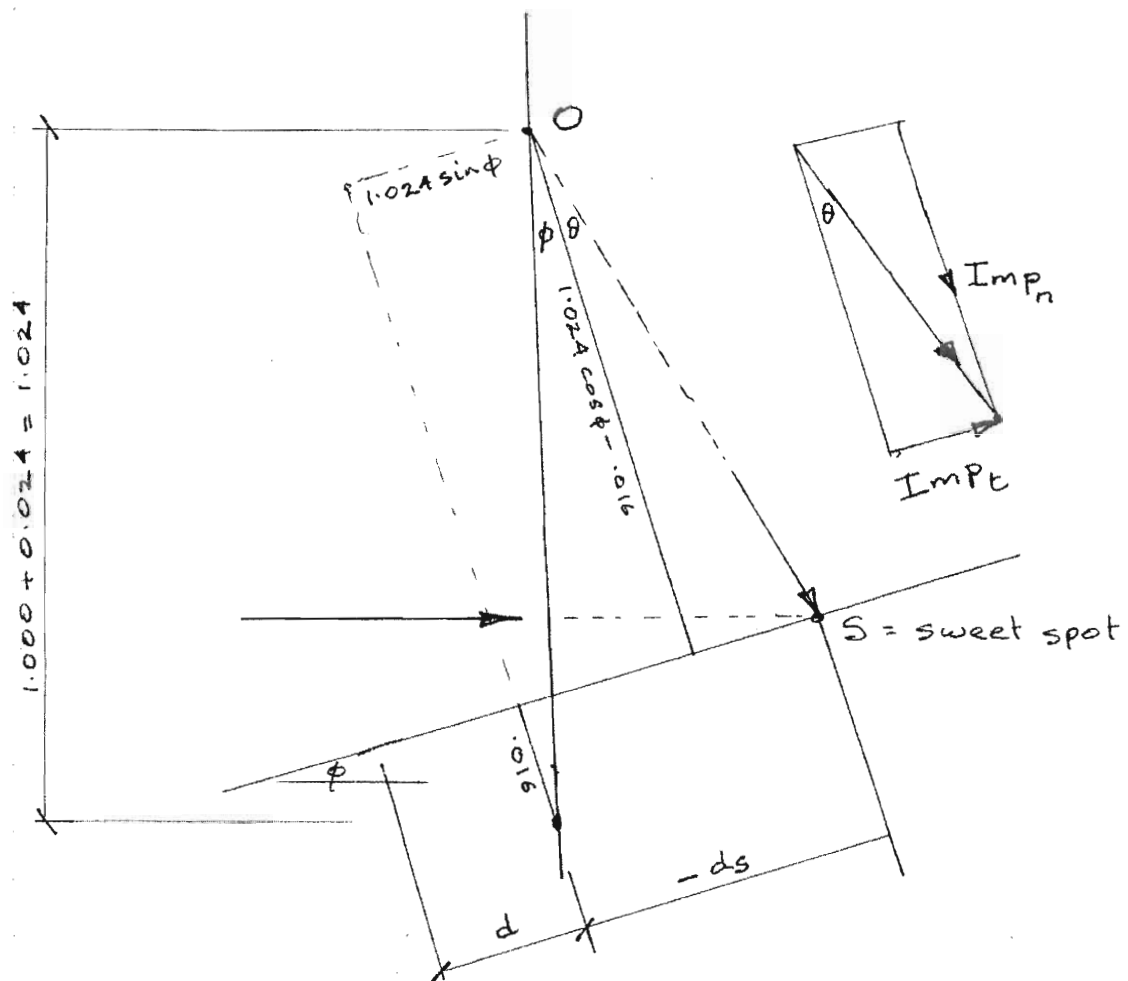
$n$	$d_n$ mm	$h_n$ mm
1	-610	-55
2	-580	-55
3	-580	-45
4	-570	-40
5	-510	-20
6	-505	-23
7	-480	-12
8	-410	-5
9	-395	10
10	-385	17
11	-335	28
12	-320	33
13	-300	39



The maximum horizontal displacement of P following impact is measured,  $= h$

Figure 3





$$\frac{Imp_t}{Imp_n} = \tan \theta = \frac{-ds - 1.024 \sin \phi}{1.024 \cos \phi - 0.016}$$

Figure 4

Figure 5

14.6° Plate

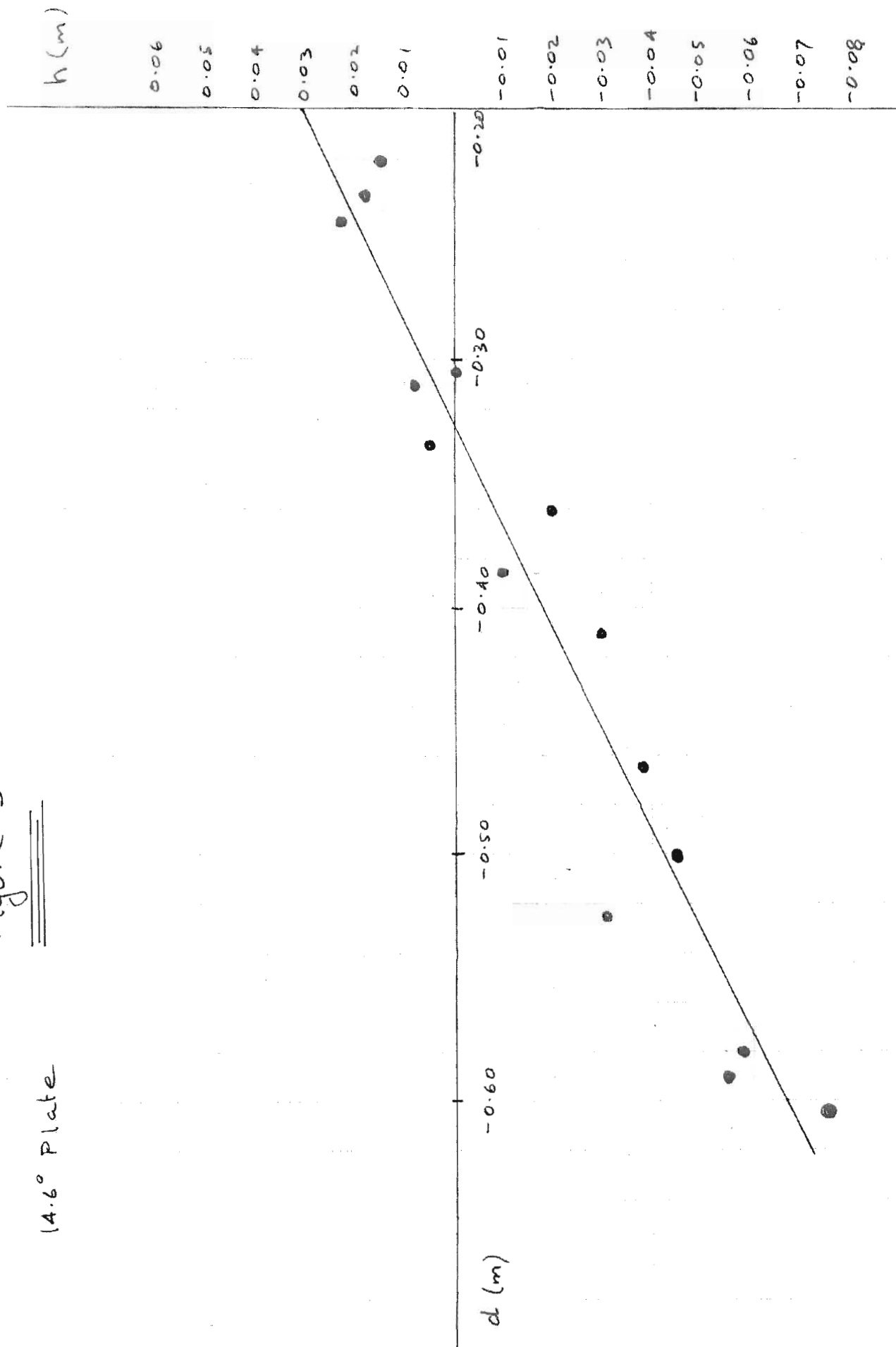


Figure 6

21.8° Plate

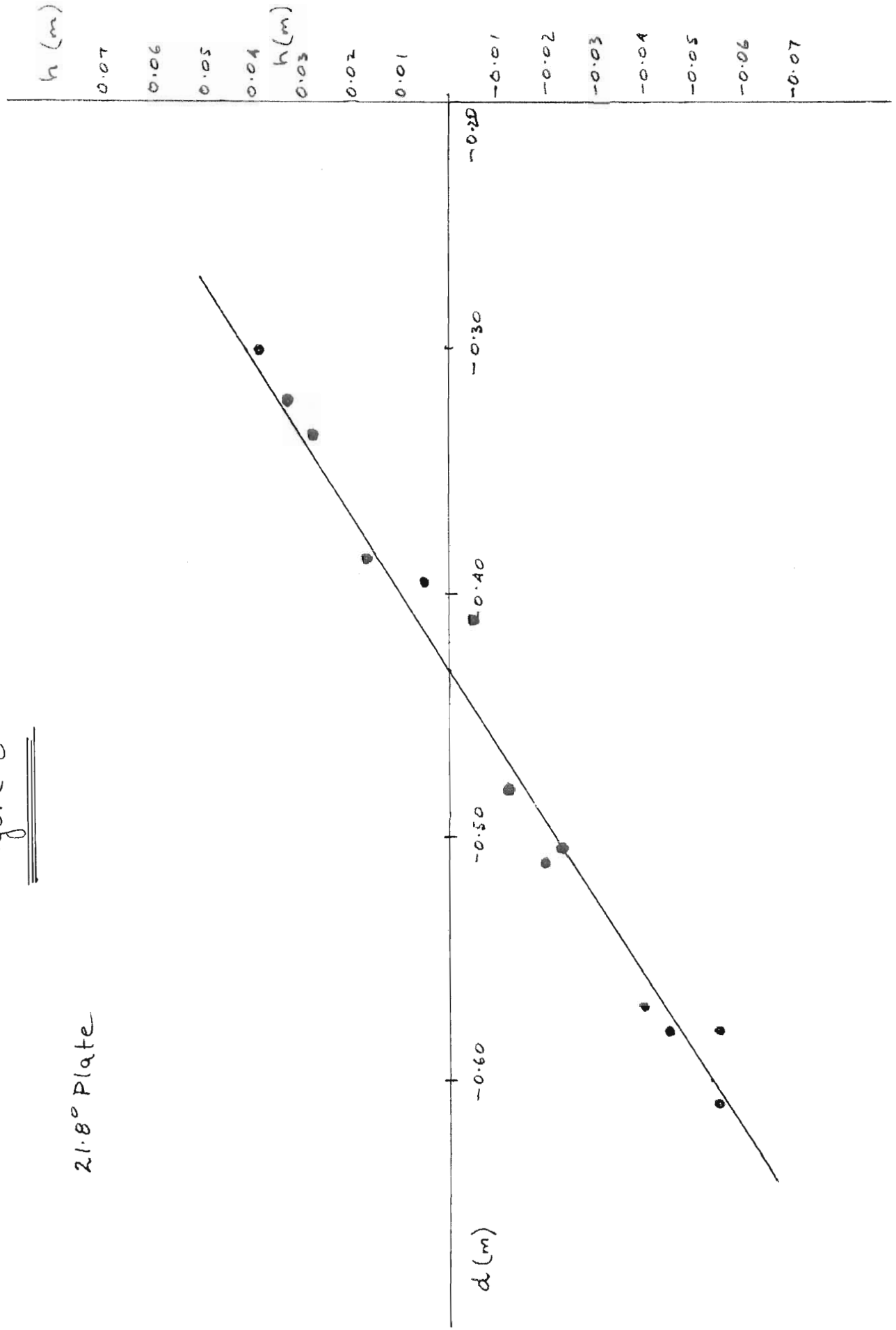






Figure 8

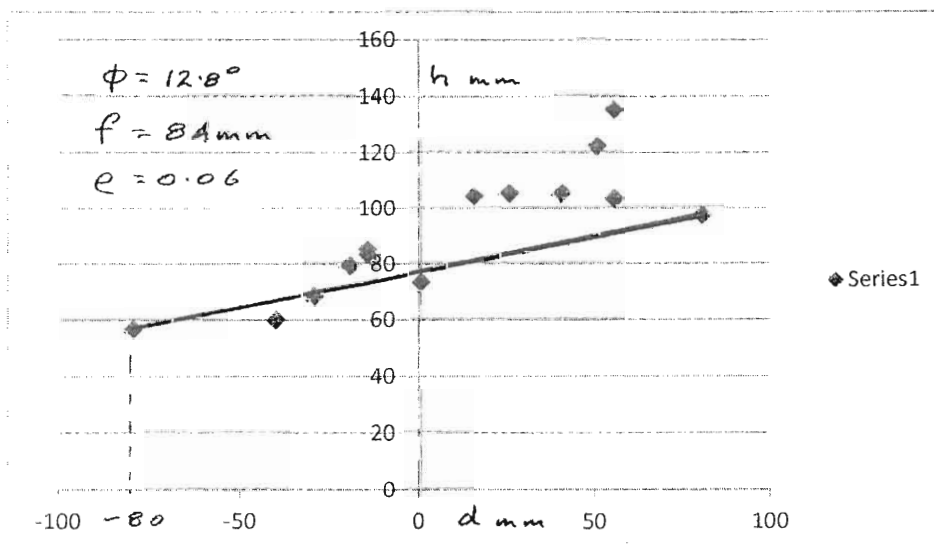
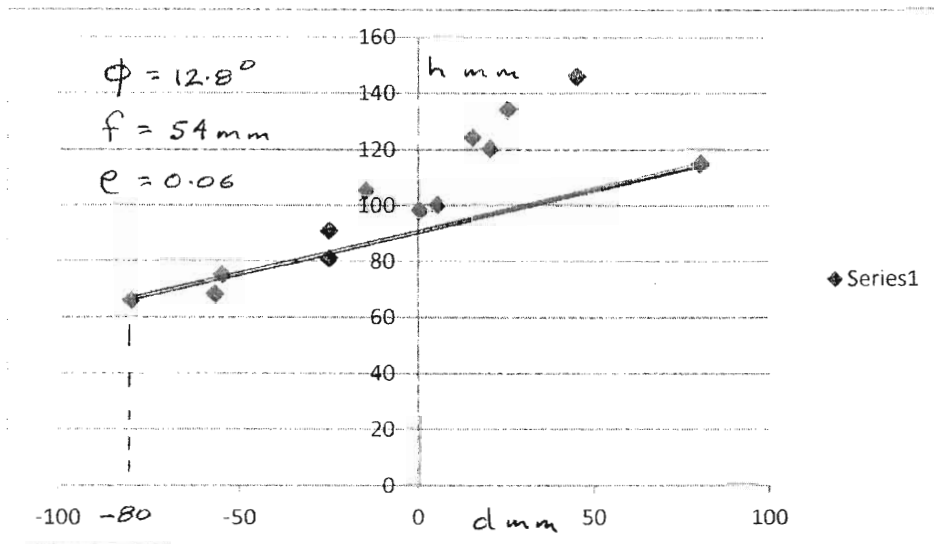
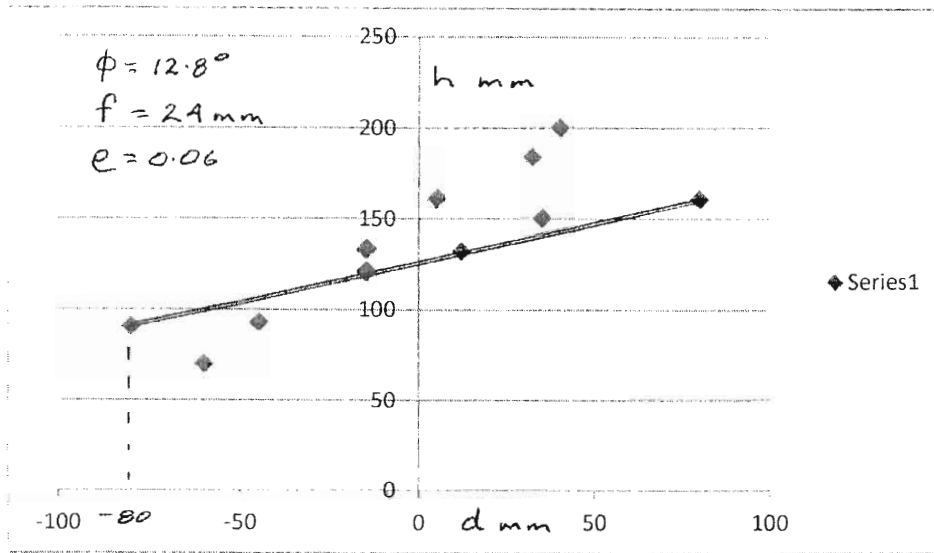


Figure 9

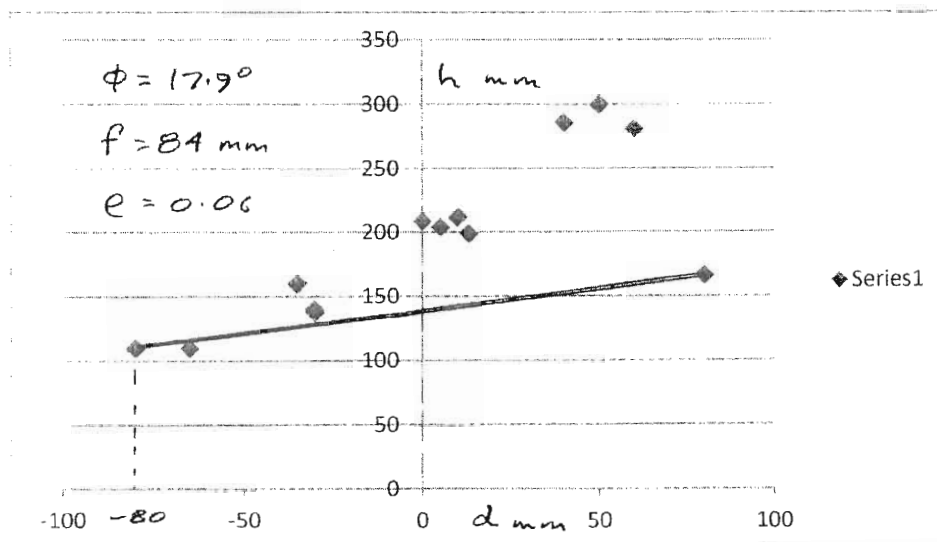
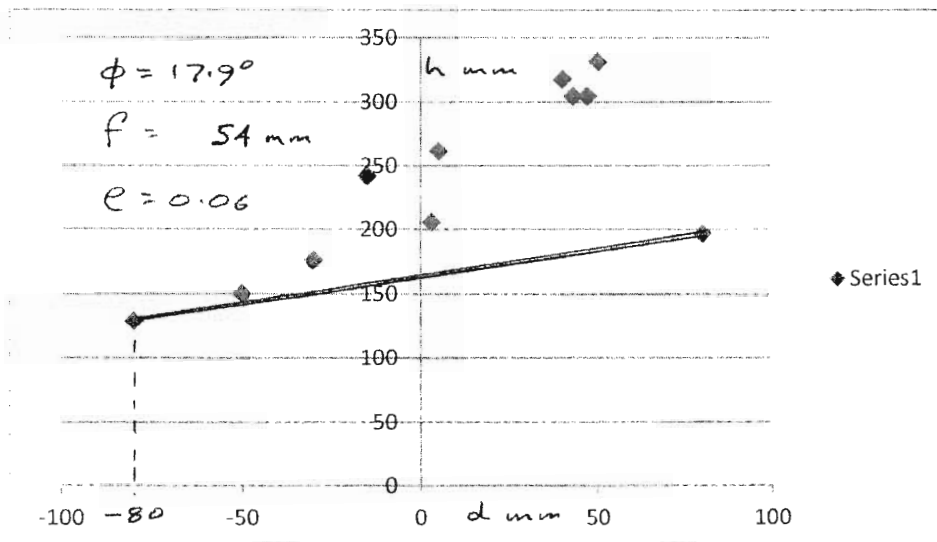
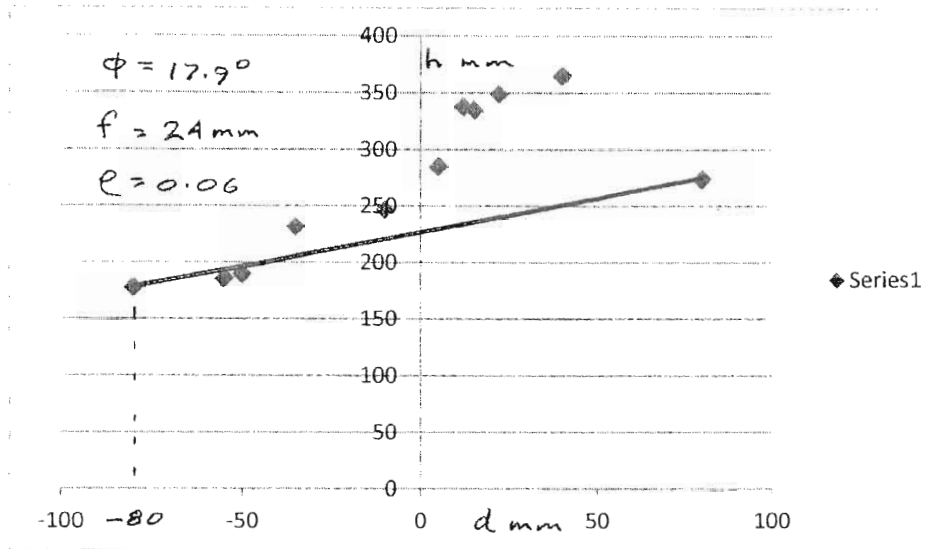
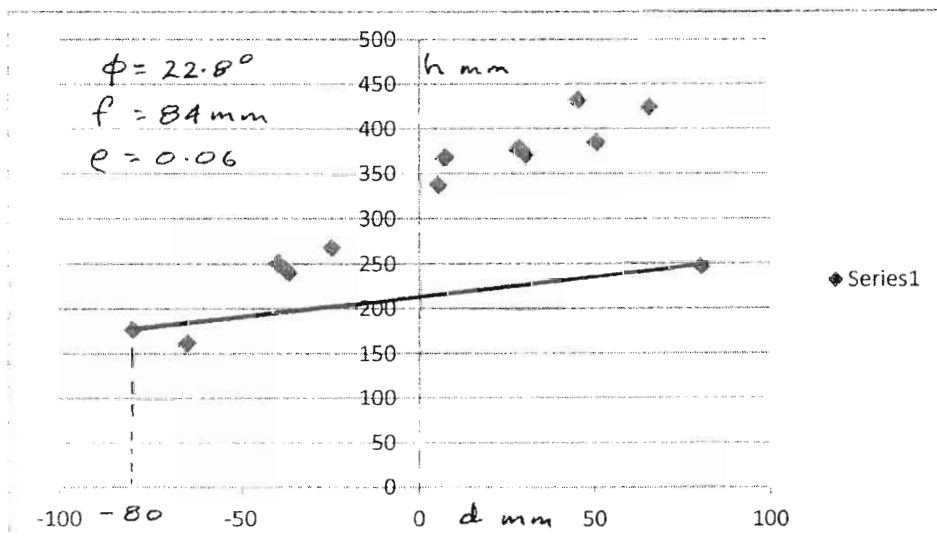
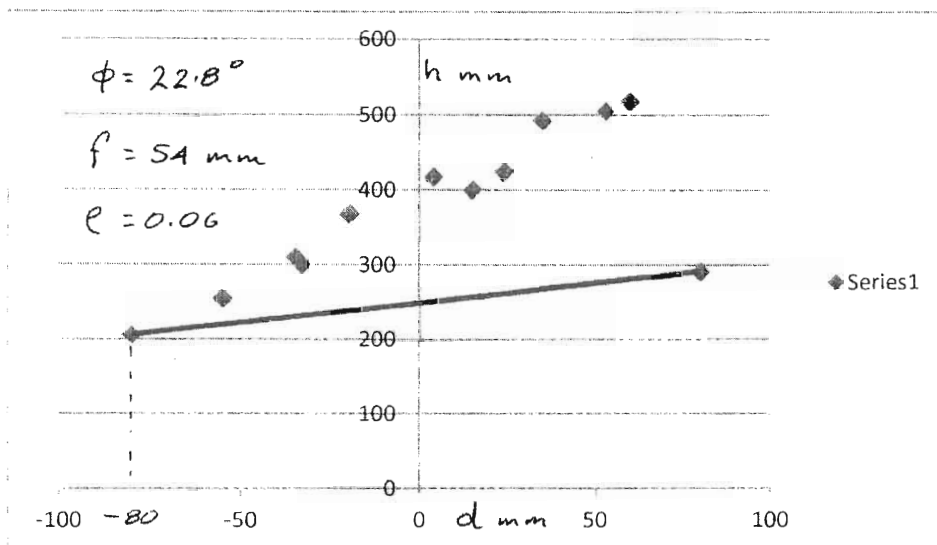
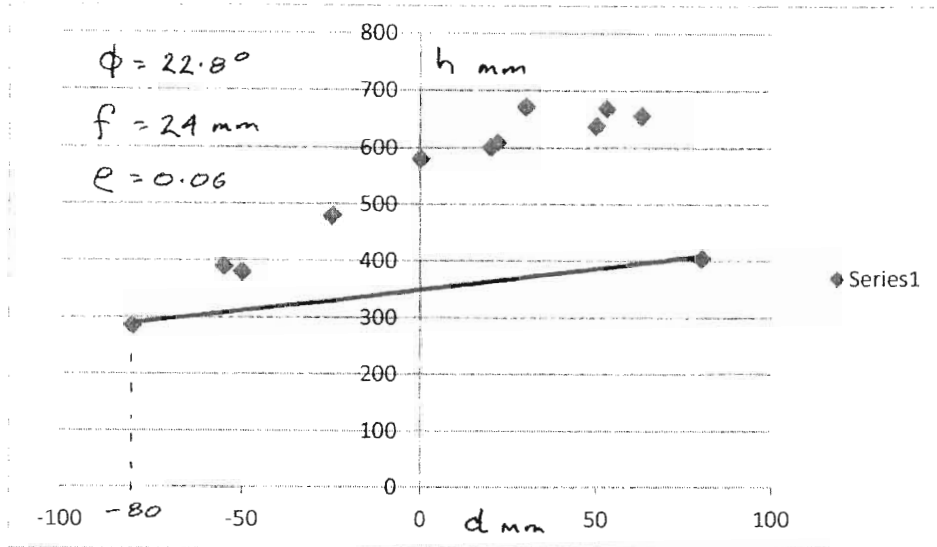


Figure 10



# **BALLISTIC PENDULUM EXPERIMENTS**

## **REPORT OF TESTS CONDUCTED ON 29-30/10/12**

Bruce Golley

### **Introduction**

Two series of ballistic pendulum tests were conducted on 29-30/10/12. The first series of tests are referred to as the sweet spot tests. The second series of tests were similar to those detailed in an earlier report. The sweet spot tests are considered in detail in this report. However only preliminary details of the second series of tests are included. The initial theoretical model of a ballistic pendulum was based on the normal and tangential impulses being applied at the centre of a roughly elliptical area where ink had been erased from the plate during impact. The theoretical response based on this assumption did not provide a satisfactory correlation with the initial experimental results, as shown herein. The experimental results showed the effect of impact position on the plate was much greater than the original theory predicted and a modified theory was developed in which the tangential impulse was related to the impact position on the plate. As fragmentation of the projectiles lead to forces on side plates which could not be dealt with theoretically, the pendulum was modified and an additional series of tests was conducted on 06-07/12/12. Details of the modified theoretical model using data from the tests on both 06-07/12/12 and 29-30/10/12 are treated in a separate report.

### **Series 1 tests**

This series of tests was conducted as an alternative procedure to determine the impulse ratio  $\rho$ , where

$$\rho = \frac{\text{Imp}_t}{\text{Imp}_n} \quad (1)$$

and  $\mathbf{Imp}_n$  and  $\mathbf{Imp}_t$  are the normal and tangential impulses during impact respectively. The maximum displacement of the pendulum depends on the point of impact, and may be positive, negative or zero. The location of the point of impact where zero displacement occurs provides a simple method to determine  $\rho$ , and hence the original experimental rig was modified to enable this point to be located. For convenience, the point is referred to as the sweet spot.

A photograph of the modified pendulum is shown in Figure 1, and a schematic drawing is shown in Figure 2.

### Location of G and determination of radius of gyration

The pendulum was fabricated as a symmetrical system using aluminium bars 2100 mm long, so the centre of gravity,  $G$ , was expected to be near the midpoint of the bars. The radius of gyration with respect to  $G$ ,  $k_G$ , was required to determine moments of inertia, and the periods of oscillation were used to determine  $k_G$  and the precise location of  $G$ . Refer to Figure 3, which simply shows the bars for convenience. Periods of oscillation were measured with five different pivots. The theoretical period with the pivot  $l_n$  above  $G$  is

$$T_n = \frac{2\pi}{\sqrt{g}} \sqrt{\frac{k_G^2}{l_n} + l_n} \quad (2)$$

For the various pivots, measured periods and corresponding values of  $l_n$  are shown in Figure 3. Lengths  $l_n$  are functions of the unknown  $x$  which is also shown in the figure. A least squares method was used to determine  $k_G$  and  $x$ . Thus

$$E_1 = \sum_{n=1}^5 \left( T_n - \frac{2\pi}{\sqrt{g}} \sqrt{\frac{k_G^2}{l_n} + l_n} \right)^2 \quad (3)$$

where

$$l_n = 0.030n - 0.006 + x \quad (4)$$

was minimised with respect to the unknowns  $k_G$  and  $x$  using  $g = 9.806 \text{ m/s}^2$ . Solving the nonlinear equations gave  $x = -0.006 \text{ m}$  and  $k_G = 1.015 \text{ m}$ . As expected,  $G$  determined using this method is close to the observed balance point. With this value of  $x$ , pivot

distances are

$$l_n = 0.030n - 0.012 \text{ m} \quad (5)$$

and the  $n^{\text{th}}$  period becomes

$$T_n = \frac{2\pi}{\sqrt{9.806}} \sqrt{\frac{1.030}{(0.030n - 0.012)} + (0.030n - 0.012)} \quad (6)$$

As the radius of gyration  $k_G$  is important in determining impulses, as a check the periods determined using this formula are compared with the observed periods in the following table, and indicate the accuracy of the formula, and hence  $k_G$ .

$n$	$T_n(\text{observed}) \text{ s}$	$T_n(\text{formula}) \text{ s}$
1	15.179	15.171
2	9.251	9.303
3	7.333	7.311
4	6.248	6.231
5	5.551	5.531

The following were also measured or were obtained in earlier tests.

Pendulum mass  $M = 8.15 \text{ kg}$

Projectile mass  $m = 0.00356 \text{ kg}$

Projectile velocity  $v_0 = 875 \text{ m/s}$

From the pendulum mass and the radius of gyration  $k_G$  the moment of inertia with respect to any pivot could be determined using the parallel axis theorem.

### Summary of equations

A projectile with initial velocity  $v_0$  and mass  $m$  impacts a plate at an angle  $\phi$  to the horizontal. Following impact, the projectile has velocity  $v_2$ . The post impact velocity is subscripted 2 for historical reasons related to earlier tests in which an intermediate velocity  $v_1$  was considered. During the impact, normal and tangential impulses  $\mathbf{Imp}_n$  and  $\mathbf{Imp}_t$  occur.

A number of equations used in determining impulses are presented without derivation. They are given here mainly for use by the writer. SI units (kg, m) are used. Dimensions

$a$ ,  $b$ ,  $f$ ,  $L$ ,  $h$ ,  $l$  and  $d$  are shown in the figures.  $\omega_0$  is the angular velocity of the pendulum following impact.  $I_O$  is the moment of inertia about the pivot  $O$  and  $I_G$  is the moment of inertia about the centre of gravity  $G$ .

$$I_G = M k_G^2 \quad (7)$$

$$I_O = I_G + M l^2 \quad (8)$$

$$L = 1.050 + f \quad (9)$$

$$\mathbf{Imp}_n = m v_0 \sin \phi \quad (10)$$

$$\mathbf{Imp}_t = m(v_0 \cos \phi - v_2) \quad (11)$$

$$a = 0.016 \sin \phi + d \cos \phi \quad (12)$$

$$b = 1.000 + f - 0.016 \cos \phi + d \sin \phi \quad (13)$$

$$\mathbf{Imp}_O = \mathbf{Imp}_n a \cos \phi + \mathbf{Imp}_n b \sin \phi + \mathbf{Imp}_t b \cos \phi - \mathbf{Imp}_t a \sin \phi \quad (14)$$

$$\omega_0 = \mathbf{Imp}_O / I_O \quad (15)$$

$$\text{maximum KE} = KE_{\max} = \frac{1}{2} I_O \omega_0^2 \quad (16)$$

$$\text{maximum PE} = PE_{\max} = M g l \left( 1 - \sqrt{1 - \left( \frac{h}{L} \right)^2} \right) \quad (17)$$

During the tests, the lowest pivot was used to maximise displacements  $h$ , and so  $f = 0.024$  in the tests, in addition to the values  $M$ ,  $m$ ,  $v_0$ ,  $k_G$  and  $x$  already noted.

Equating  $KE_{\max}$  and  $PE_{\max}$  and with appropriate substitutions the maximum horizontal displacement  $h$  can be expressed in terms of the impact distance  $d$ , the velocity  $v_2$  and plate angle  $\phi$ . For a given value of  $\phi$ ,  $h$  is then expressed as a function of  $d$  and  $v_2$ , ie

$$h = h(d, v_2) \quad (18)$$

For a given plate angle  $\phi$  with  $N$  projectile impacts there are  $N$  pairs of data points  $(d_n, h_n)$ . These data points are fitted to the theoretical function  $h = h(d, v_2)$  by minimising

$$E_2 = \sum_{n=1}^N (h(d_n, v_2) - h_n)^2 \quad (19)$$



with respect to  $v_2$ . Having determined  $v_2$  in this manner, the theoretical function becomes  $h = h(d)$  the value  $d = d_s$  locating the sweet spot is obtained by solving

$$h(d_s) = 0 \quad (20)$$

$\text{Imp}_t$  is obtained using Equation (11). As  $\text{Imp}_n$  is known from Equation (10) the required impulse ratio is determined. Alternatively, having determined  $d_s$ , the impulse ratio may be determined geometrically by noting the line of action of the resultant impulse passes through the pivot when the point of impact is the sweet spot. Thus referring to Figure 4, having located  $S$  the impulse ratio is

$$\frac{\text{Imp}_t}{\text{Imp}_n} = \frac{-d_s - 1.024 \sin \phi}{1.024 \cos \phi - 0.016} \quad (21)$$

### Series 1 results

Plate angles were measured using a digital spirit level. In the first test, the plate angle was  $14.6^\circ$  and fifteen rounds were fired. In the second test, the plate angle was  $21.8^\circ$  and thirteen rounds were fired. For future reference, the data pairs  $(d_n, h_n)$  are given in Appendix A. The data pairs are show graphically in Figures 5 and 6, together with the lines of best fit obtained by the minimisation procedure discussed above. The tangential component of  $v_0$ ,  $v_{t0} = v_0 \cos \phi$ , was also evaluated for comparison with  $v_2$ . Reduced results for the two tests are given in Table 1.

Table 1. Results for Series 1 tests

plate angle $\phi$	$14.6^\circ$	$21.8^\circ$
$d_s$ m	-0.324	-0.432
$v_2$ m/s <sup>2</sup>	832	794
$v_{t0}$ m/s <sup>2</sup>	847	812
$\frac{\text{Imp}_t}{\text{Imp}_n}$ Method 1	0.0678	0.0558
$\frac{\text{Imp}_t}{\text{Imp}_n}$ Method 2	0.0676	0.0553

## Series 2 tests

In this series of tests, the procedure followed and pendulum used were the same as detailed in the report, “Ballistic pendulum experiment, modified equations following tests 30-31/08/12” by the writer. The pendulum is shown schematically in Figure 7. Properties of the pendulum were

$$M = 3.95 \text{ kg}$$

$$k_G = 0.8476 \text{ m}$$

$$x = 0.0016 \text{ m}$$

$$g = 9.803 \text{ m/s}^2$$

$$m = 0.00356 \text{ kg}$$

Nine tests were conducted, with plate angles  $12.8^\circ$ ,  $17.9^\circ$  and  $22.8^\circ$ . With each angle, pivots were set with  $f = 0.024 \text{ m}$ ,  $f = 0.054 \text{ m}$  and  $f = 0.084 \text{ m}$ . The theoretical relationship between  $h$  and  $d$  was also determined using the impulse ratio  $\rho = 0.06$ , which is approximately the average of the two values obtained in Series 1 tests. The results are presented graphically in Figures 8, 9 and 10. The theoretical relationship in each case is the solid line drawn between two points evaluated at  $d = -80 \text{ mm}$  and  $d = 80 \text{ mm}$ , which are points at the extremes of the  $160 \text{ mm} \times 60 \text{ mm}$  target plate. Except near the upper edge of the plate where  $d = -80 \text{ mm}$  the agreement between the theoretical relationship and the observed values is poor.

During testing, it was observed that due to fragmentation of the projectiles, forces in addition to those in the elliptical impact area appeared to arise, as the welds holding light webs used to fix the impacted plate had been polished by fragments. Thus the tests to determine the impulse ratio using the original equipment involved additional unknown forces. However, these forces do not arise with impacts near the plate end where  $d = -80 \text{ mm}$ . From the graphs, the theoretical relationship appears quite close to the experimental re-

sults where  $d = -80$  mm with considerable divergence as the impact moves from that edge, which is consistent with the addition force due to some lateral fragmentation.

The pendulum was modified to eliminate any forces due to fragmentation of the projectile impacting the webs and further testing was conducted on 06-07/12/12. The results from Series 2 tests and those from the tests on 06-07/12/12 are treated in detail, together with a modified model in a later report, "Ballistic pendulum experiments, Report of tests conducted on 29-30/10/12 and 06-07/12/12 by the writer.

### **Conclusions**

The results of the tests in Series 2 showed that the original theoretical model ignored some force associated with the impact position on the plate. It appeared that a tangential force that increased with increasing distance of the impact point from the top edge of the plate arose, and this lead to a modified model being suggested. As the impact locations had not been recorded during the sweet spot tests, this places some doubt on the accuracy of the impact ratios obtained for the two angles considered. However the low ratios of  $\mathbf{Imp}_t/\mathbf{Imp}_n$  determined in those tests, 0.0678 and 0.0555 for the  $14.6^\circ$  and  $21.8^\circ$  plates respectively indicate that the normal force is much larger than the transverse force, and thus the normal stress during impact is much greater than the shear stress.

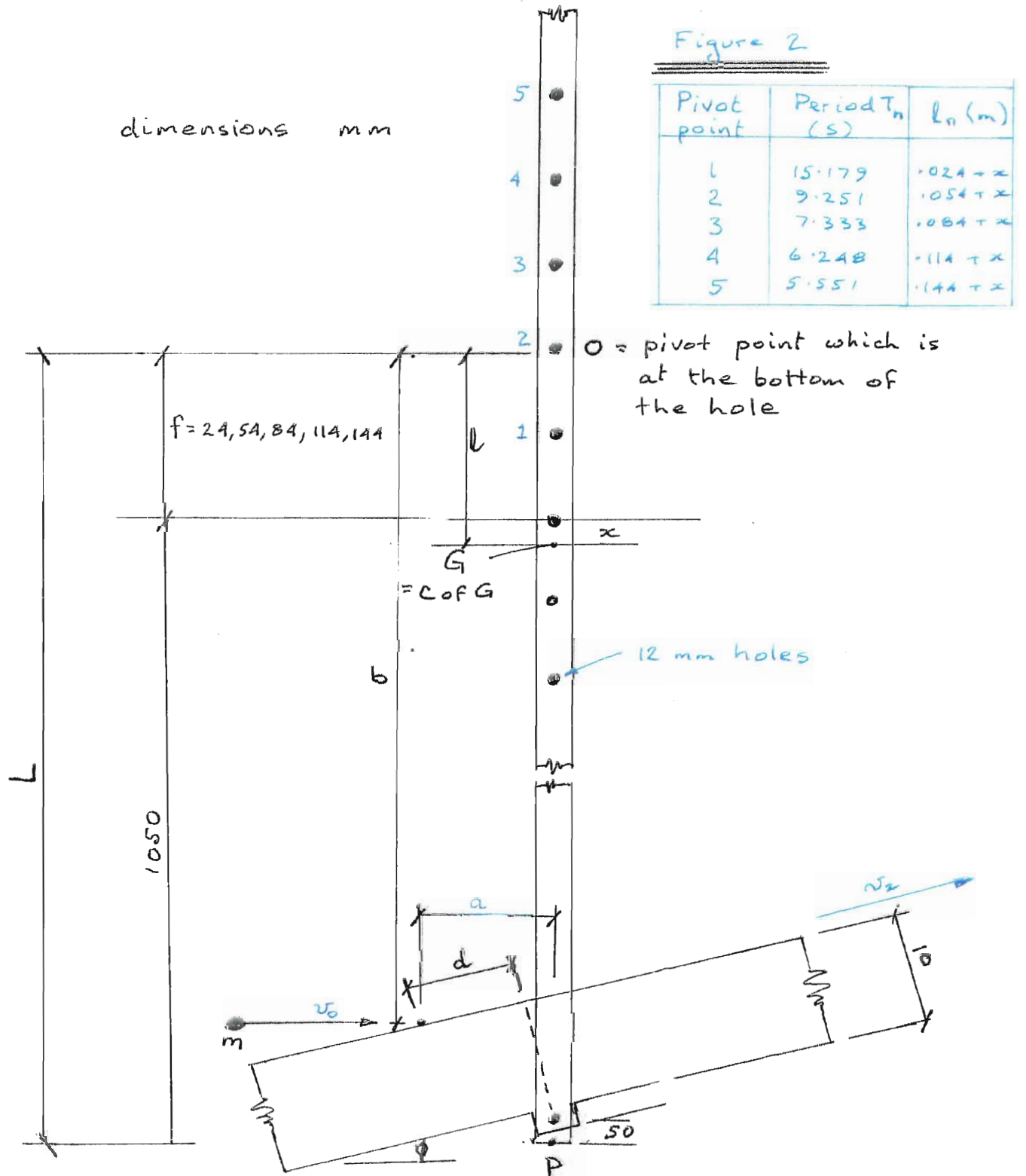
## Appendix A Series 1 test results

Table A1. Results for 14.6° plate

$n$	$d_n$ mm	$h_n$ mm
1	-605	-75
2	-590	-55
3	-580	-58
4	-525	-31
5	-500	-45
6	-465	-38
7	-410	-30
8	-385	-10
9	-360	-20
10	-335	5
11	-310	8
12	-305	0
13	-245	23
14	-235	18
15	-220	15

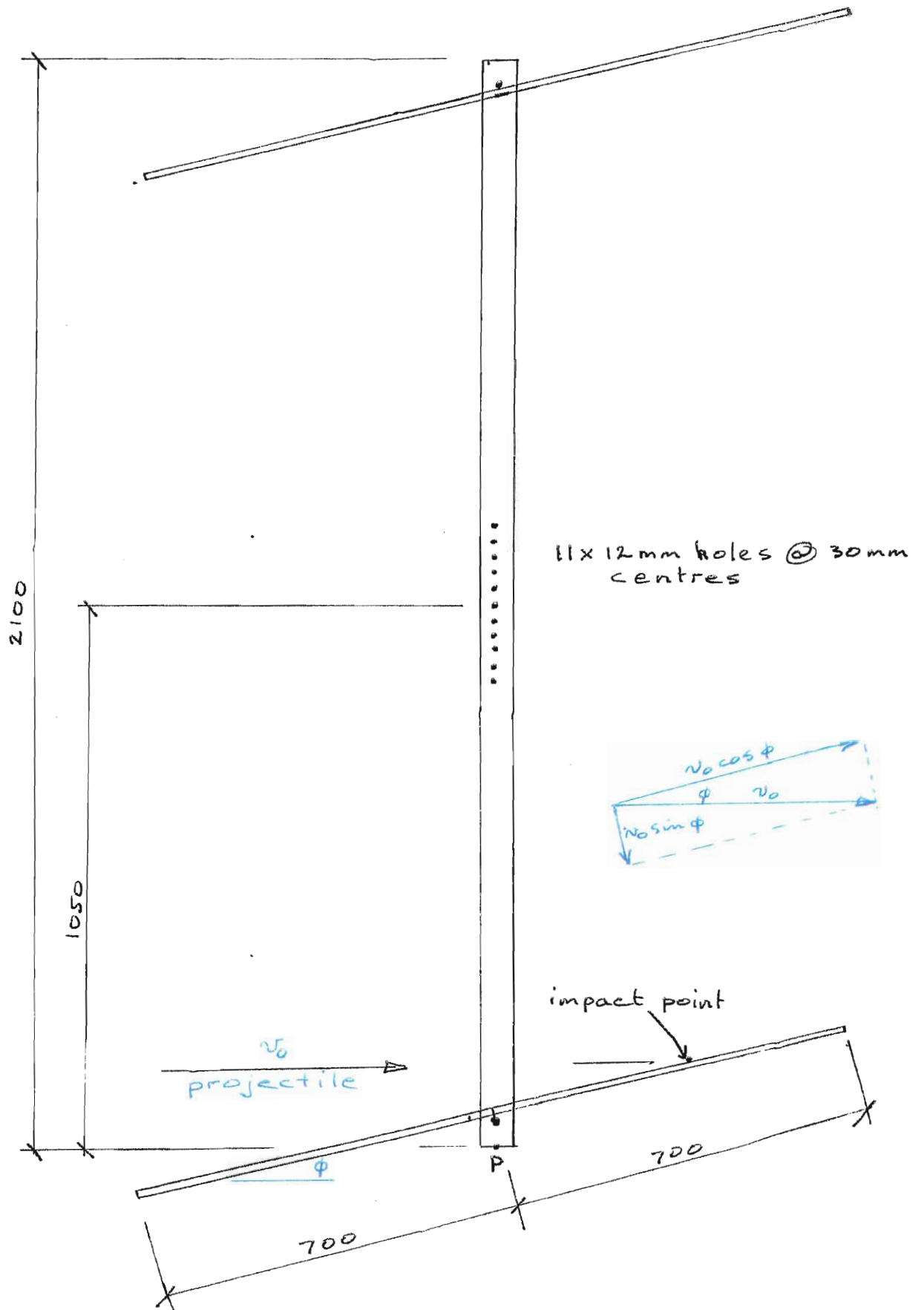
Table A2 Results for 21.8° plate

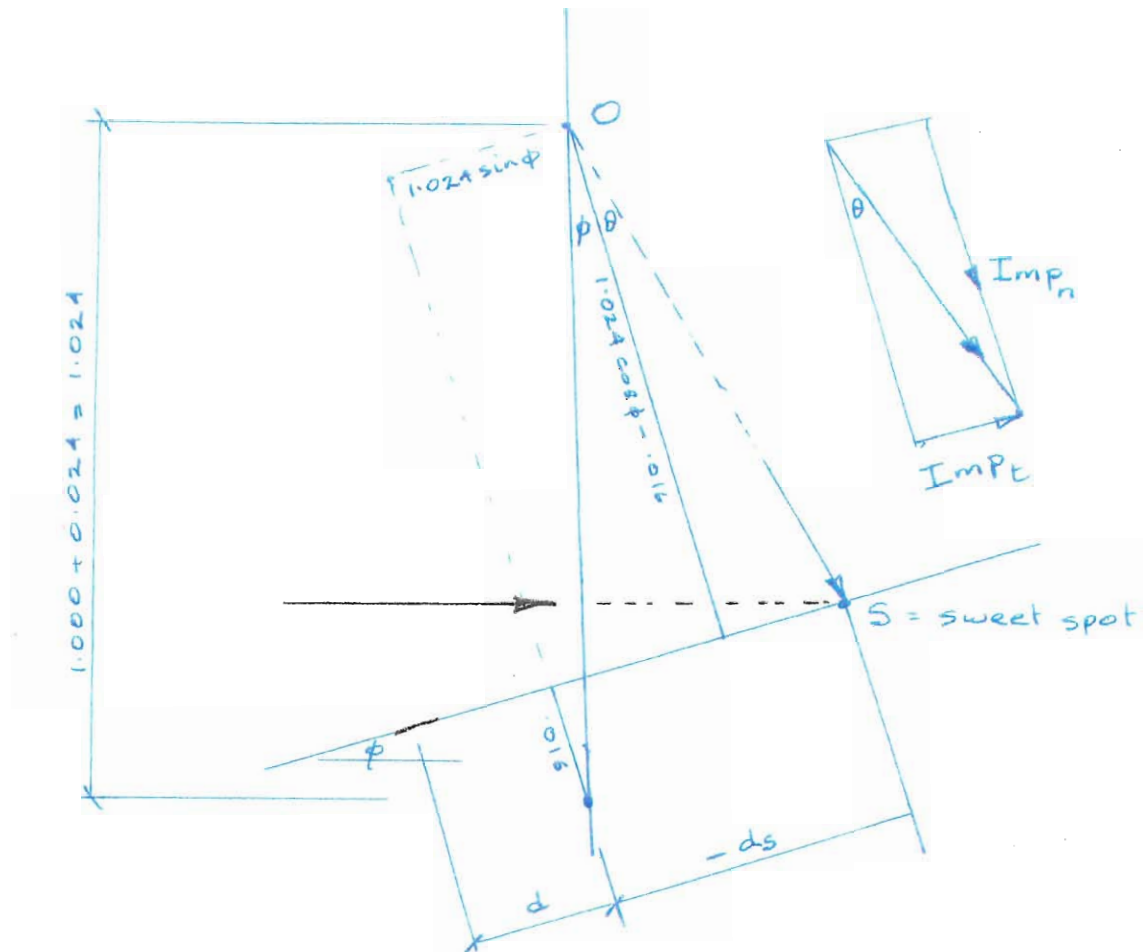
$n$	$d_n$ mm	$h_n$ mm
1	-610	-55
2	-580	-55
3	-580	-45
4	-570	-40
5	-510	-20
6	-505	-23
7	-480	-12
8	-410	-5
9	-395	10
10	-385	17
11	-335	28
12	-320	33
13	-300	39



The maximum horizontal displacement of P following impact is measured,  $= h$

Figure 3





$$\frac{Imp_e}{Imp_n} = \tan \theta = \frac{-ds - 1.024 \sin \phi}{1.024 \cos \phi - 0.016}$$

Figure 4

Figure 5

(4.6° Plate)

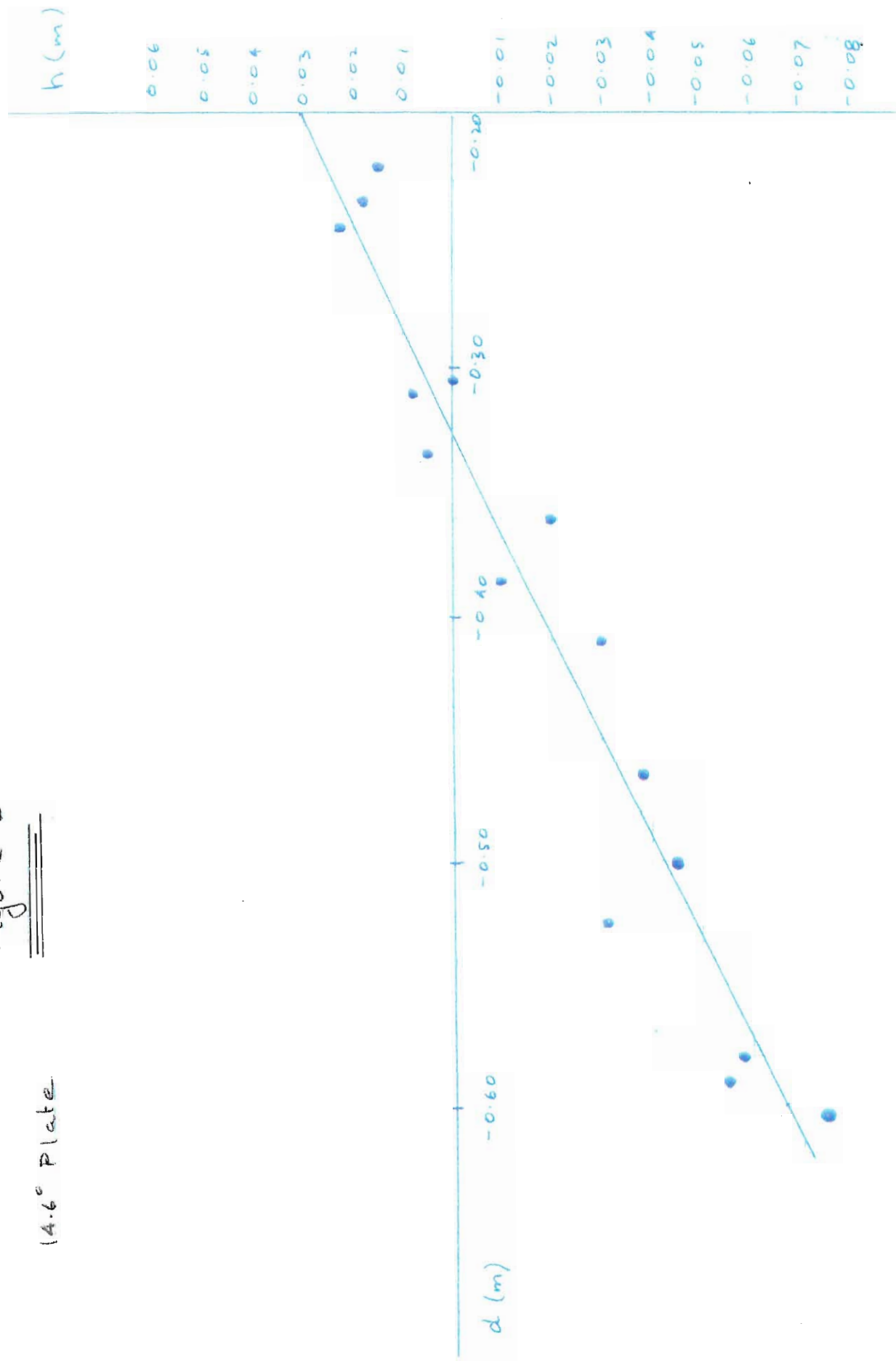
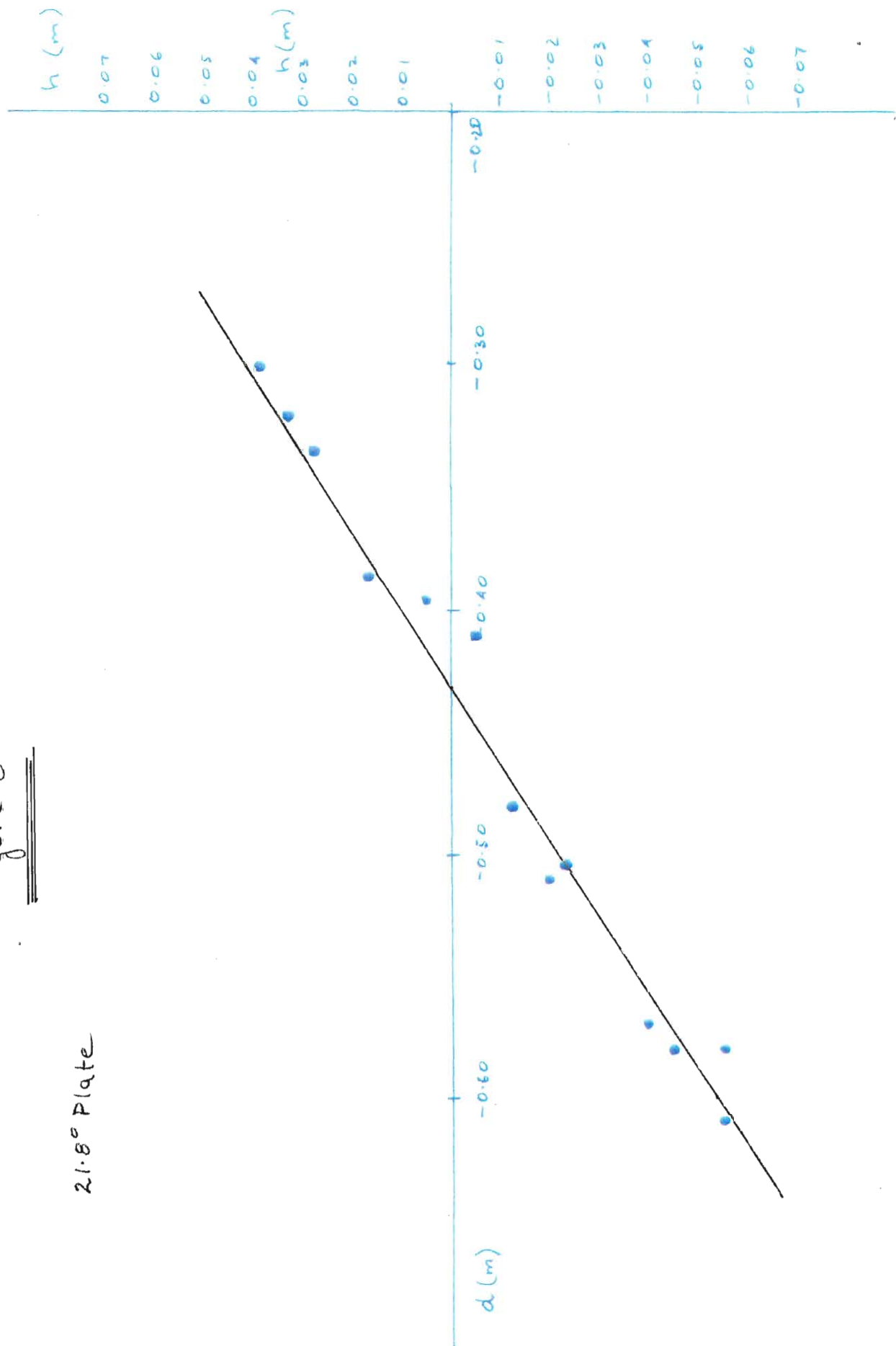




Figure 6

21.8° Plate





$$= 1000 + f - 16 \cos \phi + 2 \sin \phi \quad m m$$

Figure 8

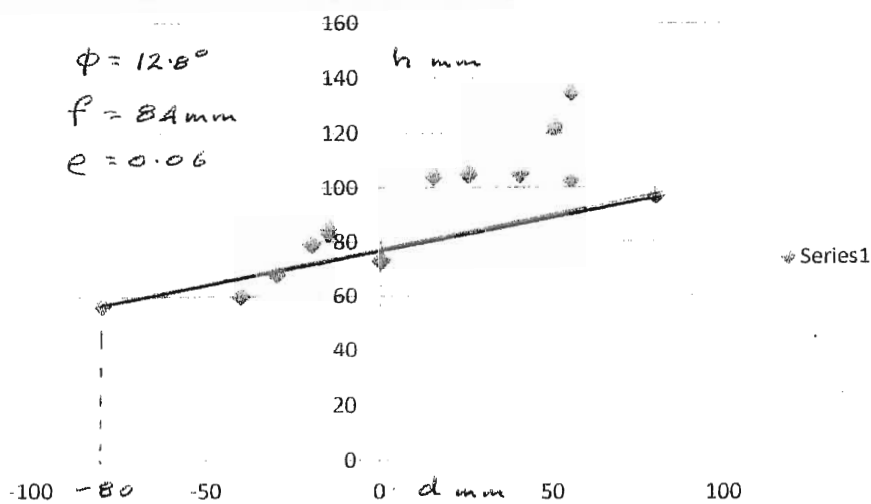
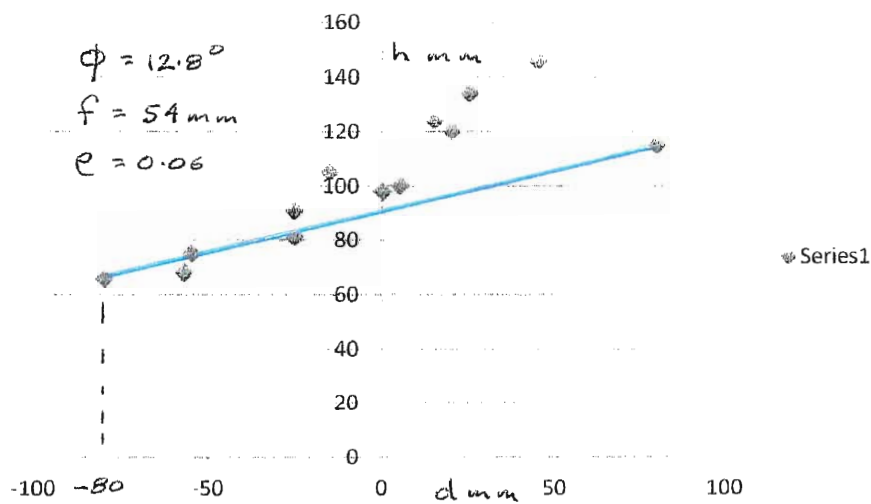
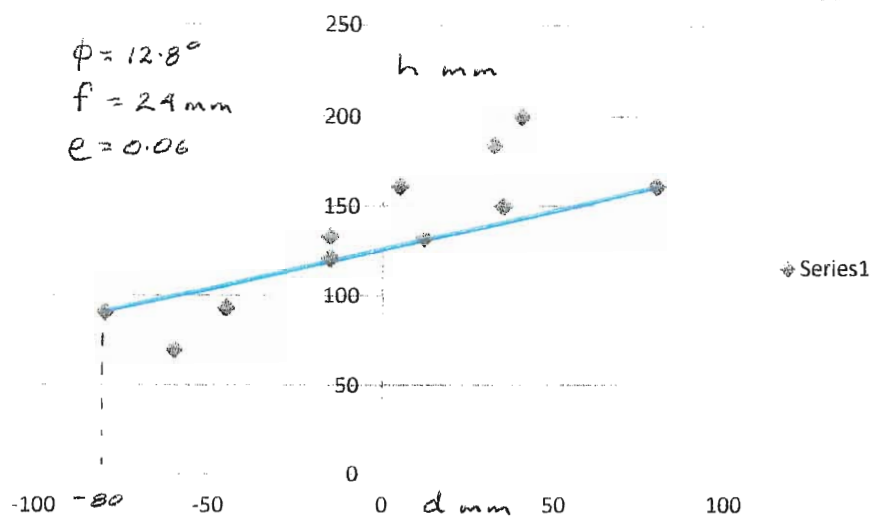


Figure 9

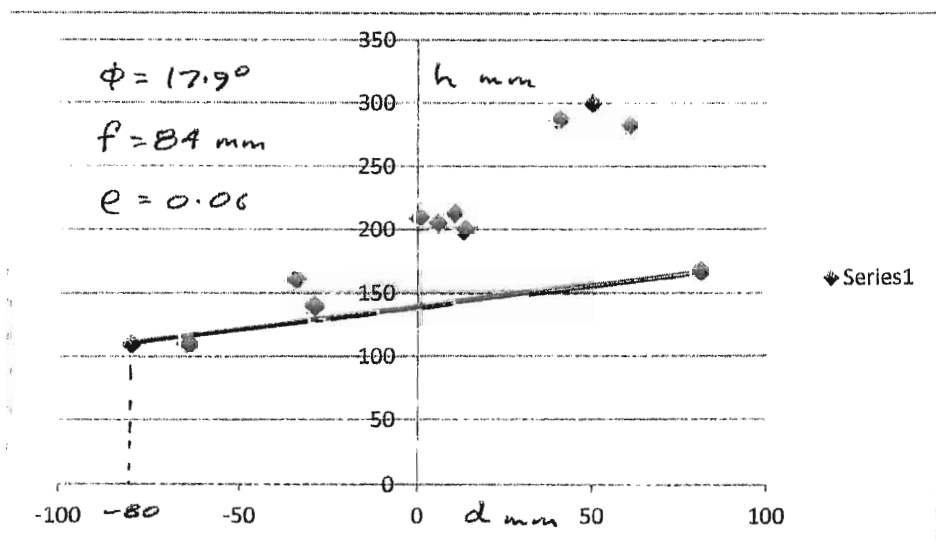
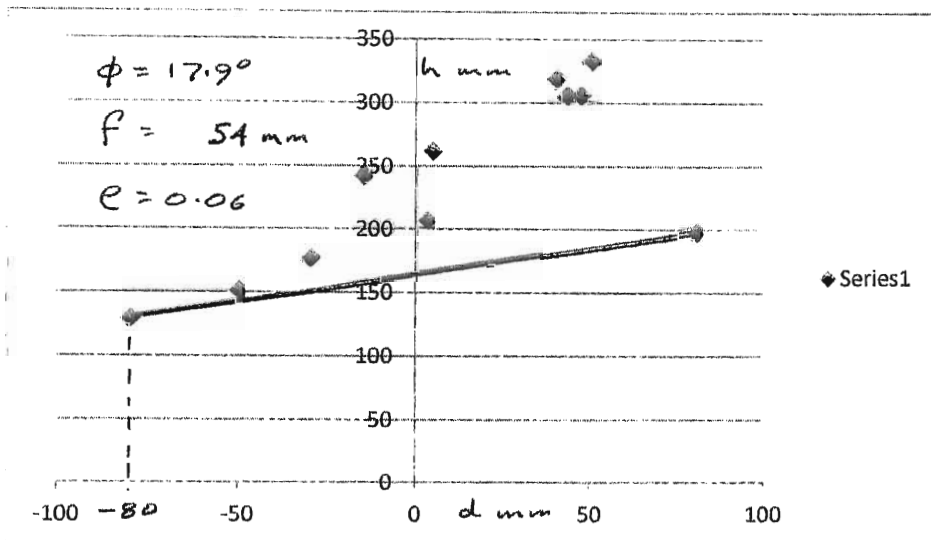
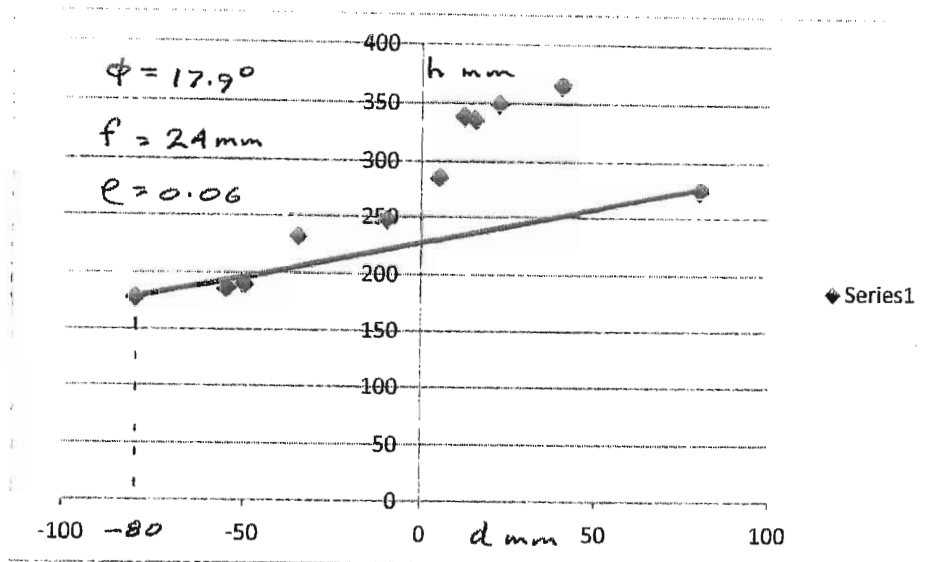
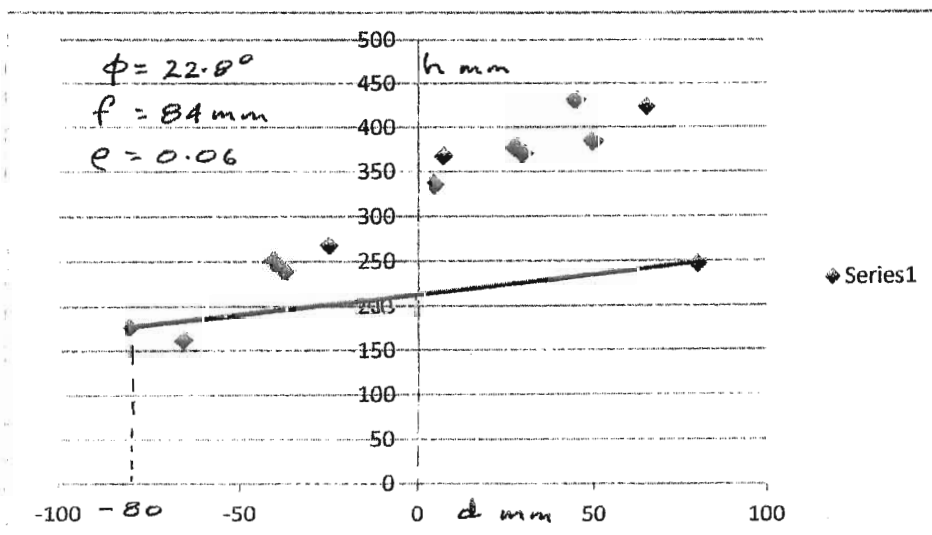
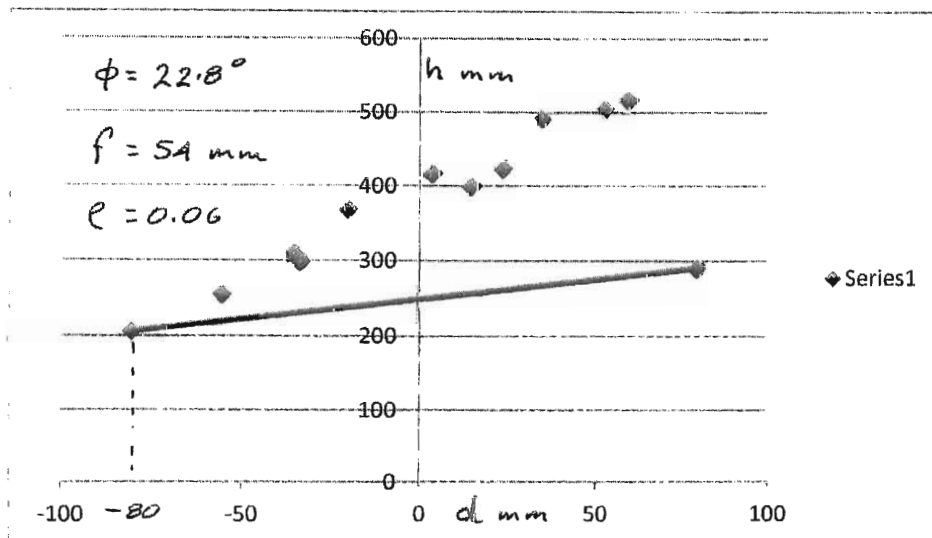
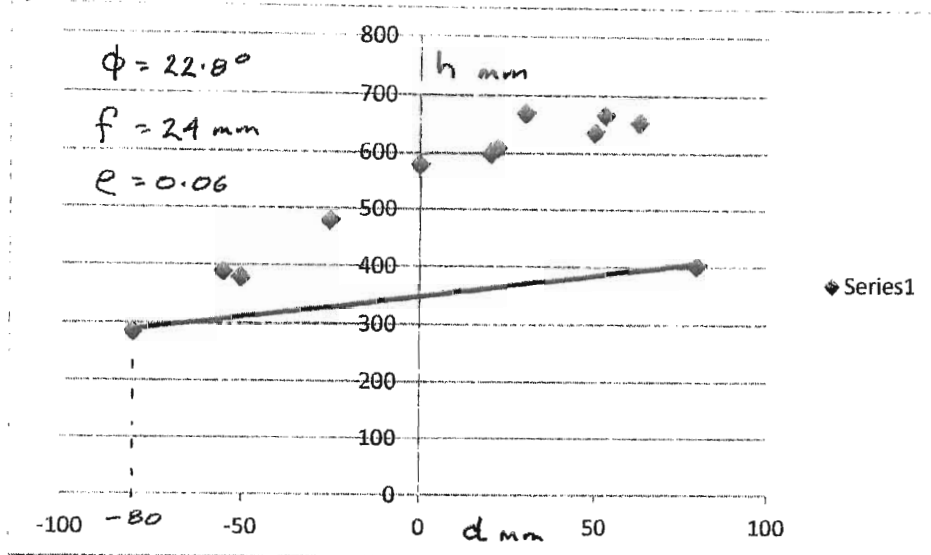


Figure 10



**PENDULUM TEST RESULTS**  
**IMPACT PLATE WITH NO SIDE PLATES**

DATE: 6 DEC 12

PLATE ANGLE (TO HORIZONTAL) – 16.7°

FULCRUM HEIGHT – 60 ~~90~~ mm

AMMUNITION – 5.56 mm SP

Shot No	Horizontal Displacement of Impact Plate (mm)	Distance of Projectile Impact Above Plate Centre Line (mm)	Distance of Projectile Impact Below Plate Centre Line (mm)
1	150	30	
2	170		25
3	180		65
4	70	78	
5	140	15	
6	100	55	
7	110	50	
8	140	4	
9	160		15
10	200		48

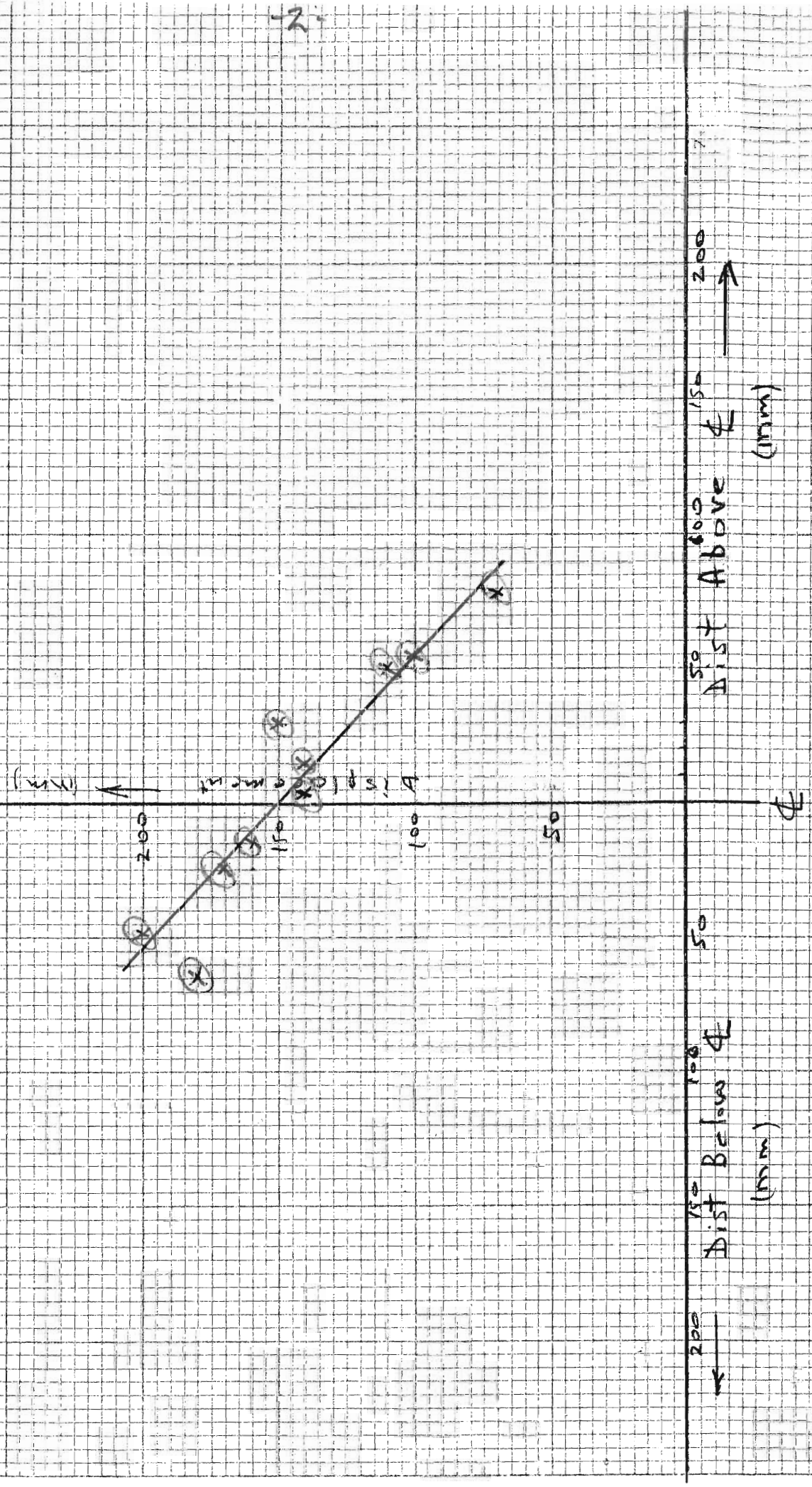
DATE: 26 DEC 12

PLATE ANGLE: 16.7°

FULCRUM HT: 90 mm

AMMO: 5.56 mm SP

2.



DATE: 6 DEC 12

PLATE ANGLE (TO HORIZONTAL) –  $9.8^\circ$

FULCRUM HEIGHT – 60 ~~90~~ mm

AMMUNITION – 5.56 mm SP

Shot No	Horizontal Displacement of Impact Plate (mm)	Distance of Projectile Impact Above Plate Centre Line (mm)	Distance of Projectile Impact Below Plate Centre Line (mm)
1	60	0	0
2	75		65
3	10	75	
4	30	43	
5	20		12
6	45		45
7	60		60
8	45		50
9	30	5	
10	10	70	



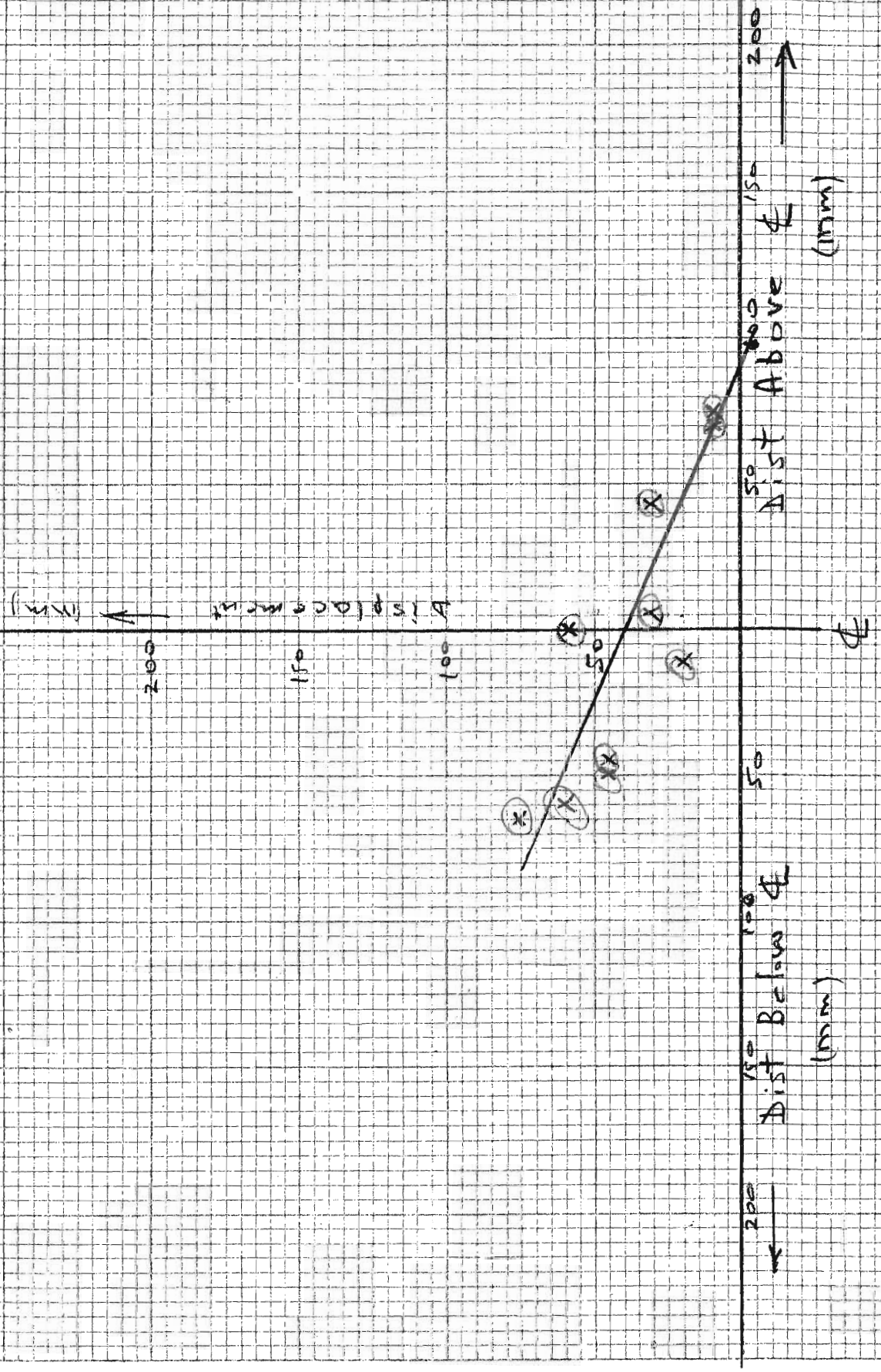
DATE: 6 DEC 12

PLATE ANGLE:  $9.8^\circ$

FULCRUM HT:  $60\text{ mm}$

NMMO:  $5.56\text{ mm SP}$

-A-



DATE: 6 DEC 12

PLATE ANGLE (TO HORIZONTAL) – 9.8°

FULCRUM HEIGHT – 30 ~~60~~ mm

AMMUNITION – 5.56 mm SP

Shot No	Horizontal Displacement of Impact Plate (mm)	Distance of Projectile Impact Above Plate Centre Line (mm)	Distance of Projectile Impact Below Plate Centre Line (mm)
1	130	0	0
2	130		45
3	100	28	
4	130		27
5	35	78	
6	110		40
7	45	70	
8	75	15	
9	105	35	
10	160		65

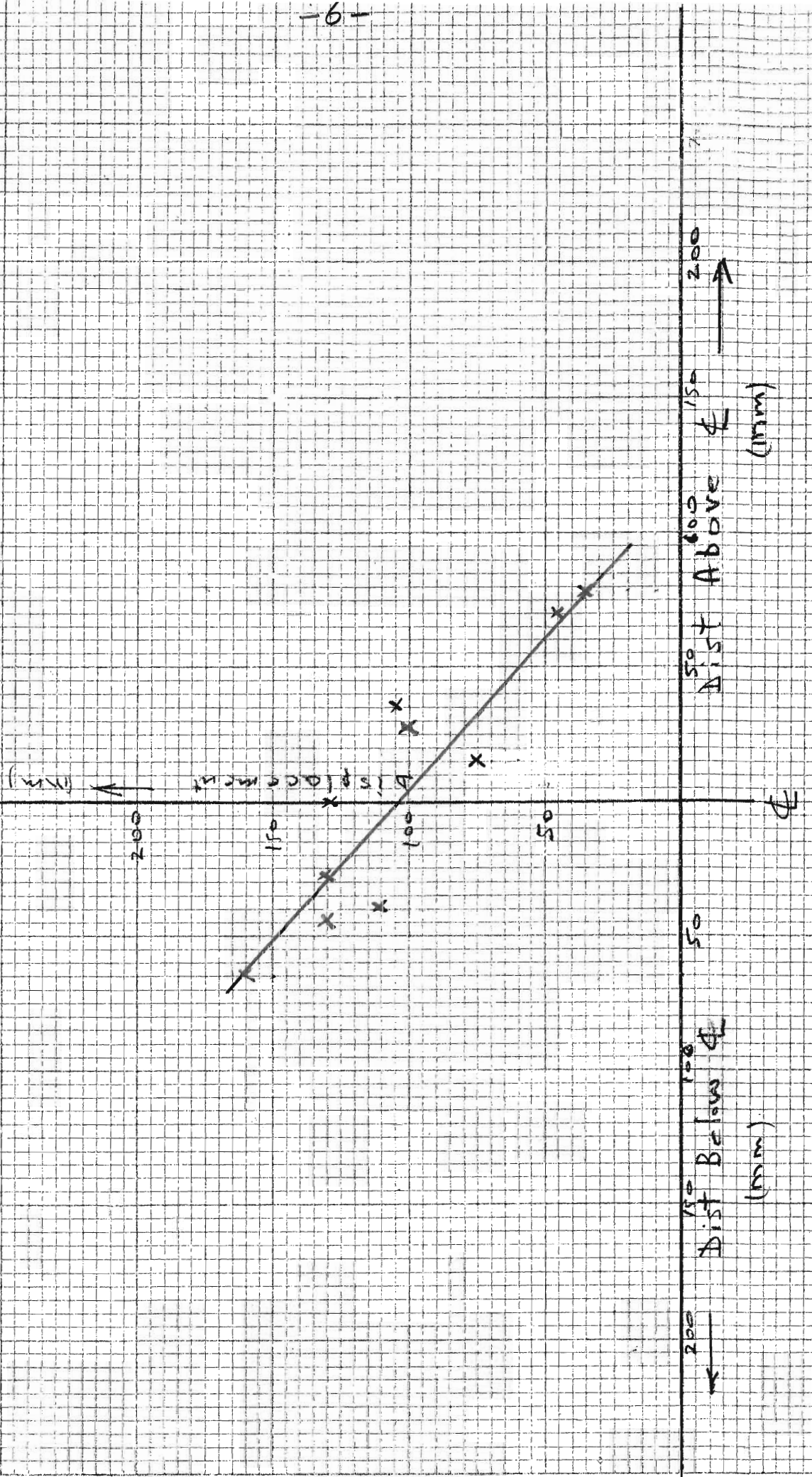
DATE: 6 DEC 12

PLATE ANGLE: 9.8°

FULCRUM HT: 30 mm

NMMO: 5.56 mm SP

-6-



DATE: 7 DEC 12

PLATE ANGLE (TO HORIZONTAL) – 16.4°

FULCRUM HEIGHT – 30 mm

AMMUNITION – 5.56 mm SP

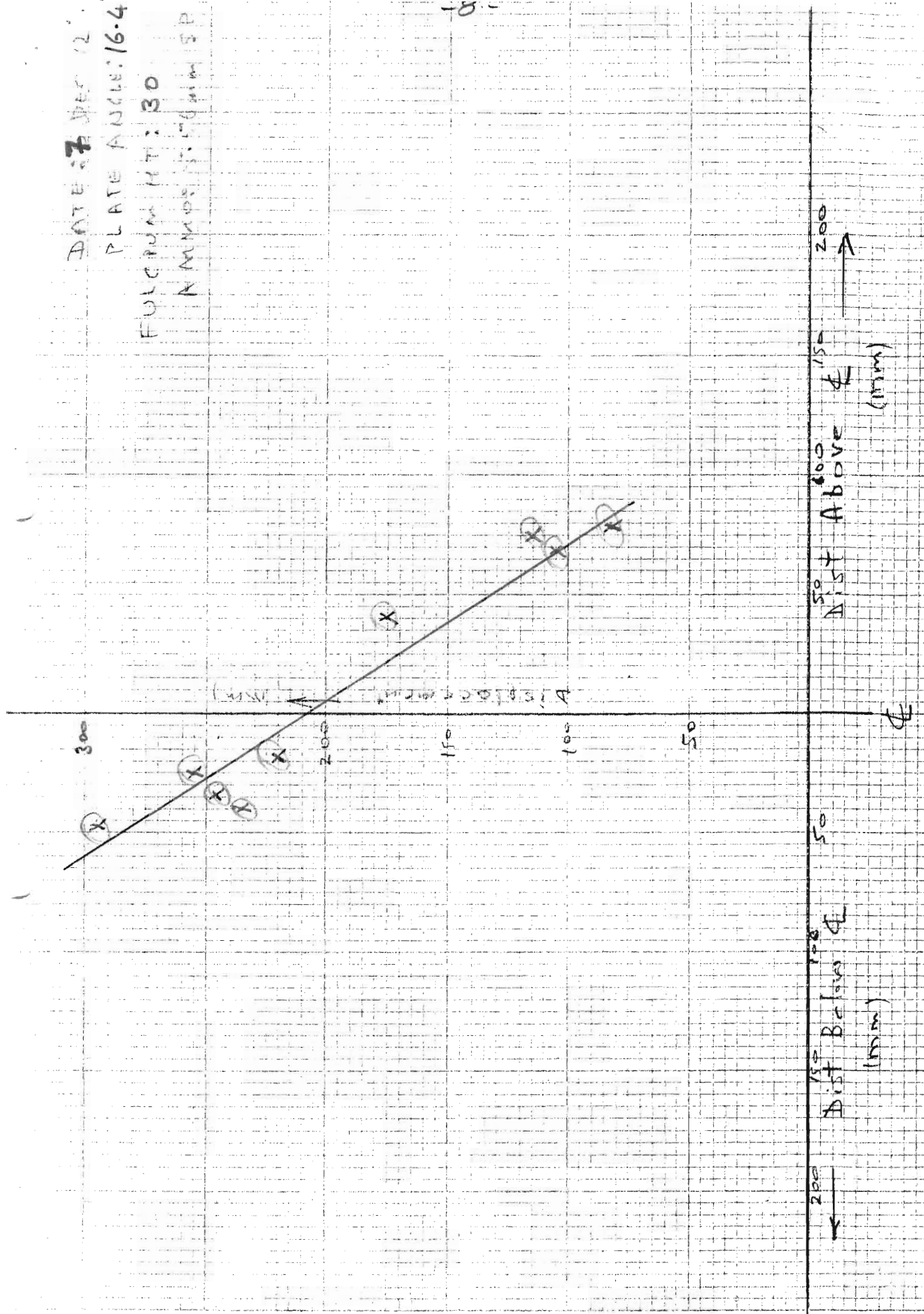
Shot No	Horizontal Displacement of Impact Plate (mm)	Distance of Projectile Impact Above Plate Centre Line (mm)	Distance of Projectile Impact Below Plate Centre Line (mm)
1	220		18
2	295		48
3	175	40	
4	105	68	
5	245		35
6	255		25
7	115	75	
8	235		40
9	83	78	

DATE: 7 DEC 12

PLATE ANGLE: 16.4

FULCRUM HT: 30

N NMDs: 5.76 mm SP



DATE: 7 DEC 12

PLATE ANGLE (TO HORIZONTAL) – 16.4°

FULCRUM HEIGHT – 90 mm

AMMUNITION – 5.56 mm SP

Shot No	Horizontal Displacement of Impact Plate (mm)	Distance of Projectile Impact Above Plate Centre Line (mm)	Distance of Projectile Impact Below Plate Centre Line (mm)
1	75	50	
2	93	0	0
3	115		35
4	112		30
5	135		40
6	88	35	
7	90	15	
8	85	45	
9	45	75	
10	130		53
11	200		68



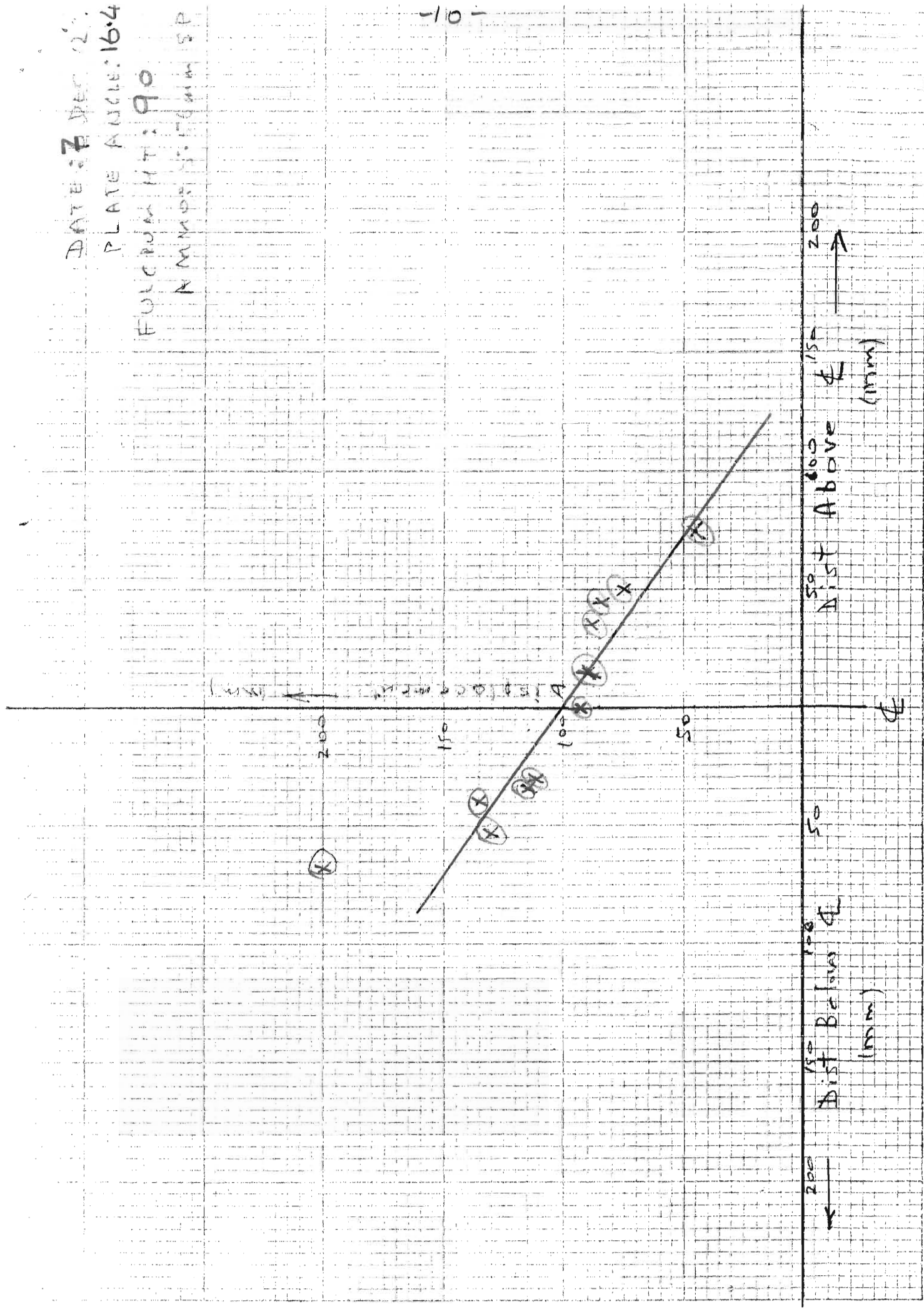
DATE: 7 DEC 12

PLATE ANGLE: 16.4

FULCRUM HT: 90

NMMDS EQUIM SP

-10-



DATE: 7 DEC 12

PLATE ANGLE (TO HORIZONTAL) – 9.6°

FULCRUM HEIGHT – 90 mm

AMMUNITION – 5.56 mm SP

Shot No	Horizontal Displacement of Impact Plate (mm)	Distance of Projectile Impact Above Plate Centre Line (mm)	Distance of Projectile Impact Below Plate Centre Line (mm)
1	38	5	
2	43		38
3	15	60	
4	28		10
5	10	78	
6	52		45
7	21	53	
8	68		60
9	85		65
10	45	40	



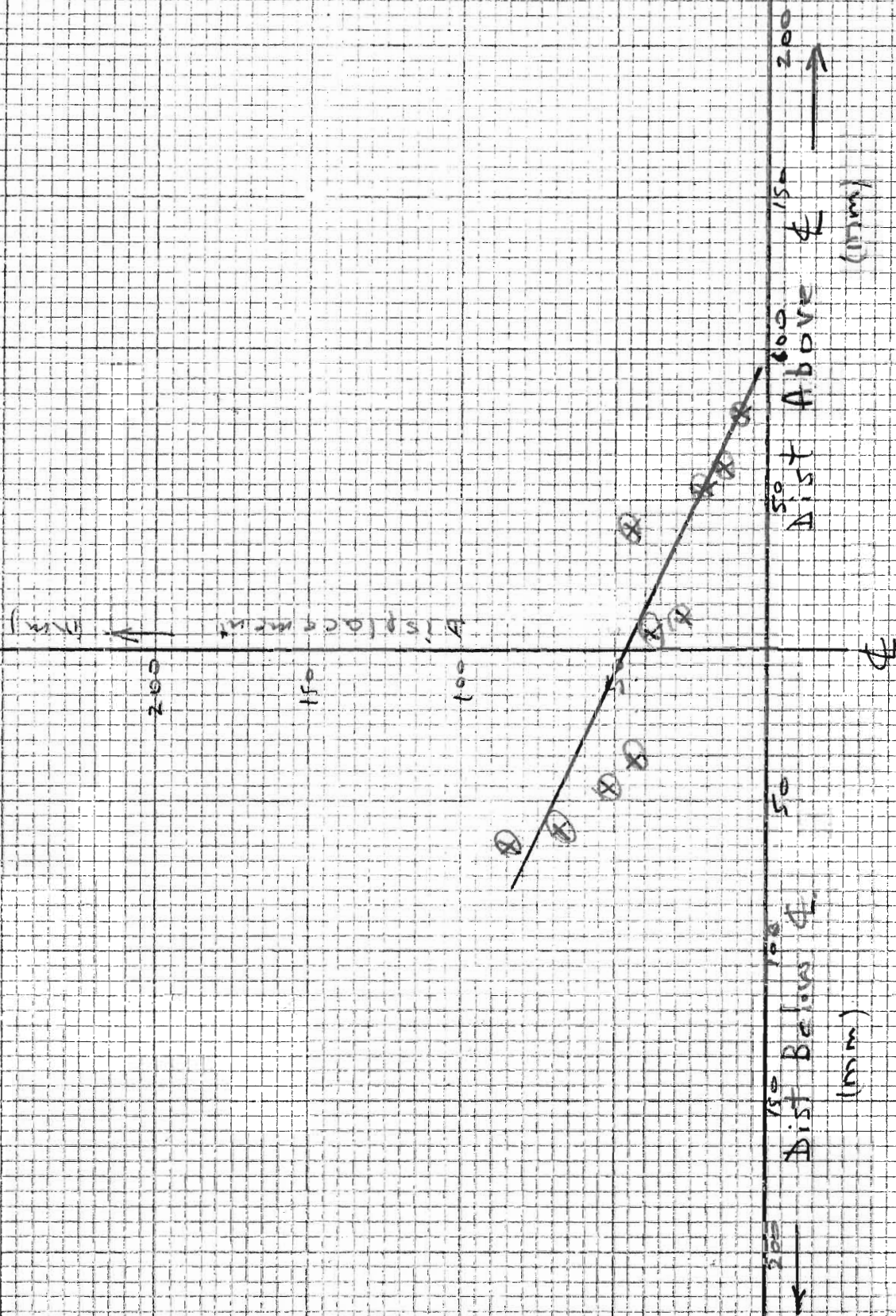
DATE: DEC 12

PLATE ANGLE: 9.6

FULCRUM HT: 90

N NUBS: 5.56 mm SP

- 12 -



**BALLISTIC PENDULUM EXPERIMENTS**  
**REPORT OF TESTS CONDUCTED**  
**ON 29-30/10/12 AND 06-07/12/12**

Bruce Golley

**Introduction**

In the heavily impacted area near the throat of the plates in a bullet trap in a firing range at [REDACTED] the lower plates had distorted concave downwards. It was felt that this distortion may be due to shot peening, which is surface yielding resulting from normal impact stresses. An experiment was designed in an attempt to determine the ratio of tangential impulse to normal impulse during impact of 5.56 mm rounds fired from M4 carbines commonly used in the range. Ballistic pendulum tests were conducted on 29/10/12 and 30/10/12. Tests referred to as sweet spot tests, have been considered in an earlier report. The second type of test is considered in this report, in addition to further tests carried out on 06/12/12 and 07/12/12 using a modified pendulum in which some side plates had been removed.

By coating the steel surface with ink from a whiteboard marker it was noted that after impact the ink had been erased in a roughly elliptical area approximately 30 mm by 10 mm. The initial theoretical model of a ballistic pendulum was based on the normal and tangential impulses being applied at the centre of this elliptical area. The theoretical response based on this assumption did not provide a satisfactory correlation with the initial experimental results. The experimental results showed the effect of impact position on the plate was much greater than the original theory predicted and a modified theory was developed in which the tangential impulse was related to the impact position on the plate. Two further series of tests were then carried out, and the results of those tests are also presented.

## Experimental details

A schematic diagram showing the bottom portion of the pendulum is shown in Figure 1. The pendulum was fabricated as a symmetrical model, with the lower portion only shown in the figure. The symmetrical scheme was adopted as a simple method to ensure the pendulum pivot was close to the centre of gravity to ensure measurable deflections of the pendulum could be obtained. The pivot point could be varied in 30 mm steps. Various pivots were used in the tests to:

- (a) enable the precise location of the centre of gravity and the radius of gyration to be accurately determined and
- (b) to provide additional data pairs for comparison with theoretical results.

A greatly simplified schematic view is shown in Figure 2. The impact surface was covered with black ink from a whiteboard marker. A 5.56 mm round was fired from an M4 carbine and the horizontal displacement of the bottom of the pendulum was measured by placing graph paper behind the pendulum and filming the motion following impact. The location of the centre of the impact area as indicated by the erasure of the ink was the measured and tabulated with the maximum horizontal displacement of the bottom of the pendulum. The vertical displacement of the centre of gravity,  $G$ , could then be determined, and hence the maximum potential energy of the pendulum following impact could be established. This is shown in Figure 3.

## Theoretical Considerations

A projectile with velocity  $v_0$  impacts a steel plate which is at an angle  $\phi$  to the horizontal, as shown in Figure 4. The projectile has components  $v_{n0}$  and  $v_{t0}$  in the normal and tangential directions as shown in the figure. The projectile is subjected to forces  $F_n(t)$  and  $F_t(t)$ . In the suggested model, the normal force is assumed to act during the time  $0 \leq t \leq t_1$  which is only related to the impact area. The tangential force is assumed to act during the time  $0 \leq t \leq t_2$  which is related to the length of the plate between the impact area and the top edge of the impacted plate. Force components and velocity components are shown in

Figure 5. Impulses during the impacts are then

$$\mathbf{Imp}_n = \int_0^{t_1} F_n(t) dt$$

$$\mathbf{Imp}_t = \int_0^{t_2} F_t(t) dt$$

It should be noted that the lever arm about pivot  $O$  associated with  $\mathbf{Imp}_t$  is independent of the impact position, as may be seen from Figure 2, although the magnitude of  $\mathbf{Imp}_t$  using this model depends on the impact position.

### Reduction of data to a common base

For each plate angle,  $\phi$ , three pivots were used and about ten rounds were fired with each pivot. The data pairs  $(h_i, d_i)$  were unable to be compared in this form, and were reduced to a common base as follows. The equations below are obtained from geometry of the pendulum, conservation of momentum during impact and equating kinetic energy immediately after impact with maximum potential energy. They are presented without further detail.

$$v_{n0} = v_0 \sin \phi$$

$$v_{t0} = v_0 \cos \phi$$

$$\mathbf{Imp}_n = m v_{n0}$$

$$\mathbf{Imp}_{t1} = m v_{t0} - m v_{t1}$$

$$\mathbf{Imp}_{t2} = m v_{t1} - m v_{t2}$$

$$\mathbf{Imp}_t = \mathbf{Imp}_{t1} + \mathbf{Imp}_{t2} = m v_{t0} - m v_{t2}$$

$$a = 0.016 \sin \phi + d \cos \phi$$

$$b = 1.000 + f_n - 0.016 \cos \phi + d \sin \phi$$

$$\omega_0 = \frac{1}{I_O} (\mathbf{Imp}_n (a \cos \phi + b \sin \phi) + \mathbf{Imp}_t ((1.000 + f_n) \cos \phi - 0.010))$$

$$h = L \sqrt{\left( \frac{I_O \omega_0^2}{M g l_n} \right) - \left( \frac{I_O \omega_0^2}{2 M g l_n} \right)^2}$$

$$l_n = f_n + x$$

$$f_1 = 0.024 \quad f_2 = 0.054 \quad f_3 = 0.084$$

$x$  located the centre of gravity with respect to the nominal centreline of the pendulum and  $I_O$  is the moment of inertia of the pendulum about the pivot  $O$ . As two series of tests are discussed in this report, these values differed in the two tests. The determination of  $x$  and  $I_O$  were obtained from the periods of the pendulum with different pivots, which is discussed in a later section. In the ballistic tests, three pivots were used, subscripted here with  $n$ .

With some substitutions using the above equations we obtain

$$h = h(d, \mathbf{Imp}_t, n)$$

Data pairs  $(d_i, h_i)$  were obtained for each pivot setting,  $n = 1, 2, 3$ .

For a particular data setting,  $n = 1, 2, 3$ , obtain for a data pair  $(d_i, h_i)$  the equation

$$h_i = h(d_i, \mathbf{Imp}_{t_i}, n)$$

This leads to a quartic equation in  $\mathbf{Imp}_{t_i}$ , one solution of which is obviously the value of  $\mathbf{Imp}_{t_i}$  corresponding to the data pair  $(d_i, h_i)$ . Thus we can consider the data pairs  $(d_i, \mathbf{Imp}_{t_i})$  which are independent of the pivot setting  $n$ .

### **Location of G and determination of radius of gyration**

The results of two series of tests are discussed in this report. Series 1 tests were carried out on 29-30/10/12, and following modification to the pendulum Series 2 tests were carried out on 06-07/12/12. The pendulums were fabricated as symmetrical systems using aluminium bars 2100 mm long, so the centre of gravity,  $G$ , was expected to be near the midpoint of the bars. For each pendulum, the radius of gyration with respect to  $G$ ,  $k_G$ , was required to determine moments of inertia, and the periods of oscillation were used to determine  $k_G$  and the precise location of  $G$ . Refer to Figure 6, which simply shows the bars for convenience.

Periods of oscillation were measured with five different pivots in Series 1 and four pivots in Series 2. The theoretical period with the pivot  $l_n$  above  $G$  is

$$T_n = \frac{2\pi}{\sqrt{g}} \sqrt{\frac{k_G^2}{l_n} + l_n}$$

For the various pivots, measured periods and corresponding values of  $l_n$  were obtained. Lengths  $l_n$  are functions of the unknown  $x$  which is also shown in the figure. A least squares method was used to determine  $k_G$  and  $x$ . Thus

$$E_1 = \sum_{n=1}^N \left( T_n - \frac{2\pi}{\sqrt{g}} \sqrt{\frac{k_G^2}{l_n} + l_n} \right)^2$$

where

$$l_n = 0.030n - 0.006 + x$$

and  $N = 5$  for Series 1 and  $N = 4$  for Series 2 was minimised with respect to the unknowns  $k_G$  and  $x$  using  $g = 9.806 \text{ m/s}^2$ . Solving the nonlinear equations the following values were obtained. Pendulum masses are also given.

*Series 1*

$$x = 0.0016 \text{ m}$$

$$k_G = 0.8476 \text{ m}$$

Pendulum mass  $M = 3.95 \text{ kg}$

*Series 2*

$$x = -0.0063 \text{ m}$$

$$k_G = 0.8626 \text{ m}$$

Pendulum mass  $M = 4.55 \text{ kg}$

Projectile mass and velocity were obtained earlier by weighing ten projectiles and measuring the velocity of ten projectiles, and the following averages were used in calculations for both series.

Projectile mass  $m = 0.00356$  kg

Projectile velocity  $v_0 = 875$  m/s

### Reduction of results

The main object of the tests was to determine relative values of normal and tangential impulses. The suggested model considers the tangential impulse to be composed of two components, and in this section the method for comparing the observations with the theoretical model is discussed.

Assume that when  $t_1 \leq t \leq t_2$  the force on the projectile,  $F_t^*$  is constant. Thus we have

$$F_t^* = -ma_t$$

where  $a_t$  is the acceleration of the projectile. Further

$$\begin{aligned} \mathbf{Imp}_t &= F_t^*(t_2 - t_1) \\ &= F_t^* \frac{2(d + 0.08)}{v_{t1} + v_{t2}} \\ &= -\frac{2ma_t(d + 0.08)}{v_{t1} + \sqrt{v_{t1}^2 + 2a_t(d + 0.08)}} \end{aligned}$$

We then have

$$\begin{aligned} \mathbf{Imp}_t &= \mathbf{Imp}_{t1} + \mathbf{Imp}_{t2} \\ &= mv_{t0} - mv_{t1} - \frac{2ma_t(d + 0.08)}{v_{t1} + \sqrt{v_{t1}^2 + 2a_t(d + 0.08)}} \end{aligned}$$

Each test on a plate for a given angle  $\phi$  had about thirty data pairs  $(d_i, \mathbf{Imp}_{t_i})$ . For each plate angle  $\phi$  a nonlinear least squares procedure was used to obtain the parameters  $v_{t1}$  and  $a_t$ . The exit velocity  $v_{t2}$  was then obtained as

$$v_{t2} = v_{t1} + \sqrt{v_{t1}^2 + 2a_t(d + 0.08)}$$

Having determined  $v_{t1}$ ,  $a_t$  and  $v_{t2}$  the impulses  $\mathbf{Imp}_t$ ,  $\mathbf{Imp}_{t1}$  and  $\mathbf{Imp}_{t2}$  and the force  $F_t^*$  derived from the data set can then be determined. The impulse  $\mathbf{Imp}_n$  is obtained simply from the initial velocity  $v_0$ , the plate angle  $\phi$  and the projectile mass. To obtain an approximate estimate of the force  $F_n(t)$ , assume the force is constant  $F_n^*$  during the time  $0 \leq t \leq t_1$ . A lengthy procedure to estimate the time  $t_1$  is given in Appendix A, which is included in this report for future use by the writer. A simpler method makes use of the observed results, which indicate that there is only a small reduction in the tangential component of velocity during impact. Hence in determining the average normal force,  $F_n^*$ , it is assumed the tangential component of velocity is constant. The time  $t_1$ , approximated by  $t_1^*$ , is the time for the projectile to travel its length plus the projection of its diameter on the inclined plate when travelling at velocity  $v_{t0}$ . Thus for a projectile of diameter 5.56 mm and length 30 mm impacting a plate at an angle  $\phi$ , the time is

$$t_1^* = \frac{1}{v_{t0}} \left( 0.030 + \frac{0.00556}{\sin \phi} \right) \text{ s}$$

An estimate of the normal force during this time is

$$F_n^* = \frac{\mathbf{Imp}_n}{t_1^*} \text{ N}$$

Thus finally an estimate of the ratio of tangential to normal force is obtained.

The impulse  $\mathbf{Imp}_t$  is a function of  $d$ , which locates the impact point. Hence the impulse ratio initially sought is not constant. The ratio  $\mathbf{Imp}_t/\mathbf{Imp}_n$  may be plotted however, and are shown in scatter plots.

## Results

Results of all tests are summarised in the tables and graphs shown in Figures 7(a,b,c) for tests with side plates and Figures 8(a,b) for tests with no side plates. The tables show the raw data, being the values of  $d$ , which located the impact on the plate and the horizontal displacement  $h$  of the bottom of the pendulum. The values of the total tangential impulse  $\mathbf{Imp}_t$  calculated as described above are also shown with those data pairs. Scatter plots of  $\mathbf{Imp}_t$  against  $d$  are also shown. In the suggested model, a theoretical curve was determined



by minimising two parameters  $v_{t1}$  and  $a_t$ , and this curve is also shown. The theoretical curve is essentially linear in the range considered. For convenience in plotting, points on the theoretical curves were evaluated at  $d = -80$  mm and  $d = 80$  mm were plotted on the scatter plots and lines drawn between those points. These points should not be confused with observed data points.

An additional table is also shown for each plate angle, in which the initial velocity component in the tangential direction,  $v_{t0}$  is given and the velocity  $v_{t1}$  which is the calculated velocity after the initial impact. Also shown is the normal impulse,  $\mathbf{Imp}_n$ , and the forces  $F_n^*$  and  $F_t^*$ , together with the ratio  $F_t^*/F_n^*$

Scatter plots of the ratio  $\mathbf{Imp}_t/\mathbf{Imp}_n$  against  $d$  are shown in Figure 9 and 10.

### Discussion of results

There is a wide degree of scatter, particularly with the smaller plate angles,  $\phi$ , but the suggested model provides a reasonable fit with the higher angles.

The initial object of the experimental program was to determine if the normal impulse during impact was significantly larger than the tangential impulse. The scatter plots show the significant influence of the position of the initial contact area on the total tangential impulse, which is spread over a much longer time than the normal impulse except if the impact is near the top edge of the plate. The normal impulse can be determined with reasonable accuracy, as the normal component of velocity is zero after initial impact. Without venturing into great detail, it is however clear that in the elliptical impact area the normal impulse is much larger than the tangential impulse. Thus from the scatter plots of the ratios  $\mathbf{Imp}_t/\mathbf{Imp}_n$  against  $d$ , even ignoring the effect of impact location, the maximum observed ratio is about 0.55 with the 22.8 degree plate. The values when the impact is near the top of the plate, that is when  $d$  is say minus 50 mm, in which case there is little effect of the tangential force after the impact zone, the maximum ratio is about 0.18 with the 22.8 degree plate, and 0.08 with the 17.9 degree plate.

The ratios  $F_t^*/F_n^*$  relating forces rather than impulses are in the range 0.067 to 0.145. The

methods for determining both values in this ratio are approximations, but the values show the tangential force is much smaller than the normal force. It should also be noted that the suggested model gives a slightly higher tangential velocity immediately after impact than before impact in some cases, reflecting the scatter of the data and probably inaccuracy of the model. However the values of  $v_{t0}$  and  $v_{t1}$  are in all cases close, reflecting the small value of the tangential impulse related to the elliptical impact area.

The tangential impulse increases with increasing plate angle as expected. Two plates with reasonably similar angles were tested, namely  $\phi = 17.9^\circ$  with side plates, and  $\phi = 16.4^\circ$  plate without side plates. The influence of the side plates is clear, as  $\mathbf{Imp}_t$  is much less with the  $\phi = 16.4^\circ$  plate than would be expected when compared with the  $\phi = 17.9^\circ$ . This is consistent with the observation that welds supporting the side plates had been impacted by fragments of the projectiles, which was the reason for modifying the initial pendulum arrangement.

## Conclusions

The tests show that the tangential component of impulse during impact is much less than the normal component of impulse. The tests were not designed to allow comparisons of tangential and normal components of force on the projectile to be accurately determined, but with some assumptions it appears the tangential component of force is much less than the normal component of force. No attempt has been made to estimate normal and shear stresses during impact, as the instantaneous contact area cannot be estimated. Although the plate surface behaviour is influenced by a combination of normal and shear stresses, it would appear that the shear component is small, and may probably be ignored. No attempt has been made to explain the physical basis of the proposed model, as the nature of the interaction involves unknown factors, but observations using high speed photography would be useful to provide some justification of the model.

## APPENDIX A

### An estimate of tangential acceleration during initial impact

In order to obtain an idea of the interface forces during impact, the following simplification was considered. Refer to Figure A1. A 5.56 mm round of length 30 mm impacts on the plate shown. An assumption is made that the projectile has an impact zone related to the projection of the projectile on the plate. It is further assumed that the tangential resistance to the projectile is proportional to the length in contact with the impact zone. Any distortion of the projectile is ignored. Three time zones are considered, corresponding to different positions of the projectile with respect to the impact zone. Thus three second order differential equations arise, integration of each giving rise to two integration constants. The constants are determined so that the displacement and tangential velocity of the leading edge of the projectile are continuous. Full details of the solutions are not presented, but sufficient detail is given for future use by the writer.

$$0 \leq t \leq t_3$$

$$m \frac{d^2x}{dt^2} = -\tau x, \quad t = 0, \quad x = 0, \quad \frac{dx}{dt} = v_{t0}$$

Solving gives

$$\begin{aligned} x &= v_{t0} \sqrt{\frac{m}{\tau}} \sin \sqrt{\frac{\tau}{m}} t \\ \frac{dx}{dt} &= v_{t0} \cos \sqrt{\frac{\tau}{m}} t \\ t &= \sqrt{\frac{m}{\tau}} \sin^{-1} \left( \sqrt{\frac{\tau}{m}} \frac{x}{v_{t0}} \right) \\ t_3 &= \sqrt{\frac{m}{\tau}} \sin^{-1} \left( \sqrt{\frac{\tau}{m}} \frac{X}{v_{t0}} \right) \\ v_{t3} &= \sqrt{v_{t0}^2 - \frac{\tau}{m} X^2} \end{aligned}$$

$$t_3 \leq t \leq t_4$$

$$m \frac{d^2x}{dt^2} = -\tau X, \quad t = t_3, \quad x = X, \quad \frac{dx}{dt} = v_{t3}$$

Solving gives

$$\begin{aligned}
x &= -\frac{\tau X}{2m}(t - t_3)^2 + v_{t3}(t - t_3) + X \\
\frac{dx}{dt} &= -\frac{\tau X}{m}(t - t_3) + v_{t3} \\
t_4 &= t_3 + \frac{v_{t3}m - \sqrt{v_{t3}^2 m^2 - 2X\tau m(L - X)}}{2X\tau} \\
v_{t4} &= \sqrt{\frac{1}{m}(v_{t3}^2 m^2 - 2X\tau m(L - X))}
\end{aligned}$$

$t_4 \leq t \leq t_1$

$$m \frac{d^2 x}{dt^2} = -\tau(X + L - x), \quad t = 0, \quad x = L, \quad \frac{dx}{dt} = v_{t4}$$

Solving gives

$$\begin{aligned}
x &= -X \cosh\left(\sqrt{\frac{\tau}{m}}(t - t_4)\right) + v_{t4}\sqrt{\frac{m}{\tau}} \sinh\left(\sqrt{\frac{\tau}{m}}(t - t_4)\right) + X + L \\
\frac{dx}{dt} &= v_{t4} \cos \sqrt{\frac{\tau}{m}} t \\
t_1 &= t_4 + \sqrt{\frac{m}{\tau}} \tanh^{-1}\left(\sqrt{\frac{\tau}{m}} \frac{X}{v_{t4}}\right) \\
v_{t1} &= \sqrt{v_{t4}^2 - \frac{\tau}{m} X^2}
\end{aligned}$$

As  $v_{t1}$  has been determined for the suggested model by data fitting, and  $v_{t4}$  can be expressed in terms of the unknown  $\tau$  using the above equations,  $\tau$  may be determined and hence the piecewise displacement function during this assumed impact is found. The acceleration and hence tangential force is obtained as a function of time by simple differentiation.

An estimate of the normal force during impact is made here by assuming the normal force is constant during the time  $0 \leq t \leq t_1$ . The time  $t_1$  has been determined above by considering the tangential displacement, as discussed above.

Figure A1

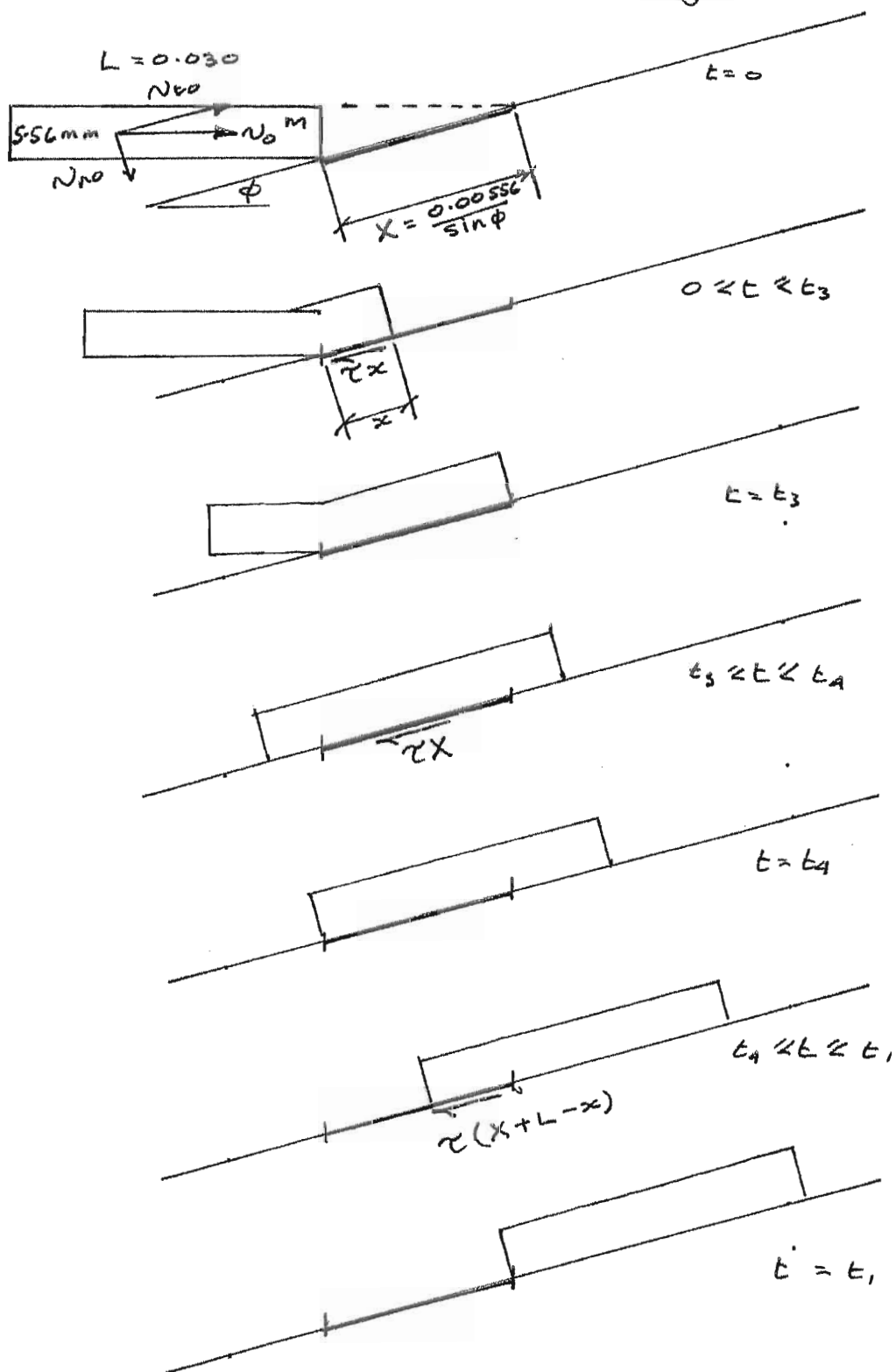


Figure 1

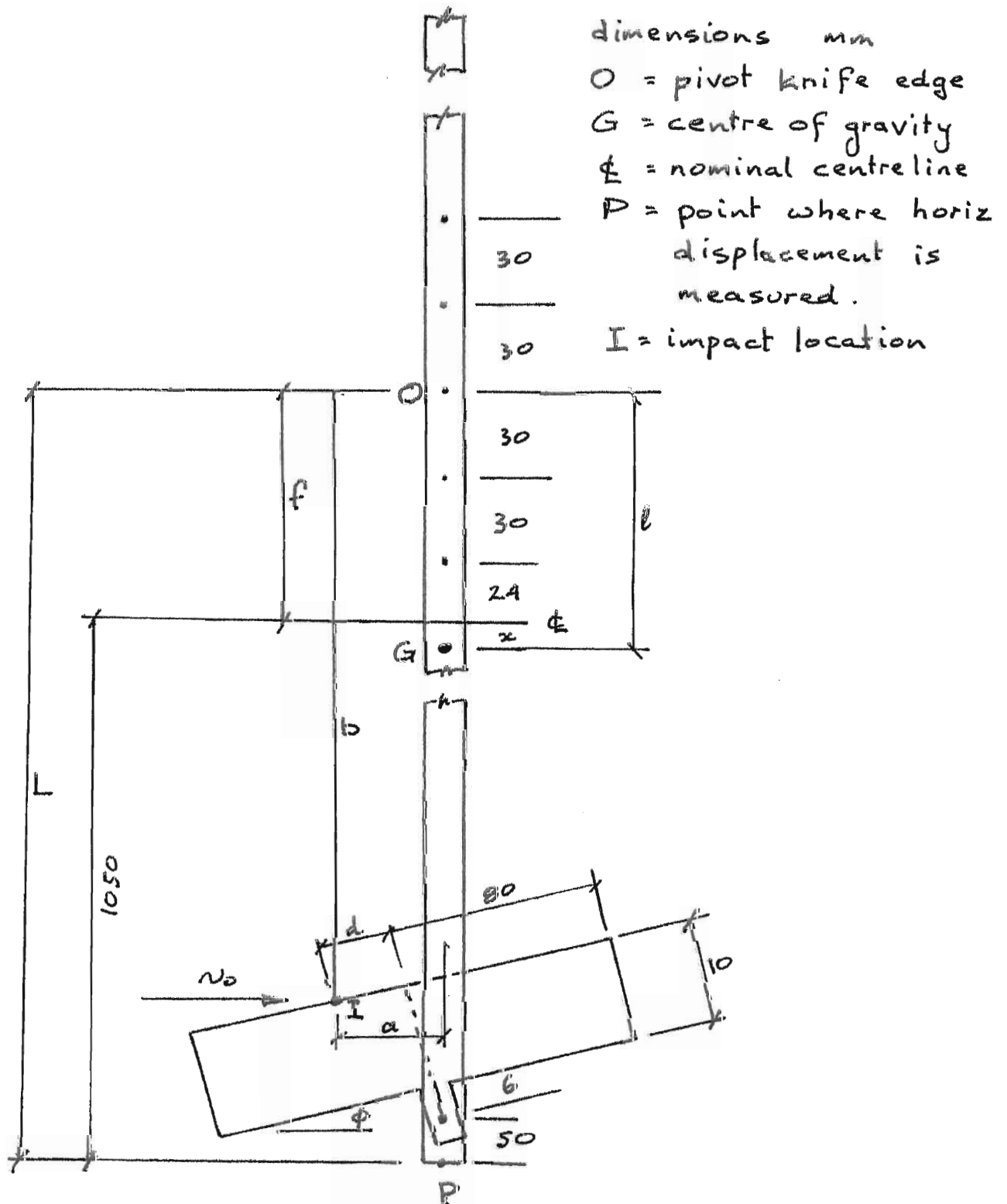
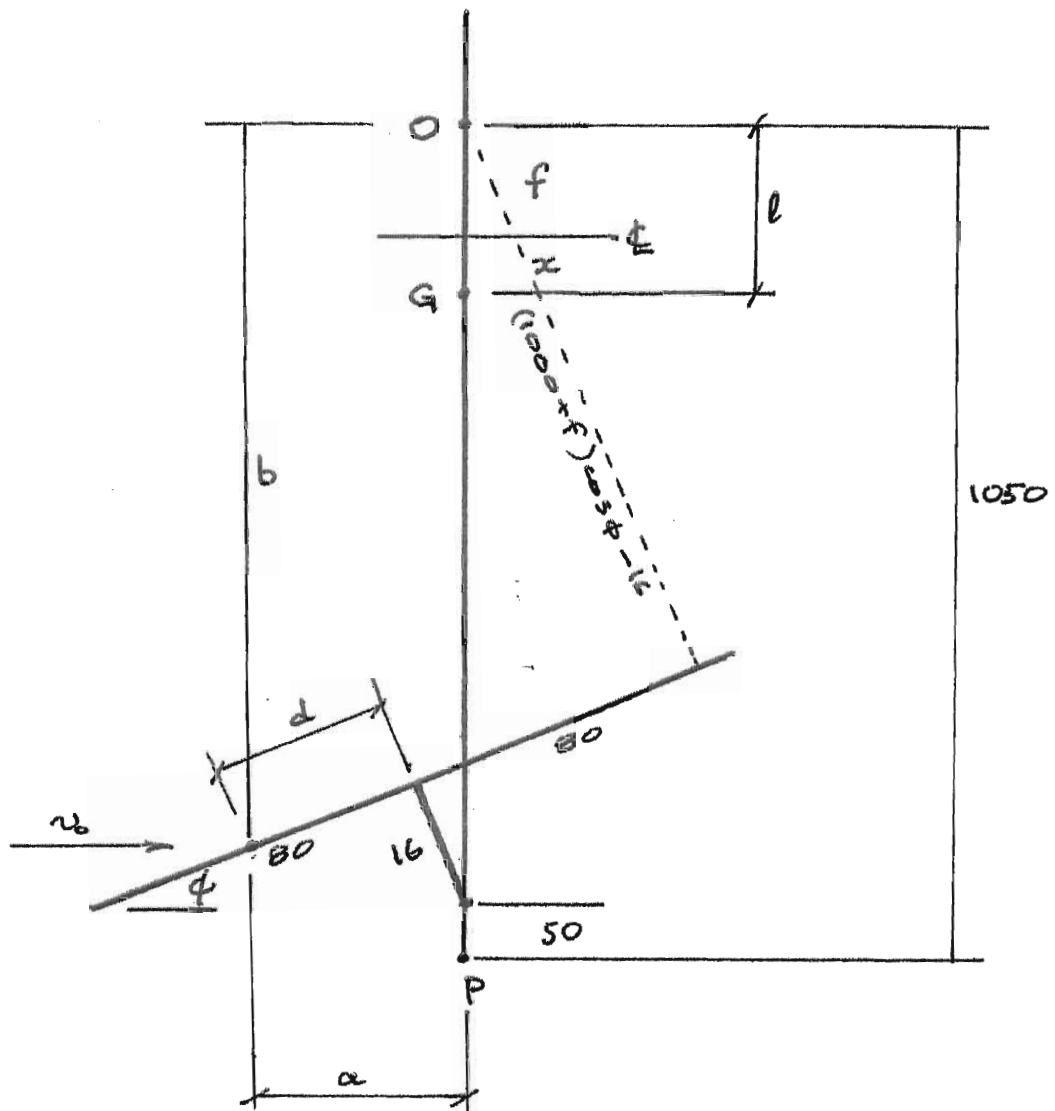


Figure 2



$$a = 16 \sin \phi + d \cos \phi \quad \text{mm}$$

$$b = 1000 + f - 16 \cos \phi + d \sin \phi \quad \text{mm}$$

Note:  $d$  is positive in the direction shown

Figure 3

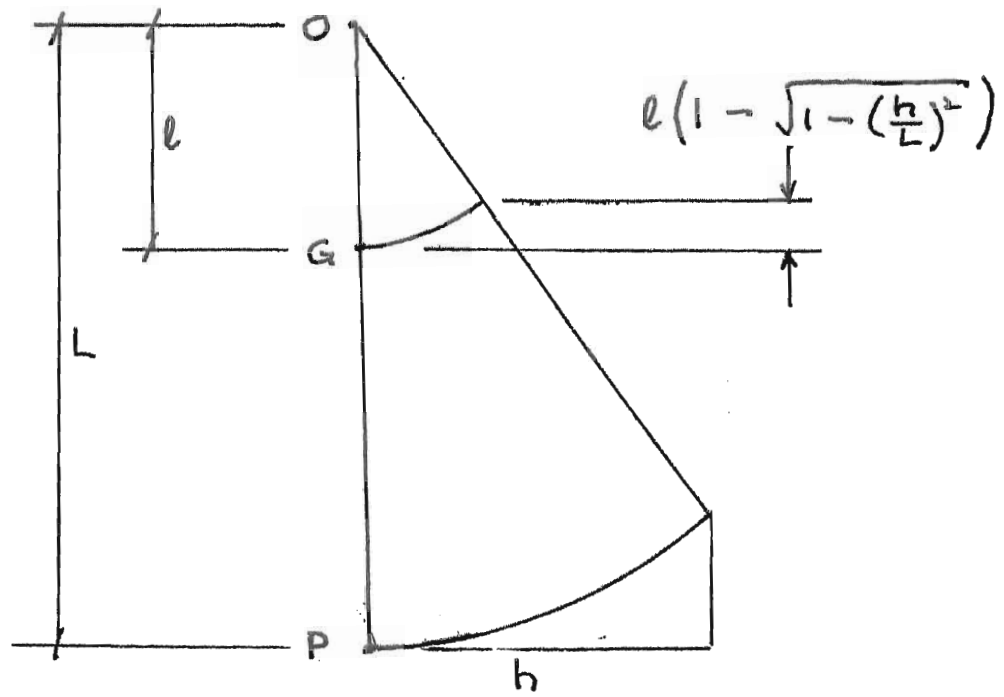




Figure 4

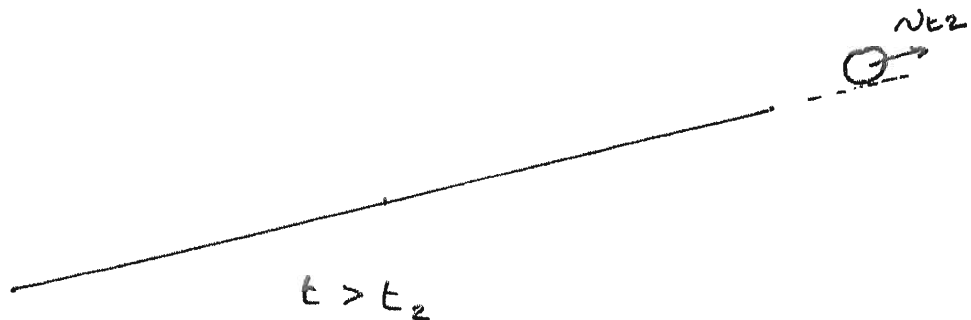
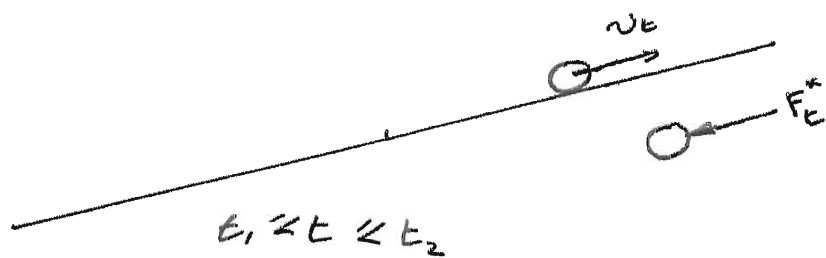
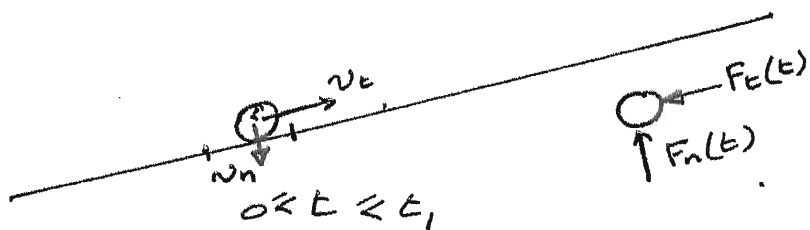
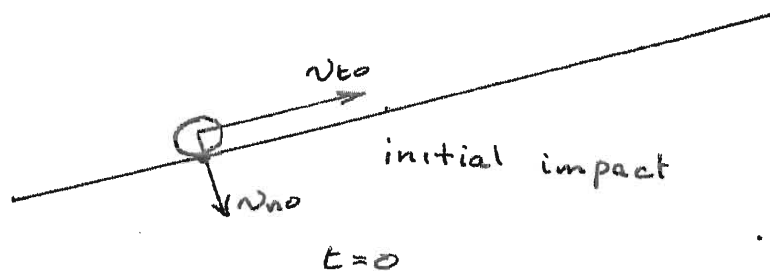
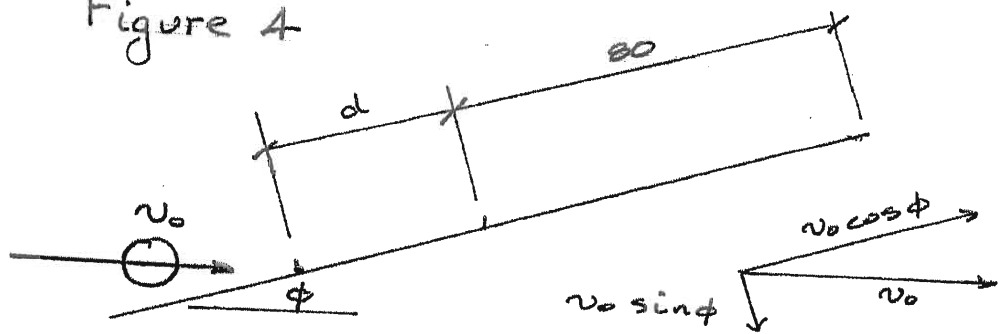


Figure 5

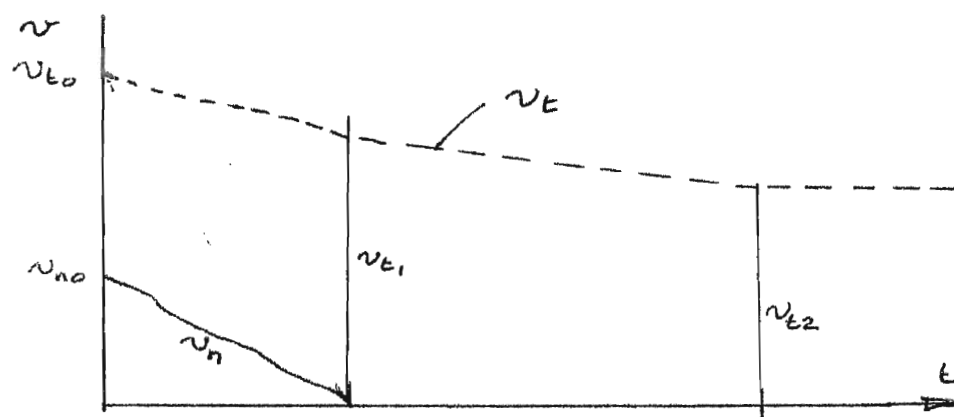
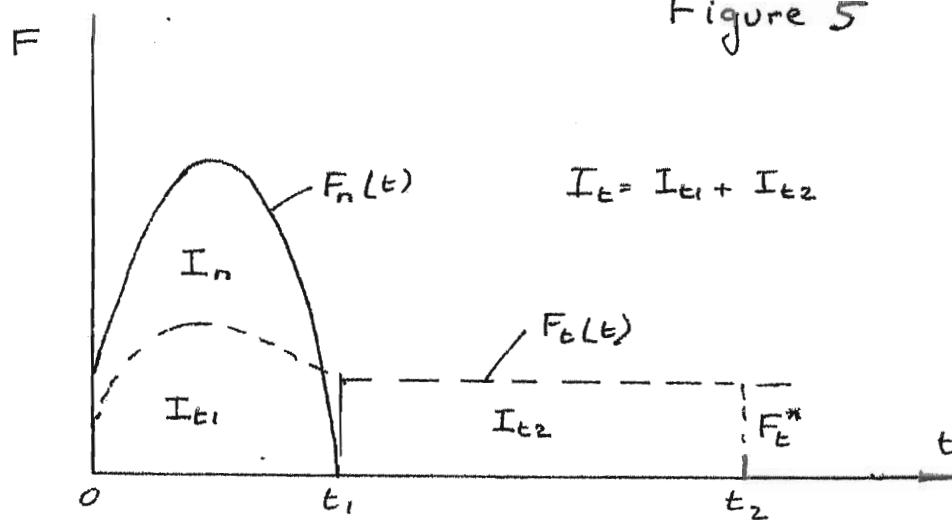
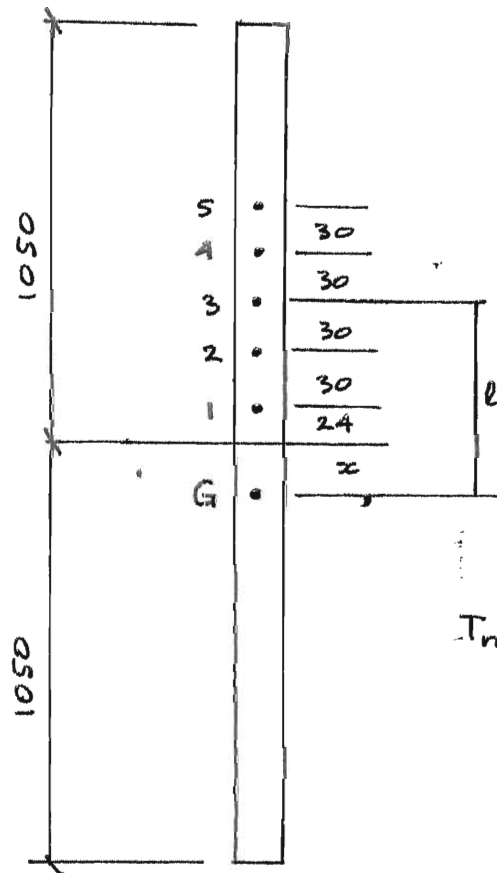


Figure 6



$$l_1 = 0.024 + x$$

⋮

$$l_5 = 0.144 + x$$

$$T_n = 2\pi \sqrt{\frac{\frac{k_G^2}{l_n} + l_n}{g}}$$

ORIGINAL PENDULUM, WITH SIDE PLATES, TESTS 29-30/10/12

17.9 degrees			
f=24 mm			
d mm	h mm	lt	
-55	186	0.045	
-50	190	0.046	
-35	232	0.1	
-10	247	0.1	
5	285	0.149	
12	338	0.23	
15	335	0.222	
22	349	0.239	
40	365	0.248	

ballistic04

17.9 degrees			
f=54 mm			
d mm	h mm	lt	
-50	150	0.076	
-30	176	0.116	
-15	242	0.252	
3	206	0.152	
5	262	0.279	
40	318	0.373	
43	305	0.342	
47	305	0.338	
50	332	0.399	

ballistic04

17.9 degrees			
f=84 mm			
d mm	h mm	lt	
-65	110	0.042	
-35	160	0.147	
-30	140	0.089	
-30	138	0.084	
0	209	0.246	
5	204	0.228	
10	212	0.245	
13	199	0.207	
40	286	0.418	
50	300	0.447	
60	281	0.385	

ballistic06

MODIFIED MODEL RESULTS REDUCED TO COMMON BASE		
Vt0 m/s		832
Vt1 m/s		841
ln Ns		0.957
Fn* kN		16.6
Ft* kN		2.41
Ft*/Fn*		0.145

17.9 degree plate, side plates

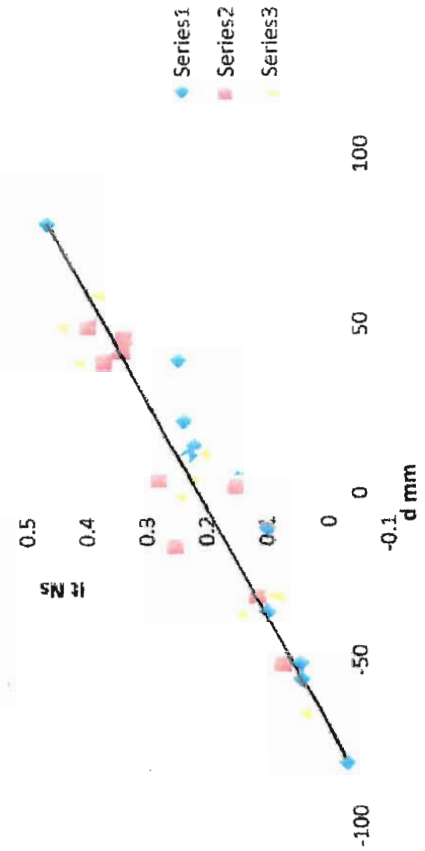


Figure 7(b)

ORIGINAL PENDULUM, WITH SIDE PLATES, TESTS 29-30/10/12

22.8 degrees f=24 mm			
d mm	h mm	lt	
-55	390	0.222	
-50	380	0.199	
-25	480	0.345	
0	580	0.498	
20	600	0.51	
22	610	0.528	
30	671	0.638	
50	638	0.546	
53	668	0.602	
63	655	0.563	

ballistic01.mw

22.8 degrees f=54 mm			
d mm	h mm	lt	
-55	255	0.155	
-35	310	0.262	
-33	300	0.235	
-20	368	0.384	
4	417	0.473	
15	400	0.418	
24	424	0.466	
35	492	0.622	
53	505	0.633	
60	518	0.658	

ballistic02.mw

22.8 degrees f=84 mm			
d mm	h mm	lt	
-65	162	0.013	
-40	251	0.23	
-37	240	0.196	
-25	268	0.26	
5	337	0.418	
7	368	0.504	
28	378	0.507	
30	371	0.484	
45	432	0.642	
50	385	0.501	

ballistic03.mw

MODIFIED MODEL	
Vt0 m/s	806
Vt1 m/s	779
In Ns	1.207
Fn* kN	22.0
Ft* kN	2.76
Ft*/Fn*	0.126

22.8 degree plate, side plates

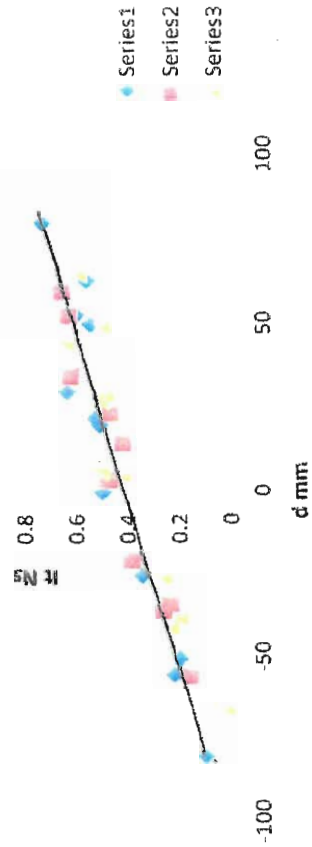


Figure 7(c)

MODIFIED PENDULUM, NO SIDE PLATES, TESTS 6-7/12/12

9.8 degrees			
f=24 mm			
d mm	h mm	lt	
-78	35	0.002	
-70	45	0.013	
-35	105	0.086	
-28	100	0.075	
-15	75	0.03	
0	130	0.106	
27	130	0.092	
40	110	0.054	
45	130	0.082	
65	160	0.118	

ballistic13

9.8 degrees			
f=54 mm			
d mm	h mm	lt	
-75	10	-0.03	
-70	10	-0.033	
-43	30	0	
-5	30	-0.019	
0	60	0.049	
12	20	-0.051	
45	45	-0.009	
50	45	-0.012	
60	60	0.019	
65	75	0.05	

ballistic14

9.6 degrees			
f=84 mm			
d mm	h mm	lt	
-78	10	-0.022	
-60	15	-0.017	
-53	21	-0.003	
-45	45	0.062	
-5	38	0.022	
10	28	-0.013	
38	43	0.016	
45	52	0.038	
55	135	0.271	
55	103	0.18	
60	68	0.077	
65	85	0.123	

ballistic15

MODIFIED MODEL RESULTS REDUCED TO COMMON BASE		
Vt0 m/s		862
Vt1 m/s		863
ln Ns		0.53
Fn* kN		7.30
Ft* kN		0.49
Ft*/Fn*		0.067

9.8 degree plate, no side plates

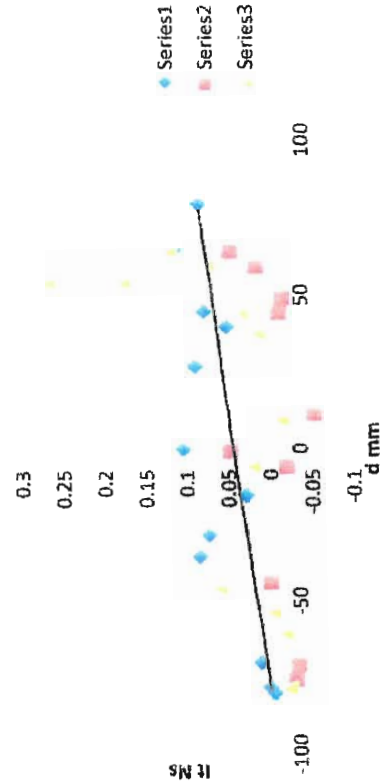


Figure 8(a)

MODIFIED PENDULUM, NO SIDE PLATES, TESTS 6-7/12/12

16.4 degrees			
f=24 mm			
d mm	h mm	lt	
-78	83	-0.061	
-75	115	-0.013	
-68	105	-0.035	
-40	175	0.05	
18	220	0.069	
25	255	0.118	
35	245	0.093	
40	235	0.073	
48	295	0.161	

16.7 degrees			
f=54 mm			
d mm	h mm	lt	
-78	70	-0.031	
-55	100	0.022	
-50	110	0.042	
-30	150	0.122	
-15	140	0.084	
-4	140	0.074	
15	160	0.106	
25	170	0.121	
48	200	0.175	
65	180	0.11	

16.4 degrees			
f=84 mm			
d mm	h mm	lt	
-75	45	-0.065	
-50	75	0.002	
-45	85	0.027	
-35	88	0.028	
-15	90	0.017	
0	93	0.013	
30	112	0.043	
35	115	0.048	
40	135	0.103	
53	130	0.077	
68	200	0.272	

MODIFIED MODEL RESULTS REDUCED TO COMMON BASE	
Vt0 m/s	839
Vt1 m/s	847
In Ns	0.879
Fn* kN	10.7
Ft* kN	0.77
Ft*/Fn*	0.072

Ballistic10

Ballistic11

Ballistic12

16.4 degrees, no side plate

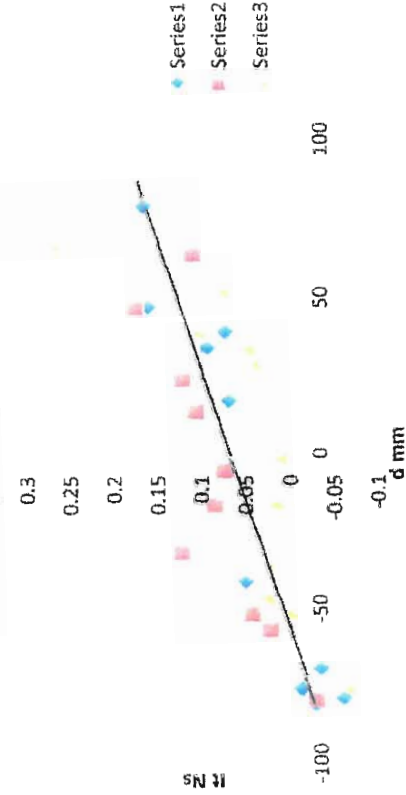


Figure 8(b)

Figure 9

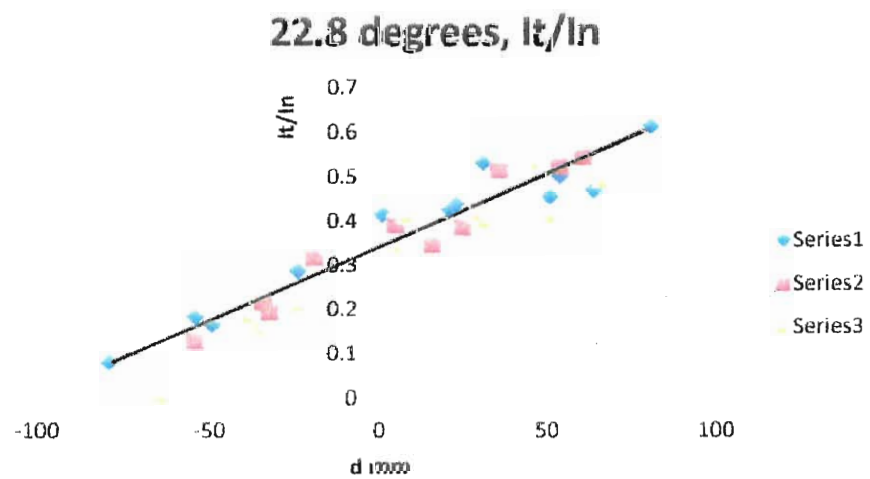
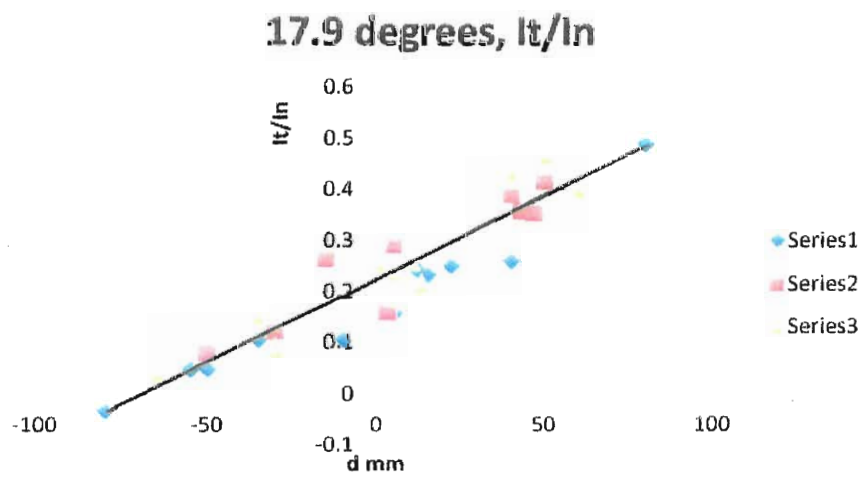
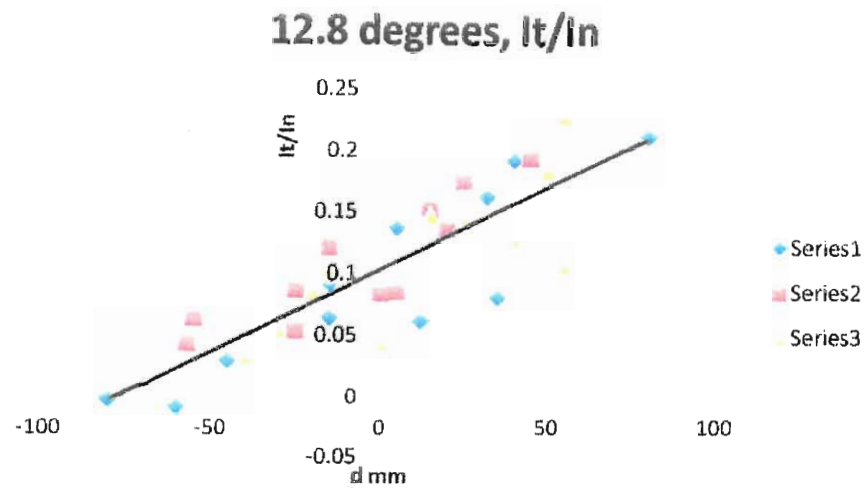




Figure 10

